

Structural Mechanisms of Binding Kinetics

Dissertation

zur Erlangung des Doktorgrades

der Naturwissenschaften

vorgelegt beim Fachbereich 14

„Molecular Sciences:

Biochemie, Chemie, Pharmazie“

der Johann Wolfgang Goethe - Universität

in Frankfurt am Main

von

Benedict-Tilman Berger

aus Berlin

Frankfurt am Main, 2020

(D30)

vom Fachbereich 14 der

Johann Wolfgang Goethe-Universität als Dissertation
angenommen.

Dekan: Prof. Dr. C. Glaubitz

Gutachter: Prof. Dr. Stefan Knapp, Prof. Dr. Eugen Proschak

Datum der Disputation: 19.10.2020

„ Corpora non agunt nisi fixata “

- Paul Ehrlich (1854 - 1915)

“A substance will not work unless it is bound ”

Goethe University FB 14:

“ From single molecules to cells ”

ACKNOWLEDGEMENT

I would like to thank all those who have contributed to the success of this PhD thesis “Structural Mechanisms of Binding Kinetics” by their professional and personal support.

First, I thank Prof. Dr. Stefan Knapp for both the possibility to work in his laboratory in the SGC at the Goethe University Frankfurt and the willingness to evaluate my PhD thesis. I would as well like to very much thank Dr. Susanne Müller-Knapp for her supervision throughout this thesis. Their suggestions and advices have contributed to the steady improvement of this work. They showed me how a scientific leader motivates employees by giving all the potential opportunities and only showing directions rather than doing micromanagement. By that I could develop my own self-motivation and self-leadership skills and become a major contributor to countless projects of other people from the group. Also, they thought me that cooperation drives science much faster than competition which resulted in many collaborations with other groups. Especially, I am grateful for the opportunity to have gained their trust on being responsible for the NanoBRET technique I learned to love to perform across the kinome and the chance to closely collaborate with the Promega corporation and Matt Robers, the techniques inventor, whom I would like to thank for his constant support and suggestions when struggling with data evaluation or assay instabilities.

I am very happy to have done my work in the kinase group of the SGC Frankfurt: I would like to especially thank Martin Schröder for being a great example of a passionate and hard-working Scientist always motivating me to strive to do the same and especially that you can be the best in your field even if you came from a completely different angle before. I would like to highlight my appreciation of Dr. Andreas Krämer, who encouraged me to do better and be more efficient in my work and for various chats about screening and crystallographic techniques, motivation and leadership skills. I did as well very much enjoy the before-work talks with Christian Kurz throughout the years in the morning gym-sessions who motivated me to keep going and which resulted in several good ideas for new projects. I would like to thank the members of the Knapp lab for supporting me, giving me a chance to understand the project-based work in a science lab better and giving me the opportunity to support them with advice and NanoBRET data produced throughout the years.

Additional to the above mentioned these are namely: Dr. Roberta Tesch, Dr. Romain Lucas, Dr. Andreas Joerger, Dr. Jelena Bozilovic, Dr. Claudia Tredup, Dr. Apirat Chaikuad, Dr. Sebastian Mathea, Dr. David Heidenreich, Dr. Thomas Hanke, Dr. Deep Chatterjee, Tim Weiser, Francesco Aleksy Greco, Sandra Röhm, Jennifer Amrhein, Nicolas Bauer, Mishal McAuley, Marcel Rak, Nadine Russ, Marek Wanior, Franziska Preuß, Anja Dölle, Xiaomin Ni, Joshua Gerninghaus, Nebojsa Miletic, Amelie Tjaden, Ralf Braden, Lilia Weizel, Haotian Wang, Anais Lucas and Kathrin Cartsburg. Also, I would like to thank Marcel Walther and Marius Kreiß who I enjoyed working with and are belonging to other groups of the pharmacy department.

I would as well like to thank the students who I was allowed to supervise during their thesis and internships for trusting me and giving me a chance to improve my leadership skills and gaining experience as a scientific advisor, namely Niklas Ostermann (2 month Bachelor Thesis), Raquel Guilharducci (6 month intern) and Melissa Ilayda Irvine (6 month Master Thesis).

I thank all colleagues in the SGC and all my collaborators for discussions with me and the opportunity to have met them and let me contribute to their projects. Specifically, I want to thank Jon Elkins and Fiona Sorrell who made my Oxford experience great and finish the STK10 story with me, Evelyne Barrey, Jörg Bomke and Daniel Schwarz for showing me how to use SPR properly, Ansgar Wegner for showing me nanoDSF, Djordje Musil for all the help with the FAK crystal structures, Matthias Frech and Marta Amaral for letting me finish the FAK project and Daria Kokh and Rebecca Wade for helping me with finishing the FAK project.

My special thanks are for my wife Lena Marie Berger who not only is the best wife you can ask for, but also professionally contributed to the improvement of this thesis by countless advices and even hands on work by producing several reagents for the assay development with me. During this work and in the after-work talks I could always count on her everlasting love and support which upheld my motivation enormously.

I would like to thank both Dr. Heinz Dürr and Mrs. Heide Dürr for constantly supporting me financially throughout this thesis, without whom I could not have overcome the rising living costs in the city of Frankfurt. Especially, I would like to thank them for taking an interest in me and the talks we had about all my plans, entrepreneurship and personal development and for all their advice that resulted from this guidance. They taught me how important it is to give back to the society, how a great leader keeps up with the flood of information and how treating employees as individuals really both motivates and makes you proud for having worked for and with them.

Finally, I want to thank my parents, Roman Berger and Patrizia Doyle-Berger, for their financial and family support - and constant worrying about whether or not this thesis might be written in time - with which they enabled my studies. As well I thank my siblings, Basti and Line, and friends for their patience and their attachment.

0 Table of contents

0 TABLE OF CONTENTS

0	Table of contents	- 9 -
1	Statutory Declaration	- 13 -
2	Publications	- 19 -
3	Summary	- 23 -
4	Zusammenfassung (long)	- 27 -
5	Zusammenfassung	- 33 -
6	Introduction	- 37 -
6.1	Cancer is often caused by deregulated protein kinases	- 37 -
6.2	Protein kinases share a conserved architecture	- 37 -
6.3	Small molecule inhibitors of Protein kinases as potential cancer treatment	- 39 -
6.3.1	Types of protein kinase inhibitors.....	- 40 -
6.4	Inhibitor binding parameters and inhibitor selectivity	- 40 -
6.4.1	Determination of equilibrium target affinity to optimize potency and selectivity of a drug	- 41 -
6.4.2	Determination of binding kinetics for optimization of selectivity <i>in vivo</i> -	- 42 -
6.4.3	Pharmacokinetics and the efficacy of a drug <i>in vivo</i>	- 43 -
6.4.3.1	Kinetic selectivity of a drug <i>in vivo</i>	- 44 -
6.4.3.2	The link between the dosage of a drug and residence time <i>in vivo</i>	- 45 -
6.4.3.3	Contraindications when optimizing for a long residence time.....	- 45 -
6.4.3.4	Limitations of the drug-target-residence-time-concept.....	- 46 -
6.5	Structure Kinetic relationships	- 47 -
6.6	Introduction to project-relevant examples of protein kinases	- 49 -
6.6.1	STK10 appears to be a frequent off-target of protein kinase inhibitors ..	- 49 -
6.6.2	Selectivity of PF-562271 on FAK over PYK2	- 50 -
7	Objectives.....	- 53 -
8	Materials and Methods.....	- 55 -
8.1	Materials.....	- 55 -

0 Table of contents

8.2	Methods	- 61 -
8.2.1	Molecular cloning.....	- 61 -
8.2.2	Protein expression and purification.....	- 62 -
8.2.3	TR-FRET assays.....	- 64 -
8.2.4	DSF assay	- 65 -
8.2.5	SPR assays.....	- 66 -
8.2.6	OMNIA assays	- 68 -
8.2.7	NanoBRET assays.....	- 68 -
8.2.8	Protein crystallization and structure determination.....	- 70 -
9	Results	- 73 -
9.1	Structural factors affecting the affinity and residence time of STK10 inhibitors.....	- 73 -
9.1.1	STK10 and SLK potently bind many clinically used kinase inhibitors <i>in vitro</i>	- 73 -
9.1.2	Intrinsic flexibility of the kinase domains of STK10 and SLK allows tight interaction with many diverse inhibitors.....	- 74 -
9.1.3	Many STK10 inhibitors show only weak cellular potency	- 77 -
9.1.4	Reasons for the large decrease in STK10 affinity of inhibitors in cells..	- 78 -
9.1.5	Influence of residence time of the clinical kinase inhibitors.....	- 81 -
9.2	Structure-kinetic-relationship reveals the mechanism of the selectivity of FAK inhibitors over PYK2	- 84 -
9.2.1	A series of PF-562271-based inhibitors shows a range of binding kinetics on FAK and PYK2.....	- 84 -
9.2.2	The hydrophobic L567-ligand interaction in FAK is crucial for high potency and long residence time inhibition	- 86 -
9.2.3	Slow off-rate inhibitors induce a helical conformation of the activation loop in FAK via a hydrophobic interaction with L567	- 88 -
9.2.4	The selectivity profile of FAK and PYK2 was dictated by the formation of a helical conformation of the DFG motif.....	- 91 -
9.2.5	Binding potency and kinetics of FAK and PYK2 in living cells	- 92 -
9.2.6	Structural mechanisms affecting the protein binding site flexibility in FAK and PYK2	- 94 -
10	Discussion.....	- 99 -
10.1	The importance of cellular characterization of inhibitor potency for inhibitor selectivity	- 99 -

0 Table of contents

10.1.1	The presence of ATP changes inhibitor potency and selectivity in cells	- 99 -
10.1.2	Examples of unexpected cellular selectivity	- 100 -
10.1.3	Comparison of the different techniques used in this study: A typical screening cascade	- 101 -
10.2	The importance of cellular characterization of inhibitor kinetics	- 102 -
10.2.1	The prolonged target residence time of erlotinib but not gefitinib might be the cause for STK10-related off target toxicity	- 103 -
10.2.2	Structural elements affecting inhibitor residence time on STK10.....	- 104 -
10.2.3	The design of slow off-rate inhibitors on FAK for improved pharmacological properties	- 105 -
10.2.4	Structural elements affecting FAK and PYK2 kinetics	- 105 -
10.2.5	Using the NanoBRET cellular wash-out assay for a kinetic compound characterization in cells.	- 106 -
10.3	Elucidation of structural mechanisms for improving binding kinetics	- 108 -
11	Supplemental Information.....	- 111 -
12	Abbreviations	- 135 -
13	References	- 137 -

0 Table of contents

1 STATUTORY DECLARATION

Except where stated otherwise by reference or acknowledgment, the work presented was generated by myself under the supervision of my advisors during my doctoral studies. All contributions from colleagues are explicitly referenced in the thesis. The material listed below was obtained in the context of collaborative research:

- Fig. 6: STK10 and SLK bind many of the clinically used inhibitors potently *in vitro*.
 - Jon Elkins, SGC Oxford: Helped with study design
 - My own contribution: ePCA and DSF data determination and evaluation
- Fig. 7: The intrinsic flexibility of the kinase domains of STK10 and SLK allows tight interaction with many diverse inhibitors.
 - Jon Elkins, SGC Oxford: Helped with study design and structure solving
 - Fiona Sorrell, SGC Oxford: Provided structural models for 6eim, 5owr, 5ajq, 6i2y, 5owr
 - My own contribution: crystals for 6eim, crystals and structure refinement for 6gtt, model interpretation and figure design for all figures.
- Fig. 8: Many of the inhibitors do not bind STK10 strongly in cells.
 - Jon Elkins, SGC Oxford: Helped with Study design
 - My own contribution: NanoBRET assays, data interpretation and figure preparation
- Fig. 9: Effect of ATP on the compound IC_{50} s in cells.
 - Jon Elkins, SGC Oxford: Helped with Study design
 - Fiona Sorrell, SGC Oxford: Production of STK10 kinase domain and STK10 full-length protein from insect cell expression
 - My own contribution: OMNIA assay data determination, evaluation, interpretation and figure design
- Fig. 10: SPR sensorgrams for STK10KD and STK10FL as indicated in the respective panel.
 - Jon Elkins, SGC Oxford: Helped with Study design
 - Fiona Sorrell, SGC Oxford: Production of STK10 kinase domain and STK10 full-length protein from insect cell expression
 - Evelyne Barrey & Daniel Schwarz & Jörg Bomke, Merck Discovery Technologies: Helped with SPR data production and interpretation (figures produced by SPR device).
 - My own contribution: SPR data production and data interpretation (figures produced by SPR device)
- Fig. 11: Effect of STK10 and SLK phosphorylation on the compound potency shift in cells.
 - Jon Elkins, SGC Oxford: Helped with Study design
 - My own contribution: NanoBRET mutagenesis and assays, data interpretation and figure preparation

1 Statutory Declaration

- Fig. 12: Could residence time be important for achieving the observed physiological effects?
 - Jon Elkins, SGC Oxford: Helped with Study design
 - My own contribution: kPCA assay setup, data generation, interpretation and figure preparation
- Fig. 13: Three substituent sites on PF-562271 R1, R2 and R3 were considered to study the interactions in the kinase binding sites.
 - Matthias Frech, Merck Discovery Technologies: Study design
 - Marta Amaral & Jörg Bomke, Merck Discovery Technologies: SPR data generation, data interpretation
 - Daria Kokh, HITS Heidelberg: Preparation of Figure E.
 - My own contribution: k_{on} - k_{off} -plot generation (figure D), data interpretation
- Fig. 14: Inhibitors with long residence times induce a helical conformation of the activation loop in FAK via a hydrophobic interaction with L567.
 - Matthias Frech, Merck Discovery Technologies: Study design
 - Marta Amaral, Merck Discovery Technologies: crystallization, model building and interpretation
 - Djordje Musil, Merck Discovery Technologies: crystallization, model building
 - My own contribution: model interpretation, figure preparation
- Fig. 15: The selectivity profile of FAK and PYK2 is dictated by the formation of a helical conformation of the DFG motif in FAK.
 - Matthias Frech, Merck Discovery Technologies: Study design
 - Marta Amaral, Merck Discovery Technologies: crystallization, model building and interpretation
 - Djordje Musil, Merck Discovery Technologies: crystallization, model building
 - My own contribution: model interpretation, figure preparation
- Fig. 16: Both binding potency and kinetics translate from *in vitro* into the cellular system.
 - Matthias Frech, Merck Discovery Technologies: Study design
 - Marta Amaral, Merck Discovery Technologies: NanoBRET data generation and interpretation
 - My own contribution: NanoBRET data generation and interpretation, figure preparation, assay design
- Fig. 17: Structural stability of the ligand binding sites in FAK and PYK2 explored by site-directed mutagenesis.
 - Matthias Frech, Merck Discovery Technologies: Study design
 - Marta Amaral, Merck Discovery Technologies: Mutagenesis design
 - Daria Kokh & Rebecca Wade, HITS Heidelberg: Mutagenesis design
 - My own contribution: Mutagenesis design, Mutagenesis, NanoBRET data generation and interpretation, figure design

1 Statutory Declaration

- Suppl. Fig. S 1: HTRF tracer 236 properties for STK10 (association kinetics and potency) and SLK (potency only).
 - Jon Elkins, SGC Oxford: Helped with Study design
 - My own contribution: kPCA assay setup, data generation, interpretation and figure preparation
- Suppl. Fig. S 2: Examples of ePCA compound titrations and resulting fits.
 - Jon Elkins, SGC Oxford: Helped with Study design
 - My own contribution: ePCA assay setup, data generation, interpretation and figure preparation
- Suppl. Fig. S 3: Examples of kPCA data curves and resulting fits.
 - Jon Elkins, SGC Oxford: Helped with Study design
 - My own contribution: kPCA assay setup, data generation, interpretation and figure preparation
- Suppl. Fig. S 8: Suppl. Fig. S 4: Mass Spec analysis of STK10 KD and STK10 FL.
 - Jon Elkins, SGC Oxford: Helped with Study design
 - Fiona Sorrell, SGC Oxford: Mass Spec generation and interpretation (figure from device)
 - My own contribution: data interpretation
- Suppl. Fig. S 9: Titration of STK10 full-length (FL) or kinase domain only (KD) proteins using 1 mM ATP and 1 mM SOX substrate in the OMNIA assay.
 - Jon Elkins, SGC Oxford: Helped with Study design
 - Fiona Sorrell, SGC Oxford: Production of STK10 kinase domain and STK10 full-length protein from insect cell expression
 - My own contribution: data interpretation: OMNIA assay performance, assay design, data interpretation and figure preparation
- Suppl. Fig. S 10: Stability of insect cell expressed STK10 proteins.
 - Jon Elkins, SGC Oxford: Helped with Study design
 - Fiona Sorrell, SGC Oxford: Production of STK10 kinase domain and STK10 full-length protein from insect cell expression
 - Lena Berger & Ansgar Wegner, Merck Discovery Technologies: nanoDSF data generation and interpretation (figure produced by device).
 - My own contribution: data interpretation
- Suppl. Fig. S 11: Tracer parameters determined in NanoBRET for FAK and PYK2.
 - Matthias Frech, Merck Discovery Technologies: Study design
 - Marta Amaral, Merck Discovery Technologies: NanoBRET data generation and interpretation
 - My own contribution: NanoBRET data generation and interpretation, figure preparation, assay design

1 Statutory Declaration

- Table 5: Chemical series based on PF-562271 investigated in this study.
 - Matthias Frech, Merck Discovery Technologies: Study design
 - Marta Amaral & Jörg Bomke, Merck Discovery Technologies: SPR data generation and interpretation
 - Timo Heinrich, Merck Discovery Technologies: Compound preparation
 - My own contribution: SPR data interpretation
- Table 6: NanoBRET target engagement and wash-out data.
 - Matthias Frech, Merck Discovery Technologies: Study design
 - Marta Amaral, Merck Discovery Technologies: NanoBRET data generation and interpretation
 - My own contribution: NanoBRET data generation and interpretation, figure preparation, assay design
- Table 7: NanoBRET site directed mutagenesis to validate FAK-L567 as the driver of slow off-rate inhibition of FAK.
 - Matthias Frech, Merck Discovery Technologies: Study design
 - Marta Amaral, Merck Discovery Technologies: Mutagenesis design
 - Daria Kokh & Rebecca Wade, HITS Heidelberg: Mutagenesis design
 - My own contribution: Mutagenesis design, Mutagenesis, NanoBRET data generation and interpretation
- Suppl. Table S 1: Data collection and refinement statistics for STK10 structures.
 - Jon Elkins, SGC Oxford: Helped with study design and structure solving
 - Fiona Sorrell, SGC Oxford: Provided structural models for 6eim, 5owr, 5ajq, 6i2y, 5owr
 - My own contribution: crystals for 6eim, crystals and structure refinement for 6gtt, model interpretation
- Suppl. Table S 2: kPCA, ePCA, DSF and NanoBRET data for STK10 and ePCA, DSF and NanoBRET data for SLK.
 - Jon Elkins, SGC Oxford: Helped with study design
 - My own contribution: all assay setup and data generation
- Suppl. Table S 3: Comparison of the Omnia activity, NanoBRET potency, SPR potency, kPCA kinetics, SPR kinetics and the NanoBRET half-lives for 8 representative compounds.
 - Jon Elkins, SGC Oxford: Helped with Study design
 - Fiona Sorrell, SGC Oxford: Production of STK10 kinase domain and STK10 full-length protein from insect cell expression
 - Evelyne Barrey & Daniel Schwarz & Jörg Bomke, Merck Discovery Technologies: Helped with SPR data production
 - My own contribution: SPR data production, NanoBRET data production, DSF data production, kPCA data production, ePCA data production, OMNIA data production

1 Statutory Declaration

- Suppl. Table S 4: Data collection and refinement statistics for FAK structures.
 - Matthias Frech, Merck Discovery Technologies: Study design
 - Marta Amaral, Merck Discovery Technologies: crystallization, model building and interpretation
 - Djordje Musil, Merck Discovery Technologies: crystallization, model building, table generation
 - My own contribution: model interpretation

Whenever a figure, table or text is identical to a previous publication, it is stated explicitly in the thesis that copyright permission and/or co-author agreement has been obtained. The following parts of the thesis have been previously published:

- Data for STK10 and SLK ePCA, kPCA, protein production and structure determination were performed as part of my Master's Thesis "The SKR of clinical kinase inhibitors binding to STK10 compared to their designed targets" (FU Berlin, 2016-04-01). This includes data usage for Fig. 6, Fig. 7, Fig. 8, Fig. 12, Suppl. Fig. S 2, Suppl. Fig. S 3 but new/different figures were generated or figures were altered.
- Suppl. Fig. S 1 is identical to figures used in the Master's Thesis.
- Data was reused for kPCA, ePCA and DSF assays after data re-evaluation in parts of Suppl. Table S 1, Suppl. Table S 2, Suppl. Table S 3
- Fig. 1A: Illustration reproduced courtesy of Cell Signaling Technology Inc. (www.cellsignal.com)
- Fig. 3: Permission granted on 2020-06-04 by Springer Nature.
- Fig. 4: Permission granted on 2020-06-03 by Elsevier.
- Fig. 18: Open access article distributed under the terms of the Creative Commons CC-BY license, which permits unrestricted use, distribution, and reproduction in any medium, provided the original work is properly cited. Not required to obtain permission to reuse this article. (<https://s100.copyright.com/AppDispatchServlet?publisherName=ELS&contentID=S2451945617303914&orderBeanReset=true>), 2020-06-03

1 Statutory Declaration

2 PUBLICATIONS

1) SGC-GAK-1: a chemical probe for cyclin G associated kinase (GAK)¹.

- Link: <https://www.ncbi.nlm.nih.gov/pubmed/30768268>
- Authors: Asquith CRM, **Berger BT**, Wan J, Bennett JM, Capuzzi SJ, Crona DJ, Drewry DH, East MP, Elkins JM, Fedorov O, Godoi PH, Hunter DM, Knapp S, Müller S, Torrice CD, Wells CI, Earp HS, Willson TM, Zuercher WJ
- Status: accepted on 19/02/15 at Journal of medicinal chemistry
- Contribution: ITC data, NanoBRET assay data and methods, figure preparation and manuscript revision

2) Development, optimization, and structure–activity relationships of covalent-reversible JAK3 inhibitors based on a tricyclic imidazo [5, 4-d] pyrrolo [2, 3-b] pyridine scaffold².

- Link: <https://www.ncbi.nlm.nih.gov/pubmed/29852068>
- Authors: Forster M, Chaikuad A, Dimitrov T, Döring E, Holstein J, **Berger BT**, Gehringer M, Ghoreschi K, Müller S, Knapp S, Laufer SA
- Status: accepted on 18/05/31 at Journal of medicinal chemistry
- Contribution: NanoBRET assay data and methods, figure preparation and manuscript revision

3) Binding kinetics survey of the drugged kinome³.

- Link: <https://www.ncbi.nlm.nih.gov/pubmed/30362749>
- Authors: Georgi V, Schiele F, **Berger BT**, Steffen A, Marin Zapata PA, Briem H, Menz S, Preusse C, Vasta JD, Robers MB, Brands M, Knapp S, Fernández-Montalván A
- Status: accepted on 18/10/26 at Journal of the American Chemical Society
- Contribution: As part of my Bachelor Thesis: ePCA and kPCA data and evaluation, SPR data and evaluation, As part of my PhD Project: manuscript revision

4) A Highly Selective Chemical Probe for Activin Receptor-like Kinases ALK4 and ALK5⁴.

- Link: <https://www.ncbi.nlm.nih.gov/pubmed/32176847>
- Authors: Hanke T, Wong JF, **Berger BT**, Abdi I, Berger LM, Tesch R, Tredup C, Bullock AN, Müller S, Knapp S
- Status: accepted on 20/03/16 at ACS Chemical Biology
- Contribution: NanoBRET assay data and methods, figure preparation and manuscript revision

- 5) **Identification of molecular targets for the targeted treatment of gastric cancer using dasatinib⁵.**
- Link: <https://www.ncbi.nlm.nih.gov/pubmed/32082487>
 - Authors: Montenegro RC, Howarth A, Ceroni A, Fedele V, Farran B, Mesquita FP, Frejno M, **Berger BT**, Heinzlmeir S, Sailem HZ, Tesch R, Ebner D, Knapp S, Burbano R, Kuster B, Müller S
 - Status: accepted on 20/01/13 at Oncotarget
 - Contribution: Scratch assay cell migration data, methods part, figure preparation and manuscript revision
- 6) **Furo [3, 2-b] pyridine: A Privileged Scaffold for Highly Selective Kinase Inhibitors and Effective Modulators of the Hedgehog Pathway⁶.**
- Link: <https://www.ncbi.nlm.nih.gov/pubmed/30569600>
 - Authors: Němec V, Hylsová M, Maier L, Flegel J, Sievers S, Ziegler S, Schröder M, **Berger BT**, Chaikuad A, Valčíková B, Uldrijan S, Drápela S, Souček K, Waldmann H, Knapp S, Paruch K
 - Status: accepted on 18/12/20 at Angewandte Chemie
 - Contribution: NanoBRET assay data and methods, figure preparation and manuscript revision
- 7) **Fast Iterative Synthetic Approach toward Identification of Novel Highly Selective p38 MAP Kinase Inhibitors⁷.**
- Link: <https://www.ncbi.nlm.nih.gov/pubmed/31702918>
 - Authors: Röhms S, **Berger BT**, Schröder M, Chaikuad A, Winkel R, Hekking KFW, Benningshof JJC, Müller G, Tesch R, Kudolo M, Forster M, Laufer S, Knapp S
 - Status: accepted on 19/11/08 at Journal of medicinal chemistry
 - Contribution: NanoBRET assay data and methods, figure preparation and manuscript revision
- 8) **NVP-BHG712: Effects of Regioisomers on the Affinity and Selectivity toward the EPHrin Family⁸.**
- Link: <https://www.ncbi.nlm.nih.gov/pubmed/29928781>
 - Authors: Tröster A, Heinzlmeir S, **Berger BT**, Gande SL, Saxena K, Sreeramulu S, Linhard V, Nasiri AH, Bolte M, Müller S, Kuster B, Médard G, Kudlinzki D, Schwalbe H
 - Status: accepted on 18/06/21 at ChemMedChem
 - Contribution: NanoBRET assay data and methods, figure preparation and manuscript revision
- 9) **Quantitative, wide-spectrum kinase profiling in live cells for assessing the effect of cellular ATP on target engagement⁹.**
- Link: <https://www.ncbi.nlm.nih.gov/pubmed/32176847>
 - Authors: Vasta JD, Corona CR, Wilkinson J, Zimprich CA, Hartnett JR, Ingold MR, Zimmerman K, Machleidt T, Kirkland TA, Huwiler KG, Ohana RF, Slater M, Otto P, Cong M, Wells CI, **Berger BT**, Hanke T, Glas C, Ding K, Drewry DH, Huber KVM, Willson TM, Knapp S, Müller S, Meisenheimer PL, Fan F, Wood KV, Robers MB

2 Publications

- Status: accepted on 17/11/22 at Cell chemical biology
- Contribution: NanoBRET assay data and manuscript revision

10) Structural factors affecting the affinity and residence time of STK10 inhibitors.

- Link: N/A
- Authors: **Berger BT**, Sorrell FJ, Salah E, Abdul Azeez KR, Berger LM, Barrey E, Schwarz D, Bomke J, Müller S, Knapp S, & Elkins JM
- Status: manuscript in preparation
- Contribution: As part of my Master's Thesis: ePCA, kPCA data, DSF data, crystallization of 6eim and 6gtt, structural refinement of 6gtt, As part of my PhD Projects: all new data evaluation and figure preparation, NanoBRET assay data, NanoBRET mutagenesis, OMNIA activity data, SPR data and manuscript preparation as first author

11) Structure-kinetic-relationship reveals the mechanism of selectivity of FAK inhibitors over PYK2.

- Link: N/A
- Authors: **Berger BT**, Amaral M, Kokh DB, Nunes-Alves A, Musil D, Heinrich T, Schröder M, Neil R, Wang J, Navratilova I, Bomke J, Elkins JM, Müller S, Frech M, Wade RC & Knapp S
- Status: Manuscript in preparation
- Contribution: Figures for SPR data, NanoBRET data and crystallographic structures, data generation for NanoBRET data, mutant construct cloning and manuscript preparation as first author

12) Quantifying Target Occupancy of Small Molecules Within Living Cells¹⁰.

- Link: <https://www.ncbi.nlm.nih.gov/pubmed/32208767>
- Authors: Robers MB, Friedman-Ohana R, Huber K, Kilpatrick L, Vasta JD, **Berger BT**, Chaudhry C, Hill S, Müller S, Knapp S, Wood KV
- Status: submitted on 20/03/24 to Annual Review of Biochemistry
- Contribution: NanoBRET data analysis and Manuscript revision

13) Controlling the Covalent Reactivity of a Kinase Inhibitor with Light.

- Link: N/A
- Authors: Reynders M, Chaikuad A, **Berger BT**, Bauer K, Koch P, Laufer S, Knapp S, Trauner D
- Status: Manuscript in preparation
- Contribution: Data and figures for NanoBRET data, data analysis and manuscript revision

14) Mutation in Abl kinase with altered drug binding kinetics indicates a novel mechanism of imatinib resistance.

- Link: N/A
- Authors: Lyczek A, Rangwala A, **Berger BT**, Tom J, Guo J, Robers M, Chodera J, Robers MB, Knapp S, Seeliger MA
- Status: Manuscript in preparation
- Contribution: Assay setup for NanoBRET, experiment planning, Data and figures for NanoBRET data, data analysis and manuscript revision

15) Development of a Selective dual DDR/p38 Inhibitor with a Novel Chemical Scaffold.

- Link: N/A
- Authors: Röhm S, **Berger BT**, Schröder M, Chatterjee D, Mathea S, Joerger AC, Pinkas D, Bullock AN, Kovooru L, Kudolo M, Pohl C, Laufer S, Knapp S
- Status: Manuscript in preparation
- Contribution: Data and figures for NanoBRET data, data analysis and manuscript revision

16) Selective targeting of the α C- and DFG-out pocket in p38 MAPK.

- Link: N/A
- Authors: Röhm S, Schröder M, Dwyer JE, Widdowson CS, Chaikwad A, **Berger BT**, Joerger AC, Krämer A, Forster M, Kudolo M, Remenyi A, Laufer S, Bagley MC, Knapp S
- Status: Manuscript in preparation
- Contribution: Data and figures for NanoBRET data, data analysis and manuscript revision

17) Macrocyclic Optimization of pyrazolo[1,5-a]pyrimidiness leads to the identification of a highly selective casein kinase 2 inhibitor.

- Link: N/A
- Authors: Krämer A, Kurz C, Celik IE, **Berger BT**, Knapp S & Hanke T
- Status: Manuscript in preparation
- Contribution: Data and figures for NanoBRET data, data analysis and manuscript revision

18) Discovery of a potent dual SLK/STK10 inhibitor based on a maleimide scaffold.

- Link: N/A
- Authors: Serafim RAM, Sorrell FJ, **Berger BT**, Vasconcelos SNS, Massirer KB, Knapp S, Bennett JM, Fedorov O, Zuercher WJ, Elkins JM
- Status: Manuscript in preparation
- Contribution: Data and figures for NanoBRET data and OMNIA data, data analysis and manuscript revision

3 SUMMARY

Human protein kinases play essential roles in cellular signaling pathways and - if deregulated - are linked to a large diversity of diseases such as cancer and inflammation or to metabolic diseases. Because of their key role in disease development or progression, kinases have developed into major drug targets resulting in the approval of 52 kinase inhibitors by the Food and Drug Administration (FDA) so far.

Within the drug discovery process, the affinity of the inhibitors is the parameter that is used most often to predict the later efficacy in humans. However, the kinetics of binding have recently emerged as an important but largely neglected factor of kinase inhibitor efficacy. To efficiently suppress a signaling pathway, the targeted kinase needs to be continuously inhibited. Thus, it has been hypothesized that fast binding on-rates and slow off-rates would be the preferred property of an efficacious inhibitor. Despite optimizing the potency of kinase inhibitors, in the past decade optimization of kinetic selectivity has therefore gained interest as a molecule cannot be active unless it is bound, as Paul Ehrlich once stated. There is increasing evidence of correlations between prolonged drug-target residence time and increased drug efficacy, and that inhibitor selectivity in cellular contexts can be modulated by altered residence times. In order to contribute to the understanding of the effect of long residence times on cellular targets we initiated two projects.

The first of these projects is related to the STE20 kinase Serine/threonine kinase 10 (STK10) and its close relative STE20 like kinase (SLK) which have been reported to be frequent off-targets for kinase inhibitors used in the clinics. Also, an inhibition of STK10 and SLK has been linked to a common side-effect of severe skin rash developed upon treatment with the EGFR inhibitor erlotinib, but not gefitinib and the severity of this rash correlated with the treatment outcome, which fits the known biology of STK10 and SLK to be regulators of lymphocyte migration and PLK kinases. However, there are yet no explanations why these two proteins show such high hit-rates across the kinome among the kinase inhibitors. Using structural analysis, we identified the flexibility of STK10 to be the main reason for this hit-rate. The observed strong *in vitro* potencies did however not translate to the cellular system which is why we investigated the inhibitors residence time on STK10. We found the same flexibility to be the main reason for slow residence times among several inhibitors. We observed large rearrangements in the hydrophobic

3 Summary

backpocket of STK10 including the α C, the P-loop enclosing the inhibitor like a lid and strong π - π -stackings to be the main reasons for prolonged residence times on STK10. Interestingly, we observed an increased residence time for erlotinib, which showed skin-related side-effects, giving rise whether the binding kinetics should be investigated for weak cellular off-target effects in future drug discovery efforts.

In the second project we initiated, we illuminate a structural mechanism that allows kinetic selection between two closely related kinases, focal adhesion kinase (FAK) and proline-rich tyrosine kinase 2 (PYK2). Using an inhibitor series designed to probe the mechanism, residence times measured *in vitro* and in cells showed a strong correlation. Crystal structures and mutagenesis identified hydrophobic interactions with L567, adjacent to the DFG-motif, as being crucial to kinetic selectivity of FAK over PYK2. This specific interaction was observed only when the DFG-motif was stabilized into a helical conformation upon ligand binding to FAK. The interplay between the protein structural mobility and ligand-induced effect was found to be the key regulator of kinetic inhibitor selectivity for FAK over PYK2.

These two projects showed that the parameter residence time should be considered for different problems among the drug discovery process. First, in an open *in vivo* system not only the potency of a drug alone, but as well its residence time might be of importance. Here we showed that the weak cellular potency translated to prolonged residence times for several inhibitors in cells and established a link between the phenotypic outcome of skin rash after erlotinib treatment and the residence time of this inhibitor on STK10 in cells. On the other hand, medicinal chemistry efforts should consider structure kinetic relationships (SKR) in the optimization process and aim to understand the molecular basis for prolonged target residence times. Here, we showed that a hydrophobic interaction that is enforced upon inhibitor binding is crucial for an unusual helical DFG conformation which arrests the inhibitor and prolongs its residence time providing the molecular basis for understanding the kinetic selectivity of two closely related protein kinases. Establishing the SKRs will help medicinal chemists to kinetically optimize their drug candidates to select a suitable molecule to proceed into further optimization programs. Hence, the projects showed that the target residence time parameter needs to be considered both as a molecular optimization parameter to improve compound potency and binding behavior as well as a parameter to be

3 Summary

understood for proceeding to the open system of *in vivo* models to later modulate the *in vivo* efficacy of protein kinase targeting drugs.

3 Summary

4 ZUSAMMENFASSUNG (LONG)

Die im Menschen vorkommenden 518 verschiedenen Proteinkinasen steuern zelluläre Signalwege und wurden als Auslöser verschiedener Krankheiten wie Krebs, entzündliche Prozesse oder metabolische Deregulation identifiziert. Wegen dieser zentralen Rolle in der Entwicklung oder der Verschlimmerung von Krankheiten sind Proteinkinasen interessante Zielmoleküle für Medikamente, die die enzymatische Proteinkinasefunktion durch Inhibition regulieren. Proteinkinasen übertragen dabei die γ -Phosphatgruppe des natürlich vorkommenden Substrates Adenosintriphosphat (ATP) auf das Zielprotein, speziell einen Tyrosin- oder einen Serin oder Threonin-Aminosäurerest. Bisher wurden 52 Medikamente zur Inhibition von Proteinkinasen von der „Food and Drug Administration“ (FDA), der amerikanischen Medikamentenzulassungsbehörde, zugelassen.

Im Medikamentenfindungsprozess ist die Affinität der zu findenden Inhibitoren der meist eingesetzte Parameter, um die spätere Wirksamkeit im Menschen abzuschätzen. Die Wirksamkeit des Medikaments im Menschen wurde vor einiger Zeit jedoch mit der Bindekinetik des Inhibitors verknüpft, was bisher noch wenig Anwendung in der pharmazeutischen Forschung findet. Um einen deregulierten Signalweg effektiv zu inhibieren, muss die Zielkinase jedoch (zeitlich) dauerhaft inhibiert werden. Entsprechend geht man davon aus, dass ein effektiver Inhibitor eine schnelle Assoziationsgeschwindigkeitskonstante und eine langsame Dissoziationsgeschwindigkeitskonstante haben sollte. Die mit der Dissoziationsgeschwindigkeitskonstante verknüpfte sogenannte Verweildauer des Inhibitors am Zielmolekül hat sich als Maß zur Quantifizierung der Bindezeit etabliert. Neben der Optimierung der Affinität von Proteinkinaseinhibitoren gewinnt daher die Optimierung der Bindekinetik eines Inhibitors zunehmend an Bedeutung, da ein Inhibitor nur wirken kann, wenn er auch gebunden ist, wie Paul Ehrlich einmal sagte. Es gibt immer mehr Beweise dafür, dass es eine Korrelation zwischen einer hohen Verweildauer des Medikamentenkandidaten und einer größeren Effektivität im Menschen gibt. Weiterhin gibt es zunehmend Beweise dafür, dass die Selektivität eines Proteinkinaseinhibitors auch über die Bindekinetik und nicht wie bisher über die Affinität reguliert werden kann.

4 Zusammenfassung (long)

Wegen der konservierten Architektur der 518 im Menschen vorkommenden Proteinkinasen ist es besonders schwierig mit dem zu entwickelnden Inhibitor Selektivität über andere Proteinkinasen zu erreichen. Es wird angenommen, dass ein unselektives Medikament mit mehr Nebenwirkungen verknüpft ist. Die Selektivität und Affinität von Inhibitoren werden in verschiedenen Ebenen untersucht. Es werden Charakterisierungen (Affinität und Kinetik, sowie auch funktionale Studien) am isolierten Enzym (*in vitro*), in Zellen (*in cellulo*) und im lebenden Organismus (*in vivo*) unterschieden. Im zellulären Umfeld kommen neben dem zu untersuchenden Zielmolekül noch die in der menschlichen Zelle beinhalteten natürlichen Substrate (z.B. ATP) und Bindungspartner, sowie verschiedene Barrieren, wie Proteinexpression, Post-translationale Modifikationen oder Kompartimentierung dazu. Im zellulären Kontext gilt es deshalb, die Selektivität und Bindestärke besonders aufmerksam zu studieren. Wir haben dazu zwei Projekte zur Untersuchung der Bindekinetik für zwei Proteinkinasen initiiert.

Das erste dieser Projekte untersucht die Serin/Threonin Kinase STK10 und die stark verwandte Proteinkinase SLK, die beide der sogenannten STE20 Familie zugerechnet werden. STK10 und SLK sind als hochfrequente sogenannte Anti-Zielmoleküle der bestehenden in der klinischen Forschung bisher eingesetzten Proteinkinaseinhibitoren bekannt und stehen im Verdacht Nebenwirkungen auszulösen. Im Speziellen wurde eine Inhibition von STK10 und SLK mit einem sehr starken Hautausschlag assoziiert, wegen welchem die Behandlung durch den zugelassenen EGFR-Inhibitor Erlotinib zur Behandlung von Lungenkarzinoma zum Teil abgesetzt wird. Erlotinib inhibiert die Kinasen STK10 und SLK stark, während ein weiterer zugelassener EGFR-Inhibitor, Gefitinib, diese Kinasen nicht bindet und Patienten als Nebenwirkungen auch keinen starken Hautausschlag bekommen. Das passt auch zu dem, was über STK10 und SLK bekannt ist, nämlich, dass beide Kinasen Lymphozytenmigration und die Proteinkinase PLK1 regulieren. Es ist jedoch nicht bekannt, warum diese beiden Proteine so hochfrequent an die klinischen Proteinkinaseinhibitoren binden.

Mithilfe struktureller Analysemethoden haben wir die Flexibilität von STK10 als möglichen Grund für diese hohe Trefferrate identifiziert. Die sehr starke Bindeaffinität, die wir für STK10 *in vitro* für die klinisch eingesetzten Proteinkinaseinhibitoren bestimmt haben, hat sich im zellulären Umfeld jedoch nicht bestätigt. Die Flexibilität von STK10

4 Zusammenfassung (long)

ermöglicht jedoch eine Vielzahl von strukturellen Veränderungen, weshalb wir die Bindekinetik untersuchten. Die strukturelle Flexibilität wurde dann als mögliche Ursache für besonders langsame Dissoziationsgeschwindigkeitskonstanten verschiedener klinischer Kinaseinhibitoren bestimmt. Es wurden große Veränderungen im hinteren, sehr hydrophoben Bereich der Bindetasche beobachtet. Im Speziellen haben wir Verschiebungen an der sogenannten αC von bis zu 8 Å beobachtet, gesehen, dass der P-Loop den Inhibitor wie ein Deckel umschließen kann und starke π - π -Wechselwirkungen mit dem Inhibitor ausbilden kann. Das deutet darauf hin, dass diese langsamen Inhibitoren an STK10 nicht wie ein Schlüssel in ein Schloss passen, sondern, dass die Konformation des Proteins durch den Inhibitor erst induziert wird. Dieser Vorgang ist prinzipiell langsamer als eine Bindung ohne Konformationsänderung. Hierbei haben wir interessanterweise im zellulären Umfeld eine deutlich langsamere Dissoziation (also eine höhere Verweildauer) des Inhibitors Erlotinib beobachtet, als für den Inhibitor Gefitinib, was darauf hindeutet, dass die Bindekinetik bei schwächer wirkenden Affinitäten untersucht werden sollte um mögliche Nebenwirkungen – hier durch Erlotinib - durch unerwünschte lange Inhibition aufzudecken. Dies sollte in zukünftigen Medikamentenfindungsprozessen implementiert werden.

Im zweiten Projekt haben wir die Selektivität des Inhibitors Inhibitor PF562271 untersucht, der dual die Focal adhesion kinase (FAK) und die verwandte proline-rich tyrosine kinase 2 (PYK2) inhibiert, wobei es der Inhibitor etwa 10-mal stärker an FAK als an PYK2 bindet. FAK und PYK2 sind involviert in der Regulation der Zellmigration, im Zellwachstum und im Zellüberleben. Diese beiden Proteinkinasen sind überexprimiert in vielen verschiedenen Krebskrankheiten und haben sich deshalb als spannende Zielmoleküle in der Onkologie etabliert. Wird FAK inhibiert kann PYK2 den Verlust der Funktion von FAK kompensieren, weshalb oft duale FAK/PYK2 Inhibitoren zur Krebsmedikation vorgeschlagen werden.

Diese Selektivität haben wir mithilfe einer chemischen Serie dem Inhibitor PF562271 strukturell ähnlicher Inhibitoren beleuchtet. Dafür haben wir die Affinität und Bindekinetik der einzelnen Inhibitoren an FAK und PYK2 *in vitro* und *in cellulo* bestimmt. Auffallend war hier eine Korrelation der Hydrophobizität einer bestimmten Teilgruppe der Inhibitoren sowohl mit der Bindestärke als auch mit der Bindedauer. Mithilfe von Röntgenstrukturanalyse haben wir herausgefunden, dass eine hydrophobe Interaktion

4 Zusammenfassung (long)

der langsamen Inhibitoren mit dem im FAK DFG-Loop befindlichen Leuzin 567 den DFG-Loop offenbar in eine helikale Struktur stabilisiert. Sowohl den helikalen DFG-Loop als auch langsame Bindekinetik der Inhibitoren haben wir im stark verwandten PYK2 Protein nicht beobachtet. Die Dissoziationsgeschwindigkeitskonstanten, die wir sowohl *in vitro* als auch in Zellen bestimmten haben, zeigten hier eine starke Korrelation. Mithilfe einer Mutagenesestudie haben wir die hydrophobe Interaktion der langsamen Inhibitoren mit dem im FAK DFG-Loop befindlichen L567 bestätigt, da bei einer Mutation von Leuzin 567 zu Alanin keiner der langsamen Inhibitoren eine lange Verweildauer zeigte. Mutagenesestudien an PYK2 haben in keinem Fall zu einem langsameren Inhibitor geführt, der vorher schnell war. Die Gesamtmobilität von PYK2 scheint hier geringer zu sein als bei FAK. Die beobachtete als Affinitätsdifferenz benannte Anomalie von PF562271 an FAK über PYK2 war nach unseren Untersuchungen daher eher der Bindekinetik und besonders der Dissoziationsgeschwindigkeitskonstante oder der Verweildauer des Inhibitors zuzuordnen, was die Regulation der Bindekinetik für das Erreichen von kinetischer Selektivität verdeutlicht. Die Verbindung der strukturellen Mobilität des Proteins mit dem nun Inhibitor-induzierten strukturellen Effekt im Zielmolekül FAK wurde als Schlüsselregulator der Selektivität identifiziert.

Beide Projekte zeigen, dass der Parameter Dissoziationsgeschwindigkeitskonstante oder die Verweildauer des Inhibitors zum Verständnis verschiedener späterer Probleme implementiert werden sollte. Die Fachmeinung, die sich immer mehr bestätigt, ist, dass die spätere Wirksamkeit des Medikaments mit der Bindekinetik korreliert werden kann und die Bindekinetik entsprechend zusätzlich zur Bindestärke analysiert werden sollte, um geeignete Medikamentenkandidaten zu finden.

Im ersten Projekt zeigten wir, dass auch eine schwache zelluläre Bindestärke von Erlotinib zu langsamer Bindekinetik an STK10 führen kann und sich diese dann in einem phänotypisch auftretenden Hautausschlag manifestiert. Im zweiten Projekt zeigten wir, dass medizinalchemische Prozesse genutzt werden sollten, um die molekulare Basis der Inhibitorinteraktion in sogenannten Strukturkinetischen Beziehungen untersucht werden sollten, um die Dissoziationsgeschwindigkeit je nach Bedarf medizinalchemisch anpassen zu können. Wir zeigten hier, dass eine bestimmte hydrophobe Interaktion der Grund für eine Besondere Konformation des DFG-Loops war, welche den Inhibitor in der

4 Zusammenfassung (long)

Bindetasche hält. Dies war auch die molekulare Basis für die beobachtete Selektivität des Inhibitors für FAK im Gegensatz zu PYK2. Die Strukturkinetik Beziehungen verschiedener Proteinkinasen zu verstehen, wird Medizinalchemikern helfen, kinetisch optimierte Inhibitoren zu entwickeln, die dann im Medikamentenfindungsprozess weiter optimiert werden.

Beide Projekte zeigten, dass die Dissoziationsgeschwindigkeit als Optimierungsparameter genutzt werden sollte, um sowohl die Inhibitoreffektivität als auch -selektivität zu steuern und zu verbessern. Es wurde jedoch auch klar, dass die *in vitro* bestimmte Bindestärke oder auch Bindekinetik deutlich abweichen kann für verschiedene Proteinkinasen. Im Falle von FAK/PYK2 hat die *in vitro* Affinität und Verweildauer sehr gut mit den *in cellulo* bestimmten Parametern korreliert. Bei STK10 haben zelluläre Faktoren, zumindest die Präsenz des natürlichen Substrates ATP in zellulären (hohen) Konzentrationen dazu geführt, dass die Bindestärke deutlich schlechter war als *in vitro* und die Bindekinetik deutlich langsamer war als von *in vitro* Daten abstrahiert.

Es wird demnach klar, dass jede Proteinkinase und weitergehend jeder Zielmolekül neu im zellulären Umfeld erforscht werden muss, um Medizinalchemikern die gewünschten Werkzeuge an die Hand zu geben, um zielgerichtet je nach Projekt die zelluläre Affinität und Verweildauer zu erreichen.

4 Zusammenfassung (long)

5 ZUSAMMENFASSUNG

Die im Menschen vorkommenden Proteinkinasen steuern zelluläre Signalwege und wurden als Auslöser verschiedener Krankheiten wie Krebs, entzündliche Prozesse oder metabolische Deregulation identifiziert. Wegen dieser zentralen Rolle in der Entwicklung oder der Verschlimmerung von Krankheiten sind Proteinkinasen interessante Zielmoleküle für Medikamente. Bisher wurden 52 Medikamente von der „Food and Drug Administration“ (FDA), der amerikanischen Medikamentenzulassungsbehörde, zugelassen.

Im Medikamentenfindungsprozess ist die Affinität der zu findenden Inhibitoren der meist eingesetzte Parameter, um die spätere Wirksamkeit im Menschen abzuschätzen. Die Wirksamkeit des Medikaments im Menschen wurde vor einiger Zeit jedoch mit der Bindekinetik des Inhibitors verknüpft, was bisher noch wenig Anwendung in der pharmazeutischen Forschung findet. Um einen deregulierten Signalweg effektiv zu inhibieren, muss die Zielkinase jedoch dauerhaft inhibiert werden. Entsprechend geht man davon aus, dass ein effektiver Inhibitor eine schnelle Assoziationsgeschwindigkeitskonstante und eine langsame Dissoziationsgeschwindigkeitskonstante haben sollte. Neben der Optimierung der Affinität von Proteinkinaseinhibitoren gewinnt daher die Optimierung der Bindekinetik eines Inhibitors zunehmend an Bedeutung, da ein Inhibitor nur wirken kann, wenn er auch gebunden ist, wie Paul Ehrlich einmal sagte. Er gibt immer mehr Beweise dafür, dass es eine Korrelation zwischen einer langsamen Dissoziationsgeschwindigkeitskonstante und einer größeren Effektivität im Menschen gibt. Weiterhin gibt es zunehmend Beweise dafür, dass die Selektivität eines Kinaseinhibitors über die Kinetik und nicht wie bisher über die Affinität reguliert werden kann. Dies gilt besonders im zellulären Kontext, weshalb wir zwei Projekte zur Untersuchung der Bindekinetik für zwei Proteinkinasen initiiert haben.

Das erste dieser Projekte untersucht die Serin/Threonin Kinase STK10 und die stark verwandte Proteinkinase SLK, die beide der sogenannten STE20 Familie zugerechnet werden. STK10 und SLK sind als hochfrequente sogenannte Anti-Zielmoleküle der bestehenden in der klinischen Forschung bisher eingesetzten Proteinkinaseinhibitoren bekannt und stehen im Verdacht Nebenwirkungen auszulösen. Im Speziellen wurde eine Inhibition von STK10 und SLK mit einem sehr starken

5 Zusammenfassung

Hautausschlag assoziiert, wegen welchem die Behandlung durch den EGFR-Inhibitor Erlotinib zum Teil abgesetzt wird. Erlotinib bindet die Kinasen STK10 und SLK stark, während ein weiterer EGFR-Inhibitor, Gefitinib, diese Kinasen nicht bindet und Patienten als Nebenwirkungen auch keinen starken Hautausschlag bekommen. Das passt auch zu dem, was über STK10 und SLK bekannt ist, nämlich, dass beide Kinasen Lymphozytenmigration und die Proteinkinase PLK1 regulieren. Es ist jedoch nicht bekannt, warum diese beiden Proteine so hochfrequent an die klinischen Proteinkinaseinhibitoren binden. Mithilfe struktureller Analysemethoden haben wir die Flexibilität von STK10 als möglichen Grund für diese hohe Trefferrate identifiziert. Die sehr starke Bindeaffinität, die wir für STK10 bestimmt haben, hat sich im zellulären Umfeld jedoch nicht bestätigt. Die Flexibilität von STK10 ermöglicht jedoch eine Vielzahl von strukturellen Veränderungen, weshalb wir die Bindekinetik untersuchten. Die strukturelle Flexibilität wurde dann als mögliche Ursache für besonders langsame Dissoziationsgeschwindigkeitskonstanten verschiedener klinischer Kinaseinhibitoren bestimmt. Es wurden große Veränderungen im hinteren, sehr hydrophoben Bereich Bindetasche beobachtet. Im Speziellen haben wir Veränderungen an der sogenannten αC von bis zu 8 Å beobachtet, gesehen, dass der P-Loop den Inhibitor wie ein Deckel umschließen kann und starke π - π -Wechselwirkungen mit dem Inhibitor ausbilden kann. Hierbei wurde im zellulären eine deutlich langsamere Dissoziation des Inhibitors Erlotinib beobachtet, als für den Inhibitor Gefitinib, was darauf hindeutet, dass die Bindekinetik bei schwächer wirkenden Affinitäten untersucht werden sollte, um mögliche Nebenwirkungen durch unerwünschte lange Inhibition aufzudecken. Dies sollte in zukünftigen Medikamentenfindungsprozessen implementiert werden.

Im zweiten Projekt, welches die potentielle kinetische Selektivität der Focal adhesion kinase (FAK) und der verwandten proline-rich tyrosine kinase 2 (PYK2) für den Inhibitor PF-562,271 untersucht, haben wir mithilfe einer chemischen Serie strukturell ähnlicher Inhibitoren den Bindeprozess beleuchtet. Die Dissoziationsgeschwindigkeitskonstanten, die wir sowohl *in vitro* als auch in Zellen bestimmten, haben hier eine starke Korrelation gezeigt. Mithilfe von Röntgenstrukturanalysen und einer Mutagenesestudie haben wir eine spezifische hydrophobe Interaktion der langsamen Inhibitoren mit dem im FAK DFG-Loop befindlichen Leuzin Nr. 567 beobachtet, welche den DFG-Loop in eine helikale Struktur stabilisierte. Dies wurde im PYK2 Protein nicht beobachtet. Diese als Affinitätsdifferenz

5 Zusammenfassung

benannte Anomalie war nach unseren Untersuchungen eher der Bindekinetik des Inhibitors zuzuordnen, was die Regulation der Bindekinetik für das Erreichen von Selektivität verdeutlicht. Die Verbindung der strukturellen Mobilität des Proteins mit dem nun Inhibitor-induzierten strukturellen Effekt im Zielmolekül FAK wurde als Schlüsselregulator der Selektivität identifiziert.

Beide Projekte zeigen, dass der Parameter Dissoziationsgeschwindigkeitskonstante zum Verständnis verschiedener späterer Probleme implementiert werden sollte. Die Fachmeinung bleibt bestehen, dass die spätere Wirksamkeit des Medikaments mit der Bindekinetik korreliert werden kann und die Bindekinetik entsprechend zusätzlich zur Bindestärke analysiert werden sollte, um geeignete Medikamentenkandidaten zu finden. Im ersten Projekt zeigten wir, dass auch eine schwache zelluläre Bindestärke von Erlotinib zu langsamer Bindekinetik an STK10 führen kann und sich diese dann in einem phänotypisch auftretenden Hautausschlag manifestiert. Im zweiten Projekt zeigten wir, dass medizinalchemische Prozesse genutzt werden sollten, um die molekulare Basis der Inhibitorinteraktion in sogenannten Strukturkinetischen Beziehungen untersucht werden sollten, um die Dissoziationsgeschwindigkeit je nach Bedarf medizinalchemisch anpassen zu können. Wir zeigten hier, dass eine bestimmte hydrophobe Interaktion der Grund für eine Besondere Konformation des DFG-Loops war, welche den Inhibitor in der Bindetasche hält. Dies war auch die molekulare Basis für die beobachtete Selektivität des Inhibitors für FAK im Gegensatz zu PYK2. Die Strukturkinetik Beziehungen verschiedener Proteinkinasen zu verstehen, wird Medizinalchemikern helfen, kinetisch optimierte Inhibitoren zu entwickeln, die dann im Medikamentenfindungsprozess weiter optimiert werden. Beide Projekte zeigten, dass die Dissoziationsgeschwindigkeit als Optimierungsparameter genutzt werden sollte um sowohl die Inhibitoreffektivität als auch -selektivität zu steuern und zu verbessern.

5 Zusammenfassung

6 INTRODUCTION

6.1 CANCER IS OFTEN CAUSED BY DEREGULATED PROTEIN KINASES

Cancer is the second leading cause of death in the United States¹¹. This year, the American Cancer Society projects 1.8 million new cancer cases and over 600,000 cancer death in the US. While the leading cancer types are lung, colorectal, breast and prostate cancer, lung cancer alone caused more death than the other cancer types combined. The most common new cancer cases are prostate cancer in male and breast cancer in female. Happily, the overall cancer death rate has decreased by 29% over the past decades (2008-2017), often due to improved treatment.

To describe the complex biology of cancerous cells in comparison to healthy cells, 10 hallmarks have been proposed by Hannahan and Weinberg¹² and refined to 7 more organized hallmarks¹³. Cancer cells show selective growth and proliferative advantage, altered stress response favouring overall survival, vascularization, invasion and metastasis, metabolic rewiring, an abetting microenvironment, and immune modulation. Hallmarks can be developed upon genome mutations that dysregulate control mechanisms in various biochemical signalling pathways and alter gene expression. The most commonly dysregulated family of proteins in the signalling circuits of the cell is protein kinases.

Protein kinases fulfil various functions as regulators in cell signalling pathways and therefore have emerged as therapeutic targets for many human diseases including cancer, metabolic diseases and neurologic disorders¹⁴.

6.2 PROTEIN KINASES SHARE A CONSERVED ARCHITECTURE

Kinases are a family of enzymes that transfer a γ -phosphate of an adenosine triphosphate (ATP) molecule to a hydroxyl-group of their substrates. Protein kinases phosphorylate three potential amino acids as substrates and are grouped into serine/threonine and tyrosine kinases according to their substrate preference. Protein kinases share a highly conserved tertiary structure and catalytic mechanism and were therefore clustered based on their sequence identity by Manning *et al*¹⁵ and subsequently organized into a phylogenetic tree¹⁶ (**Fig. 1A**). The 518 human kinase genes are depicted as endpoints of the phylogenetic tree that is based on a sequence comparison of the catalytic domains, and additional factors such as sequence similarity

6 Introduction

and overall protein domain structure. The protein kinases were subclustered into 7 subfamilies: The AGC family comprises PKA, PKC and PKG kinases, the CAMK family includes calcium/calmodulin-dependent protein kinases, the CK1 family consists of casein kinase 1 homologs, the CMGC family includes subfamilies CDK, MAPK, GSK3 and CLK, the STE family includes homologues of yeast sterile 7, sterile 11 and sterile 20 kinases and the remaining two groups are called tyrosine kinases (TK) and tyrosine kinase-like (TKL)¹⁶.

Kinases are located in various parts of the cell. Receptor tyrosine kinases are transmembrane proteins localized in the plasma membrane of the cell and transduce external signals. Other kinases have very different subcellular locations, e.g. the nucleus or cytoplasm¹⁷. Kinases currently targeted in cancer are for example kinases involved in several hallmarks like proliferation, e.g. MEK1 and MEK2 in the MAPK pathway, mTOR in the PI3K-Akt signalling pathway or RSK in the FGFR dependant proliferation¹⁸. Kinases involved in cell cycle regulation and mitosis are CDKs, Aurora kinases or PLKs and are therefore oncology targets.

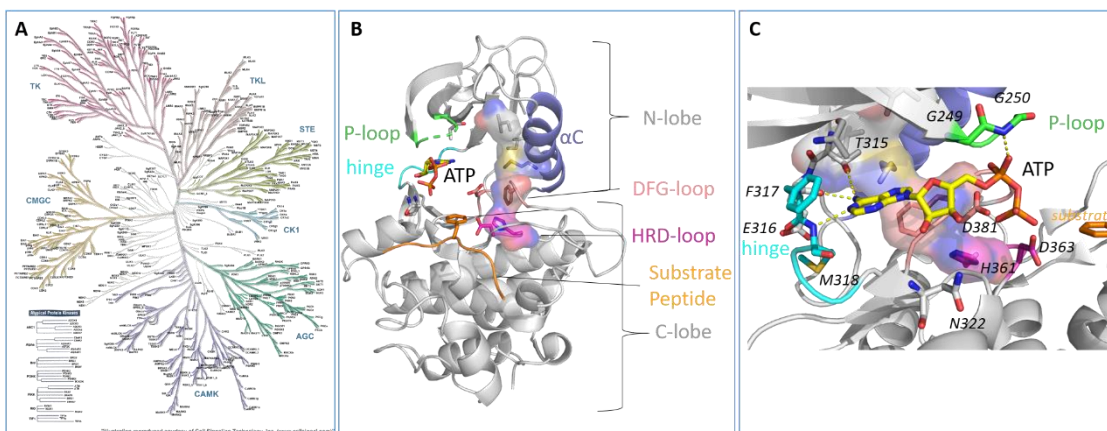


Fig. 1: Protein kinases share a conserved architecture. (A) Manning *et al*¹⁵ identified 518 protein kinases in the human genome and organized these by sequence similarity into the kinase phylogenetic tree¹⁶. (B) The protein kinases domain is highly conserved and consists of two lobes (N-lobe, C-lobe) that are connected via the hinge region and contain the P-loop, DFG-loop and HRD-loop for substrate recognition and their catalytic function. The regulatory spine consists of hydrophobic residues of the kinase and stabilizes the kinase conformation to be active if the spine is intact or inactive if the spine is broken. PDB 2g2i was used for figure creation. (C) The substrate ATP is highly complexed via G249/G250 in the P-loop (ATP-phosphates), polar hinge interactions with E316/F317/M318 (adenosine ring) and a magnesium-mediated bond with D381. PDB 2g2i was used for figure creation. ATP = adenosine triphosphate.

Nearly all kinases share conserved arrangements of secondary structure in 12 subdomains that are forming into a bi-lobed catalytic core structure with the ATP binding in a deep cleft located between these lobes¹⁸ (**Fig. 1B**). While the N-terminal lobe consists primarily of beta sheets and at least one alpha helix called the α C, the C-terminal lobe consists primarily of alpha helices. The N- and C-terminal lobes are

6 Introduction

connected by the hinge region that is involved in ATP binding via polar backbone hydrogen bonds with the adenosine ring of ATP. The ribose moiety of ATP often is connected to a nearby located polar amino acid, e.g. N322 in ABL1 (**Fig. 1C**). The so-called P-loop, G-loop or glycine rich loop contains a glycine rich motif GxGxxG that forms hydrogen bonds with the phosphate residues of ATP. The activation loop, as well called DFG-loop, contains a conserved DFG and APE motif and is involved in regulating kinase activity. This activation loop can assume many conformations and is often a determinant of an active or inactive state of the protein kinase dependant on whether it is in an inward position (DFG-in) or faced outside of the ATP pocket (DFG-out). The aspartate residue within the DFG-motif is responsible for chelating a magnesium ion that positions the ATP phosphates for phototransfer. If the chelating aspartate residue faces outwards, the reaction will not take place. Most kinases (except the with no lysine kinases (WNK)) share a conserved lysine in the active site β -sheet that is involved in both the binding of the co-substrate ATP and interacting with a glutamic acid residue located in helix α C when the kinase is in an active conformation¹⁹. The aspartate located in the catalytical loop or HRD-loop is critical for the phosphor transfer.

In the overall structure, a kinase catalytical domain contains a hydrophobic regulatory spine that holds the kinase structure in place (**Fig. 1B**). In a DFG-out conformation the hydrophobic phenylalanine points towards the ATP active site, thereby disrupting the hydrophobic interactions necessary for the regulatory spine. Likewise, there is a catalytical spine that is complemented by the adenosine residue of ATP. Only if all motifs of this architecture are located in the exact right position and angle, the protein kinase will be active to phosphorylate a substrate residue.

6.3 SMALL MOLECULE INHIBITORS OF PROTEIN KINASES AS POTENTIAL CANCER TREATMENT

The deep-binding pocket of protein kinases for the co-substrate ATP makes them targetable with small molecule inhibitors. The use of small molecule BCR-ABL tyrosine kinase inhibitors like e.g. imatinib increased the 5-year related survival for patients with chronic myeloid leukemia from 22% in 1970 to 70% for patients diagnosed 2009-2015¹¹. Despite this significant progress, only a small group of kinases has been the focus of research suggesting that more disease mechanisms will be targeted by kinase inhibitors in the future^{18,20}. Currently, there are 52 protein kinase inhibitors approved²¹.

6 Introduction

6.3.1 Types of protein kinase inhibitors

Four different classes of kinase inhibitors have been defined based on their binding mode for the targeted kinase^{18,22}.

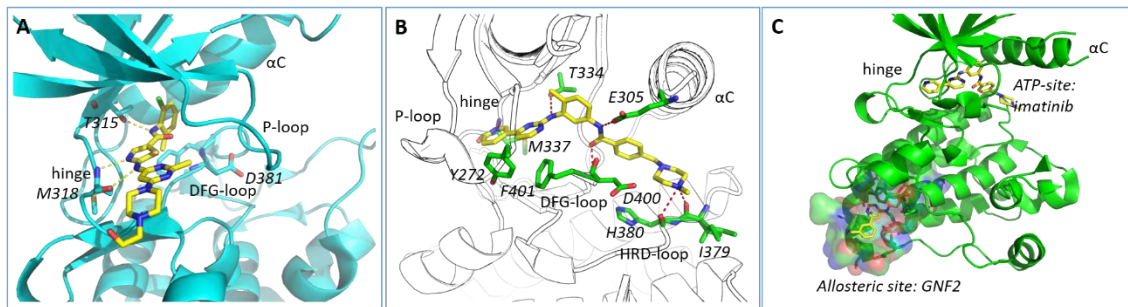


Fig. 2: Protein Kinase inhibitor Types. (A) Type I inhibitors such as dasatinib on ABL1 (PDB 2gqg) bind the active site of the active kinase conformation (intact regulatory spine) and share polar hinge interactions similar to the binding mode of the natural substrate ATP. (B) Type II inhibitors such as imatinib on ABL1 (PDB 3k5v) bind the active site of the inactive kinase conformation expanding into the hydrophobic backpocket thereby forcing a DFG-out conformation and disrupting the regulatory spine. Type III inhibitors bind the backpocket of the active site of the inactive kinase conformation occupying the hydrophobic backpocket thereby disrupting the regulatory spine (not shown). (C) Type IV inhibitors such as GNF2 on ABL1 (PDB 3k5v) bind to an allosteric binding site on the protein surface.

Type I inhibitors are ATP-competitive inhibitors binding to the hinge within the ATP-pocket when the kinase is in an active state conformation defined by an active “in” conformation of the DFG motif and an intact hydrophobic regulatory spine²³. Type II inhibitors are ATP competitive and bind to the hinge and additionally are extending into the adjacent pocket made available by a conformational change of the DFG-motif in the activation loop (DFG-out). This conformational change keeps the kinase in an inactive state and breaks the regulatory spine of the domain. Type III inhibitors are non-competitive allosteric inhibitors and bind only to the adjacent hydrophobic pocket opening because of a DFG-out conformation. Type IV inhibitors are non-competitive allosteric inhibitors that are binding to a site remote from the ATP binding site. This kind of inhibitor is most frequently of high selectivity as it exploits a unique site in the particular kinase, however, has a risk of being identified as a binder but does not alter kinase activity. Lastly, the binding mode of inhibitors can be reversible or irreversible. Covalent inhibitors are forming an irreversible bond to the kinase active site typically by reacting with a nucleophilic cysteine residue. Recently, reversible covalent kinase inhibitors²⁴ have been described closing the kinase inhibitor space.

6.4 INHIBITOR BINDING PARAMETERS AND INHIBITOR SELECTIVITY

Because protein kinases are a large superfamily of enzymes that share highly similar active sites, achieving selectivity for disease associated targets remains a major challenge in this field and insufficient target selectivity has limited the applications of

6 Introduction

kinase inhibitors mainly to the oncology area where broader kinome wide non-selectivity of inhibitors is often tolerated during short treatment circles and sometimes even is desired. The development of large selectivity screening panels that are now widely available transformed our knowledge of kinase inhibitor selectivity²⁵. However, even with these data in hand, the cellular targets of kinase inhibitors remain largely enigmatic due to the complexity of factors that can influence inhibitor efficacy in cells. Some of these mechanisms have been elucidated: Kinases are highly dynamic enzymes that are rapidly activated by phosphorylation, interaction with domains flanking the kinase catalytic domain and by a diversity of regulatory proteins. These interactions and modifications have a profound effect on the structure and dynamic features of the catalytic domain and therefore the binding and efficacy of inhibitors in cells. In addition, kinases differ significantly in their affinity for the co-factor ATP. Within a family of 518 protein kinases and over 2000 other nucleotide-dependant enzymes like polymerases, chaperones, motor proteins, reductases and methyltransferases¹⁸ it remains challenging optimizing a particular inhibitor to be selective in order to avoid off-target toxicity due to kinome cross-reactivity. In order to achieve the desired selectivity profile, different parameters can be optimized. To find a potential starting molecule for developing a lead compound most drug discovery processes are starting with large screening-campaigns of drug-like molecule libraries. More recently rational drug design is used in order to make the drug discovery process more efficient. Some of the optimization parameters used in the drug optimization are described in the following section.

6.4.1 Determination of equilibrium target affinity to optimize potency and selectivity of a drug

Target affinity is often assessed in cell-free *in vitro* assays that measure compound binding to a target (binding assays) or compound effect on the biochemical activity (enzyme activity assays)²⁶. The binding strength of a compound binding to a protein target is quantified by the half-maximal inhibitory concentration (IC_{50} ²⁷), or for binding assays the equilibrium dissociation constant (K_D) of the drug (L)-target (R) binary complex (RL) or the equilibrium inhibitory constant (K_i) of the receptor-inhibitor complex can be obtained²⁸ from the IC_{50} . The affinity of a drug for a target in equilibrium is given by the thermodynamic equation for the free binding energy of the drug to the target ($\Delta G_{binding}$) that is dependent on the free gas constant (R) and the temperature (T) (**Equ.**

1) and this free binding energy can be referred to the equilibrium dissociation constant (K_D), defined by the law of mass action.

$$\Delta G_{binding} = -RT \ln(K_A) = RT \ln(K_D) = RT \ln\left(\frac{[R] * [L]}{[RL]}\right) \quad \text{Equ. 1}$$

According to the law of mass action in equilibrium (**Equ. 1**) the affinity and more explicitly the free energy are higher, the lower the K_D . The K_D additionally is defined as the concentration of a binding partner for which half of the receptors are bound.

Systematic quantitative selectivity studies have been done on kinases, showing that e.g. the very promiscuous ATP-competitive type I compound staurosporine binds various kinases from various kinase families with high affinity, whereas potential drugs more often only inhibit specific kinases with high affinity²⁹⁻³². The potency of an inhibitor is a way of optimizing drug selectivity.

6.4.2 Determination of binding kinetics for optimization of selectivity *in vivo*

The question why the binding kinetics of a drug-target-interaction might be an important parameter for optimization of selectivity is given in the section **6.4.3**. First, the underlying concept of kinetic drug-target-interaction will be explained here.

There are two different models in current usage when describing the interaction between a target (R) and its compound (L) to form a drug-target-complex (RL) kinetically (**Fig. 3**). The simple model (**Fig. 3A**) mostly known as the lock-and-key-model just considers a simple one-step association and dissociation of both receptor and ligand where the rate of RL formation is described with the association rate constant (k_a) and dissociation rate constant (k_d). In this model, the association rate constant equals the on-rate of the ligand (k_{on}) and the dissociation rate constant equals the off-rate of the ligand (k_{off}).

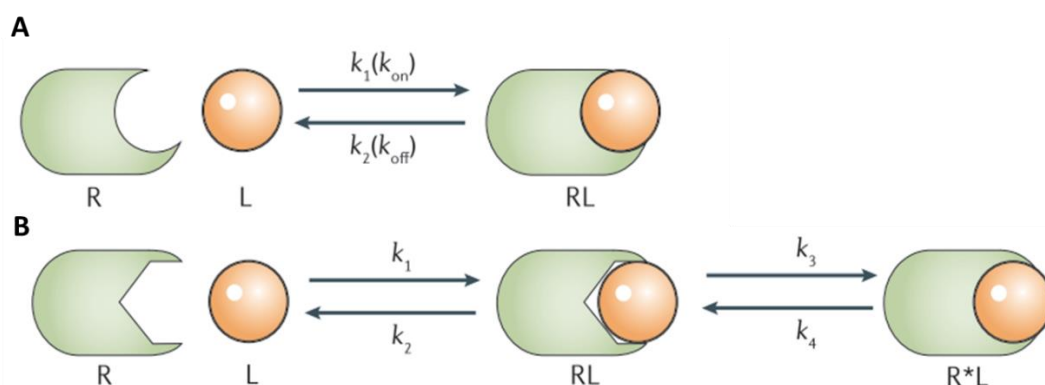


Fig. 3: Schematic mechanism of a drug-target interaction. Lock-and-key model (**A**) and Induced-fit-model (**B**). R = receptor, L= ligand, RL = (initial) receptor-ligand complex, k_x = rate constant; R^*L = energetically favored receptor-ligand-complex. Picture was taken and slightly derived from Copeland .

However, the commonly used lock-and-key-model for assessing the drug-target residence time, where the residence time is simply characterized as the ratio of the off-rate of the decay of a drug-target complex and its on-rate upon complex formation is not enough and has been replaced by the more sophisticated induced-fit-model (**Fig. 3B**). Here, the drug and target form an initial complex determined by an on- and off-rate and then the complex undergoes an internal isomerization forming an energetically favored induced drug-target-complex, which kinetically ‘traps’ the inhibitor in the target resulting in a high-affinity binary complex between receptor and ligand (RL^*). The determination of the off-rate is than not only dependant of the initial RL decay but also on the high-affinity complex formation and decay.

6.4.3 Pharmacokinetics and the efficacy of a drug *in vivo*

Recently it has been shown that the *in vivo* efficacy of a potential drug is more often related to the binding kinetics of a compound rather than to its affinity alone where the same (high) affinity can be obtained via different ratios of on- and off-rate^{26,34-39} (**Equ. 2**) referring to the statement of Paul Ehrlich around the turn of the 20th century “*corpora non agunt nisi fixate*”⁴⁰ („a substance will not work unless it is bound“).

$$K_D = \frac{k_{\text{off}}}{k_{\text{on}}} \quad \text{Equ. 2}$$

In an open system, the efficacy of a drug is rather determined by the k_{on} and k_{off} of the drug-target complex²⁶. This off-rate can be translated to both a residence time (RT, τ) of the drug for the target and a dissociative half-life which makes the off-rate an important optimization factor *in vitro* for later *in vivo* efficacy (**Equ. 3**⁴¹).

6 Introduction

$$RT = \tau = \frac{1}{k_{\text{off}}} = \frac{t_2^1}{\ln(0.5)} \quad \text{Equ. 3}$$

In the human body (*in vivo*) the concentration of drug that is given differs in different compartments and tissues which ultimately means the drug concentration is no longer constant but varies with time after dosing. Hence, in this system considered 'open' the drug concentration varies and is influenced by factors different than the molecular interactions with the target²⁶ identified in the 'closed' system (*in vitro*). In an open system pharmacokinetics have to be considered for the evaluation of the drug.

It has been shown that many clinical and especially approved drugs show a prolonged residence time for their targets⁴²⁻⁴⁴. Different optimization opportunities for long residence time drugs will be briefly summarized here.

6.4.3.1 Kinetic selectivity of a drug *in vivo*

Because *in vivo* the duration of drug action is related to the rate of drug dissociation, the residence time of a drug for the target is a potential optimization parameter that can improve the selectivity of the drug by kinetic binding properties⁴⁵. If the target is inhibited much longer than a hypothetical equipotent off-target, pharmacokinetically the target effect will outlast the off-target effect. This is considered kinetic selectivity. In the open setup, the drug concentration would peak after oral dosing. The equipotent off-target with fast on-, fast off-kinetics would be inhibited much faster than the target as oral bioavailability was linked to the on-rate of a compound. However, the slow off- slow on-rate target would be inhibited more slowly but outlasts the wash-out effect of the steady blood flow. The fast off off-target will not be inhibited longer. The on-rate is ultimately limited by the velocity of diffusion that is estimated to be $10^8 \frac{1}{Ms}$ ²⁶. A nice example for kinetic selectivity has been shown for a drug named Tiotropium that is binding the three muscarinic receptors M1, M2 and M3 with similar affinity, but completely different binding kinetics⁴⁶. This behaviour causes a kinetic selectivity for its original target M3, being inhibited for 35 hours whereas the off targets are only inhibited for much shorter periods of time.

When the residence time of the biological complex is long, a significant level of receptor occupancy can be sustained even when the systemic levels of ligand diminished significantly⁴⁷. Kinetic selectivity has an effect on the therapeutic window if a drug

6 Introduction

displays a long residence time at its primary target and short residence time on off-targets over the course of dosing⁴³.

6.4.3.2 *The link between the dosage of a drug and residence time in vivo*

The dosing of a compound is affected by drug residence time. If a target is inhibited longer *in vivo* because of longer receptor occupancy by the drug, the dosing interval can be regulated and optimized²⁶. Using the same example of muscarinic receptor M3, different inhibitors showed different binding kinetics, but similar affinity⁴⁸. The slow-off-rate compound Tiotropium was able to inhibit its target for 35 hours in comparison to the competitor drugs Clinidium (30 minutes), Ipratropium (10 minutes) and Atropium (2 minutes). With an occupancy of over 24h, a daily dosing interval can be considered which increases patient comfort. Other examples for beneficial long residence times are angiotensin II type 1 antagonism used for lowering of blood pressure in the long residence time inhibitor candesartan versus the slow residence time inhibitor losartan^{49,50}. Highest residence times would be reached with irreversible, covalent inhibitors like Aspirin, which inhibits the COX2-receptor via a covalent cysteine bondage⁵¹. Irreversible inhibition always bears the risk of drug safety problems as described in the next section.

6.4.3.3 *Contraindications when optimizing for a long residence time*

The optimization of residence time is target dependant. For some targets a prolonged duration of action leads to a complete inhibition and hence to a more efficient, comfortable or selective drug. Some targets, however, are linked to serious side-effects when inhibited for long duration. Here, the residence time should be optimized to only shortly inhibit the target⁵². A potent compound would here have a very high on-rate if the residence time should be short. A fast on-rate is related to a good bioavailability whereas the slow on-rate of a slow off-rate compound gives poor bioavailability. Having a long residence time, drugs can accumulate, and local drug concentration might outreach the therapeutical window, which is the window between action of the drug, and drug toxicity. Examples for residence time dependant toxicity³⁶ are the dopamine receptor antagonists used as antipsychotics which caused immediate adverse effects through mechanism based toxicity, N-methyl-D-aspartate receptor antagonists used for Alzheimer's disease or cyclooxygenase inhibition where aspirin with its long (irreversible) binding profile increases the risk of bleeding events.

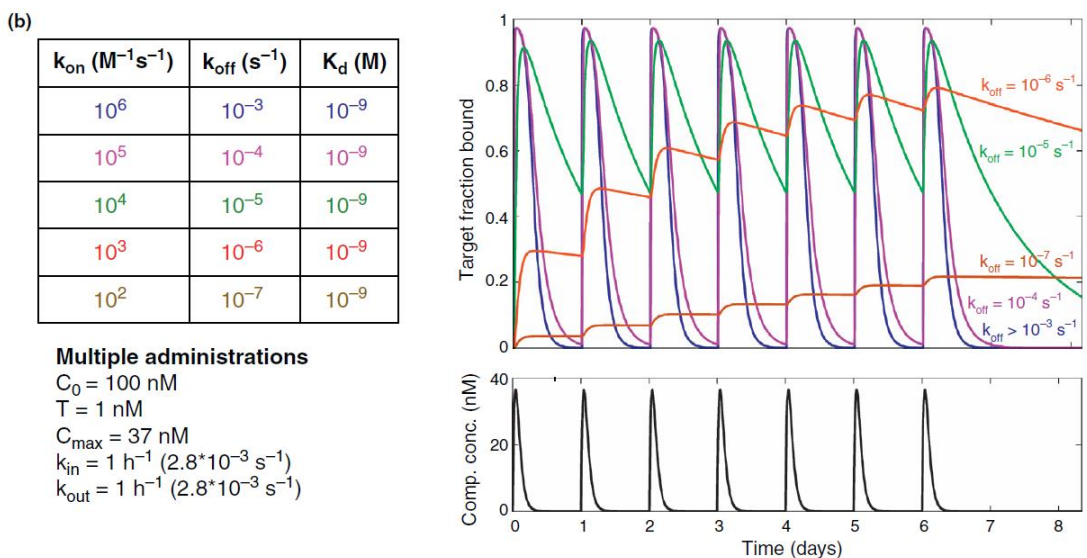
6.4.3.4 *Limitations of the drug-target-residence-time-concept*

Although an optimization of the residence time is advantageous, there are some limitations of the concept.

The drug-target residence time is linked to the pharmacokinetic half-life of target degradation or new target synthesis³³. Optimization of the residence time only has an impact on pharmacodynamics when the residence time is longer than the pharmacokinetic terminal half-life. When the pharmacological effect of the drug outlasts the lifetime of pharmacological concentrations of drug in systemic circulation. If drug target residence time is less or similar to the pharmacokinetic half-life no extended effect will be realized because the target engagement would be equally well driven by simple mass-balance effects. This was nicely depicted by a simulation of Dahl *et al*⁵³ (**Fig. 4**).

Receptor degradation has an effect on binding kinetics⁵⁴. The value in optimizing the residence time for a target is *in vivo* limited to the lifetime of the biological target protein in cells where physiological inhibition is achieved when the residence time of the drug-target complex equals or exceeds the half-life of protein biosynthesis within the cell population that is targeted⁴⁵. If new target protein is rapidly synthesised by the cell, such that the concentration of new protein exceeds the intracellular drug concentration, the newly synthesized protein will perform its biochemical function unrelated to the presence of drug inhibiting pre-existing proteins³³. This happens e.g. in rapidly proliferating organisms.

6 Introduction



Drug Discovery Today

Fig. 4: Pharmacological simulation of a theoretical equipotent drug with different binding kinetics from Dahl *et al*⁵³: Drugs with an off-rate in the range up to $10^{-4} \text{ (s}^{-1}\text{)}$ do not outlast the pharmacokinetic effect. A residence time beyond this will have a pharmacological effect even after complete wash-out of the dosed drug.

In summary the optimization of residence time is target dependent. Fast kinetics lead to short, ultimate physiological inhibition having good bioavailability whereas slow kinetics lead to shortened dosing intervals and longer duration of action, which can cause problems with bioavailability, mechanism-based-toxicity or drug accumulation^{12,14,1833}.

6.5 STRUCTURE KINETIC RELATIONSHIPS

In lead optimization, medicinal chemists typically use the described equilibrium binding parameters IC_{50} and K_{D} or K_{I} (6.4.1). In a structure activity relationship (SAR) medicinal chemists attribute incremental changes in affinity to the desired target to certain chemical functional groups using a systematic series of test compounds⁵⁵. Taking the kinetic binding parameters into account (6.4.2), in a structure kinetic relationship (SKR), medicinal chemists attribute incremental changes in binding kinetics to certain chemical functional groups, similar to a SAR. As affinity and residence time are thermodynamically linked (Equ. 2), the parameter chosen to describe a SKR should be independent of the one describing an SAR.

In the induced fit model of drug and target, the internal isomerization of the RL complex to the high affinity RL* complex typically leads to an occlusion of the binding pocket from bulk solvent, thereby strengthening hydrophobic-hydrophobic interactions

6 Introduction

and thereby the RL* state^{33,41}. In this case, often loops and other structural elements are ordered to form a lid for the drug binding pocket kinetically 'trapping' the inhibitor⁵⁶.

Mechanisms, that have been reported to cause the drug to be kinetically trapped and were shown to prolong the compounds binding kinetics include structural rearrangements upon compound binding, Ligand specific induced fit⁵⁷, conformational adaptation of the system⁵⁸, water rearrangements and changes in the water network^{59,60}, shielded h-bonds⁶¹, transient interactions with covalent or reversible character² or halogen-aromatic interactions⁶².

Especially the activation loop might be interesting when considering the induced-fit model for kinases. The DFG-out conformation was e.g. described for BIRB796 analogues as a mechanism for a slow on-rate⁶³ and hence high residence time given the potency of the compound. Also, the kinetic difference between type I and type II inhibitor is linked to DFG-in and -out states because of a significantly higher free-energy barrier⁶⁴. A DFG flip in FGFR1 was reported to influence binding kinetics⁶⁴. Type I PDA was enthalpically driven and fast and ponatinib (type II) entropically driven and slow.

A binding of drugs into the deep binding pocket requires a desolation of water molecules which decelerates the binding process^{55,65} which was termed 'displacement of energetically unhappy waters' that are displaced or stabilized by the compound. Contrary, the association rate of the compound might be enhanced by introducing polar moieties to the ligand⁶⁵. Here it is to consider that fast association kinetics can be linked to a rebinding of the drug that leads to a higher pharmacological action and target occupancy⁶⁶.

Structure kinetic relationships do yet not contain enough information to be generalized for future guidance of medicinal chemists beyond the target studied⁶⁷. However it has been shown that an introduction of methylene linkers on DOTL1⁶⁸, halogens on Haspin⁶² and CRF-1⁶⁹, bulky hydrophobic groups on IGF-1R⁷⁰ or methyl groups on p38 kinase⁶³ and HSP90⁶¹ did prolong target residence times. Generally, the hydrophobicity of sulfonamides on carbonic anhydrase⁷¹ additional to the examples mentioned before seem to prolong the target residence time by making the compound more 'sticky'.

6.6 INTRODUCTION TO PROJECT-RELEVANT EXAMPLES OF PROTEIN KINASES

In this thesis we identified potential cases of residence time relevant follow up projects.

6.6.1 STK10 appears to be a frequent off-target of protein kinase inhibitors

In this study we investigated serine/threonine kinase 10 (STK10) also known as lymphocyte-oriented kinase, LOK and STE20 like kinase (SLK). The two serine/threonine kinases are reported to be binding various kinase inhibitors in large scale screens^{25,72-76}. STK10 is a 112kDa protein⁷⁷ which is highly expressed in hematopoietic tissues⁷⁸ and in lymphoid organs and lymphocytes⁷⁹. The homogenous kinase SLK (143 kDa) is expressed ubiquitously. STK10 and SLK share a highly similar kinase domain (73% identical sequence) and contain characteristics for the family of STE20 kinases¹⁹. An activation segment exchange mechanism was shown on STK10 and SLK upon homodimerization and was facilitated by a dimerization of their coiled coil domains⁸⁰.

STK10 has been shown to downregulate the production of IL-2 in lymphocytes by negatively regulating the MEKK1 pathway, which activates cytokine transcription and leads to inflammatory responses^{79,81}. STK10 phosphorylates ERM (Ezrin/radixin/moesin) proteins^{82,83}. STK10 has been also shown to activate PLK1 *in vitro* in cooperation with its relative SLK leading to cell cycle progression^{78,84,85}. Therefore, STK10 may have some potential as an anti-cancer target.

Many epidermal growth factor receptor (EGFR) inhibitors show a severe skin rash as a side-effect^{86,87}. Unfortunately, this side-effect can be severe enough to necessitate dose-reduction or termination of treatment⁸⁸, and shows a range of severity between patients. For erlotinib or gefitinib – two EGFR inhibitors – the presence of the skin rash correlated with a more positive treatment outcome⁸⁹⁻⁹³, which indicated a dose-escalation until the onset of severe skin rash would yield better treatment outcomes for NSCLC⁹⁴.

If the skin rash is severe, cytokine release, inflammation, and a large infiltration of leukocytes, especially monocytes and lymphocytes was reported^{86,95}. It may be that the higher doses of EGFR inhibitors are related to off-targets and that these off-targets even contribute to the treatment outcome.

6 Introduction

Erlotinib was reported to induce a much worse skin rash than gefitinib⁹⁶⁻⁹⁸. The unwanted skin related side-effects were linked to an off-target inhibition of STK10 and SLK by erlotinib⁹⁹. While an up-regulated IL-2 secretion and cell migration in lymphocytes was observed for erlotinib, but not gefitinib, these effects did not occur after siRNA knockdown of STK10⁹⁹.

6.6.2 Selectivity of PF-562271 on FAK over PYK2

Focal adhesion kinase (FAK) and its relative Protein tyrosine Kinase 2 (PYK2) are non-receptor tyrosine kinases involved in cell migration, proliferation and survival¹⁰⁰. While PYK2 is expressed in brain, vascular smooth muscle, endothelium, spleen, kidney and hematopoietic cells, FAK is expressed ubiquitously¹⁰¹⁻¹⁰³. Both kinases share 46% sequence identity with similar overall architecture. They contain an N-terminal FERM domain followed by the central kinase domain that shares 61% sequence identity, followed by a proline rich region and the C-terminal focal adhesion targeting (FAT) domain¹⁰⁴. The activation pattern for FAK and PYK2 differ, where FAK is activated by integrins, growth factor receptors and cytokine receptors, PYK2 is activated by intracellular calcium mobilization¹⁰². Both are focal adhesion kinases that promote tumour proliferation and metastasis and are long known targets in the fight of several cancers¹⁰⁵⁻¹⁰⁷. Studies have shown that an inhibition of FAK results in an upregulation of PYK2 which lead to cancer drug resistance. To overcome this, several dual FAK/PYK2 inhibitors have been tested by Pfizer in the clinics¹⁰⁸: PF-431396¹⁰⁹, PF-562271¹¹⁰ and PF-8554878 (defactinib)¹¹¹, as well as selective FAK PF-573228¹¹² and selective PYK2 PF-719¹¹³ inhibitors. Crystal structures have been solved for PF-562271 for both FAK (3bz3) and PYK2 (5tob), showing an uncommon helical DFG-motif in FAK but not PYK2 (**Fig. 5**). This mechanism has been identified as the cause for the approximately 9-fold improved potency of PF-562271 for FAK ($IC_{50} = 1.5$ nM) over PYK2 ($IC_{50} = 13$ nM)¹¹⁰.

6 Introduction

7 OBJECTIVES

The aim of this thesis is to identify examples of a translation of molecular structures of proteins to a defined residence time or of cases where the target-residence-time should be considered in the drug optimization process. Therefore, this thesis aims to investigate two projects:

1. The aim of the first study was to understand the structural mechanisms resulting in the binding of a large diversity of clinical inhibitors to the STK10 off-target and if STK10/SLK are indeed inhibited in cellular systems. Additionally, we were interested whether it might be the residence time of STK10/SLK inhibitors causing the reported skin rash side effects of FDA approved kinase inhibitors erlotinib but not gefitinib with STK10/SLK off-target activity.
2. In the second study, we wanted to explore the kinetic properties of the PF-562271 series of FAK and PYK2 inhibitors to study if differences in residence times could be utilized for the development of kinetically selective or balanced dual FAK/PYK inhibitors. In order to understand the distinct kinetic profiles of FAK or PYK2 binding, we performed surface plasmon resonance assays, in-cell binding experiments and structural and site-directed mutagenesis studies to gain insights into the protein residues determining kinetic selectivity, and the dynamics of protein-ligand interactions.

7 Objectives

8 MATERIALS AND METHODS

8.1 MATERIALS

Table 1: List of devices used.

Description	Name	Company (Headquarter)
Centrifuges	Table centrifuge HERAEUS PICO 21 Centrifuge	Thermo Fischer Scientific Inc. (US-Waltham)
	Centrifuge 5810 R	Eppendorf (GE-Hamburg)
	Avanti JXN-26	Beckman Coulter (US - California)
	Plate centrifuge HERAEUS MEGAFUGE 16 Centrifuge	Thermo Fischer Scientific Inc. (US-Waltham)
Crystallization Imager and storage	Minstrel UV	Rigaku (J - Tokyo)
Gel power supply	PowerPac HC	Bio-Rad Laboratories, Inc. (US-Hercules)
Gelfiltration system	ÄKTA xpress	GE Healthcare Life Science (UK-Chalfont St Giles)
Incubators	Multriton Incubator Shaker	Infors HT AG (CH-Bottmingen)
	INCU-Line Digital Mini-Incubator	VWR International GmbH (GE-Darmstadt)
	Sanyo CO ₂ incubator	Sanyo (J – Osaka)
Cell culture hood	MaxiSafe2020	Thermo Fischer Scientific Inc. (US-Waltham)
Liquid handlers	ECHO and Access	Labcyte Inc. (US - Sunnyvale)
	ECHO 550	Labcyte Inc. (US - Sunnyvale)
	Multidrop Combi with Small tube plastic tip dispensing cassette, #835023437	Thermo Fischer Scientific Inc. (US-Waltham)
	Mosquito	TTP Labtech (UK - Melbourn)
Mass Spec	6530 Accurate-mass Q-TOF LC/MS with 1290 Infinity LC Injector HTC	Agilent Technologies (US-Santa Clara)
Measuring instrument	PHERASTAR FS, PHERASTAR FSX, CLARIOstar	BMG Labtech GmbH (GE-Offenburg)
	Stratagene Mx3005P	Agilent Technologies (US-Santa Clara)
Molecular Gel Imager	Gel Doc XR+ with Image Lab Software	Bio-Rad Laboratories, Inc. (US-Hercules)
PCR machine	Thermo-cycler	Biometra (GE-Göttingen)
pH Meter	3510 pH Meter	Jenway Bibby Scientific Ltd. (UK - Straffordshire)
Photometer	UV/visible Spectrophotometer Ultraspec 1100 pro	GE Healthcare Life Science (UK-Chalfont St Giles)
Pipettes	Eppendorf Research Plus 0.1-2.5	Eppendorf AG (GE-Hamburg)
	Eppendorf Research Plus 2-20	Eppendorf AG (GE-Hamburg)
	Eppendorf Research Plus 20-200	Eppendorf AG (GE-Hamburg)
	Eppendorf Research Plus 100-1000	Eppendorf AG (GE-Hamburg)
	Pipetus Pipettor	Hirschmann Laborgeräte GmbH & Co. KG (GE-Eberstadt)

8 Materials and Methods

	Thermo E1 Clip-Tip 200	Thermo Fischer Scientific Inc. (US-Waltham)
	Thermo E1 Clip-Tip 12.5	Thermo Fischer Scientific Inc. (US-Waltham)
Sonicator	Vibra cell	Sonics & Materials, Inc. (US-Newtown)
Heat Sealer	PlateLoc	Agilent Technologies (US-Santa Clara)
Shaker	MixMate	Eppendorf AG (GE-Hamburg)
SPR	Biacore T200	GE Healthcare (US-Illinois)

8 Materials and Methods

Table 2: List of materials used.

Description	Name	Company (Headquarter)
Äkta columns	ÄKTA column S75 16/60 or S200 16/60	GE Healthcare Life Science (UK-Chalfont St Giles)
Baffled glass for expression	Pyres Fernbach baffled culture flask	Sigma Aldrich Corp. (US-St. Louis)
Baffled plastic for preculture	250 ml Corning Erlenmeyer baffled cell culture flask	Sigma Aldrich Corp. (US-St. Louis)
Centrifuge bottle	Centrifuge bottle with Screw (1000 mL)	Beckman Coulter, Inc. (UK-Brea)
	Centrifuge bottle with Screw (40 mL)	Beckman Coulter, Inc. (UK-Brea)
Concentrator	Protein Concentrators 30 kDa	Thermo Fischer Scientific Inc. (US-Waltham)
Cuvettes	Cuvette UV 2.5 ml	Thermo Fischer Scientific Inc. (US-Waltham)
Dialysis membrane	SnakeSkin Dialysis Tubing 3.5K MWCO	Thermo Fischer Scientific Inc. (US-Waltham)
Gel	Novex life technologies NuPAGE 4-12% Bis-Tris Midi Gel	Thermo Fischer Scientific Inc. (US-Waltham)
Microplates	Echo qualified, 384 well polypropylene microplate, clear, F-bottom, LBCYPP-0200	Labcyte Inc. (US-Sunnyvale)
	Echo qualified, 384 well COC microplate, clear, F-bottom, LBCYLP-0200	Labcyte Inc. (US-Sunnyvale)
	Masterblock 384 well, deep well, #782170	Greiner Bio-One GmbH (GE-Frickenhausen)
	Microplate 1536 well, black, #782900	Greiner Bio-One GmbH (GE-Frickenhausen)
	Microplate 384 well, small volume, #784201	Greiner Bio-One GmbH (GE-Frickenhausen)
	Microplate 384 well, small volume, F-bottom #784900	Greiner Bio-One GmbH (GE-Frickenhausen)
	Microplate, 384 well, F-shape, black, #781209	Greiner Bio-One GmbH (GE-Frickenhausen)
	Microplate, 384 well, F-shape, white, PP, #781207	Greiner Bio-One GmbH (GE-Frickenhausen)
Plates	Masterblock 96 well, 2 mL, V-shape, #780270	Greiner Bio-One GmbH (GE-Frickenhausen)
	Microplate 96 well, F-bottom, black, #655900	Greiner Bio-One GmbH (GE-Frickenhausen)
	Microplate 96 well, V-bottom, natural, #651201	Greiner Bio-One GmbH (GE-Frickenhausen)
	Standard PCR plate for LC480	4titude Ltd. (US-Sacramento)
Seals	Nunc Sealing Tapes Aluminium Acrylate	Thermo Fischer Scientific Inc. (US-Waltham)
	Nunc Sealing Tapes Polyethylene Silicone	Thermo Fischer Scientific Inc. (US-Waltham)
	VIEWseal for crystallization plates	Greiner Bio-One GmbH (GE-Frickenhausen)
Syringe	10 mL Syringe	Medicina Ltd. (UK-Bolton)

8 Materials and Methods

Table 3: List of reagents used.

Description	Name	Company (Headquarter)	
Antibiotics	Chloramphenicol	Sigma-Aldrich Corp. (US-St. Louis)	
	Kanamycin	Sigma-Aldrich Corp. (US-St. Louis)	
	Streptomycin	Sigma-Aldrich Corp. (US-St. Louis)	
Buffer ingredients	Bovines Serum Albumin (BSA), # A-7906	Invitrogen AG (US-Carlsbad)	
	DL- Dithiothreitol >98% (DTT)	Sigma-Aldrich Corp. (US-St. Louis)	
	Glycerol	Melford Laboratories Ltd. (UK-Chelsworth)	
	HEPES buffer solution	Sigma-Aldrich Corp. (US-St. Louis)	
	Imidazole, 99+%, crystalline	Thermo Fischer Scientific Inc. (US-Waltham)	
	KCl	Thermo Fischer Scientific Inc. (US-Waltham)	
	MgCl ₂	VWR Chemicals (US-Radnor)	
	MnCl ₂	Thermo Fischer Scientific Inc. (US-Waltham)	
	MOPS >99.5%	Sigma-Aldrich Corp. (US-St. Louis)	
	Sodium chloride	Sigma-Aldrich Corp. (US-St. Louis)	
	TCEP	Thermo Fischer Scientific Inc. (US-Waltham)	
	TRIS Base	Merck KGaA (GE-Darmstadt)	
	Tween 20	Cisbio Bioassays (FR-Codolet)	
	E.coli Cells	lambda-phosphatase birA	Apollo Scientific Ltd. (UK-Bredbury)
		lambda-phosphatase cells	Apollo Scientific Ltd. (UK-Bredbury)
MACH 1 cells		Thermo Fischer Scientific Inc. (US-Waltham)	
Cleaning	Neutracon	Generon Ltd. (UK-Maidenhead)	
Cloning reagent	5x DNA Loading Buffer, Blue	Bioline (GE-Luckenwalde)	
	BSA I	Santa Cruz Biotechnology, Inc. (US-Dallas)	
	dCTP	Invitrogen AG (US-Carlsbad)	
	dGTP	Invitrogen AG (US-Carlsbad)	
	dNTP	Invitrogen AG (US-Carlsbad)	

8 Materials and Methods

	Dpn I	Thermo Fischer Scientific Inc. (US-Waltham)
	GeneRuler and O'GeneRuler DNA Ladders	Thermo Fischer Scientific Inc. (US-Waltham)
	Gold cloning cells	Agilent Technologies (US-Santa Clara)
	Herculase 2 buffer	Agilent Technologies (US-Santa Clara)
	Herculase 2 Fusion DNA Polymerase	Agilent Technologies (US-Santa Clara)
	Miniprep Kit	Qiagen N.V. (NL-Venlo)
	MyTag DNA polymerase	Bioline (GE-Luckenwalde)
	NEBuffer 2	New England Biolabs (US-Ipswich)
	PCR purification kit	Qiagen N.V. (NL-Venlo)
	pfx buffer	Invitrogen AG (US-Carlsbad)
	pfx enhancer	Invitrogen AG (US-Carlsbad)
	pfx polymerase	Invitrogen AG (US-Carlsbad)
	Phusion polymerase	Bioline (GE-Luckenwalde)
	Phusion polymerase buffer	Bioline (GE-Luckenwalde)
	Primer	see appendix
	Q5 DNA polymerase	Invitrogen AG (US-Carlsbad)
	Q5 DNA polymerase buffer	Invitrogen AG (US-Carlsbad)
	Sucrose	Thermo Fischer Scientific Inc. (US-Waltham)
	SYBR Safe DNA Gel Stain	Sigma-Aldrich Corp. (US-St. Louis)
	T4 DNA polymerase	Merck KGaA (GE-Darmstadt)
	T4 DNA polymerase buffer	Merck KGaA (GE-Darmstadt)
	Vector pNic28-BSA4	provided by SGC
Midi-Prep	MidiPrep Kit	Qiagen N.V. (NL-Venlo)
Compounds	Compounds	available from SGC and SelleckChem
Crystallization screen	HCS core screen	Qiagen N.V. (NL-Venlo)
	HIN core screen	Qiagen N.V. (NL-Venlo)
	JCSG core screen	Qiagen N.V. (NL-Venlo)
	LFS core screen	Qiagen N.V. (NL-Venlo)
DSF	Sypro Orange	Sigma-Aldrich Corp. (US-St. Louis)
Expression	Biotin	Sigma-Aldrich Corp. (US-St. Louis)
	IPTG >99%	Sigma-Aldrich Corp. (US-St. Louis)
Lanthanide	Streptavidin-Terbium #610SAXLB	Cisbio Bioassays (FR-Codolet)
Media	Agar, pure, powder	Sigma-Aldrich Corp. (US-St. Louis)
	LB broth (MILLER)	Sigma-Aldrich Corp. (US-St. Louis)

8 Materials and Methods

	Peptone from casein (Tryptone)	Merck KGaA (GE-Darmstadt)
	Yeast Extract Granulated	Sigma-Aldrich Corp. (US-St. Louis)
Cell culture media	DMEM Dulbecco's modified eagles medium (Gibco)	Thermo Fischer Scientific Inc. (US-Waltham)
	Opti-MEM (Gibco)	Thermo Fischer Scientific Inc. (US-Waltham)
	Trypsin 0.1% (Gibco)	Thermo Fischer Scientific Inc. (US-Waltham)
	FBS, Fetal Bovine Serum (Gibco)	Thermo Fischer Scientific Inc. (US-Waltham)
	PBS, Phosphate Buffered Saline (Gibco)	Thermo Fischer Scientific Inc. (US-Waltham)
	PenStrep (Gibco)	Thermo Fischer Scientific Inc. (US-Waltham)
NaOH	Sodium hydroxide – pellets	Merck KGaA (GE-Darmstadt)
Purification	Ni-sepharose beads	GE Healthcare Life Science (UK-Chalfont St Giles)
	PEI	Sigma-Aldrich Corp. (US-St. Louis)
	Precision Plus Protein Unstained Standards	Bio-Rad Laboratories, Inc. (US-Hercules)
	Quick Coomassie Stain	Generon Ltd. (UK-Maidenhead)
	TEV protease	homemade by SGC
Solvent	DMSO, Dimethyl sulfoxide	Sigma-Aldrich Corp. (US-St. Louis)
Tracer	kinase tracer 236 #PV5592	Thermo Fischer Scientific Inc. (US-Waltham)
	Tracer 1710	Thermo Fischer Scientific Inc. (US-Waltham)
	Tracer 199	Thermo Fischer Scientific Inc. (US-Waltham)
	Tracer 222	Thermo Fischer Scientific Inc. (US-Waltham)
NanoBRET	NanoBRET Plasmids	Promega (US-Madison)
	NanoBRET NanoGlo Substrate and extracellular NLuc inhibitor	Promega (US-Madison)
	NanoBRET Tracer K5	Promega (US-Madison)
	NanoBRET Tracer K10	Promega (US-Madison)
	FuGene HD	Promega (US-Madison)
	Transfection Carrier DNA	Promega (US-Madison)
	Tracer Dilution Buffer	Promega (US-Madison)
	HEK293T cells ATCC-CRL-3216	LGC standrds GmbH (GE-Wesel)
OMNIA	STK10 peptide	AssayQuant (US-Massachusetts)
SPR	SA-Chips	GE Healthcare (US-Illinois)
	HBS-N-Buffer	GE Healthcare (US-Illinois)

8.2 METHODS

8.2.1 Molecular cloning

QuickChange Mutagenesis was performed as described elsewhere¹¹⁴. In brief, the PCR conditions used are a standard three step PCR that consists of an initial denaturation phase (30 s at 98°C) followed by an amount of cycles for PCR product amplification: Here, 25 Cycles were used of: 10 s at 98°C for DNA template denaturation, 45 s at 55°C for allowing the primers to anneal and 300 s at 72°C for elongation by the polymerase used at the 5' end of the annealed primer (extension). A final extension of 10 minutes was done at 72°C after completing the cycles. PCR products were then Dpn I treated to digest the original template DNA plasmid that contained an antibiotics selection marker resistance and then transformed in MACH1 cloning strain cells: MACH1 cells were thawed on ice prior to the addition of 40 µL MACH1 cells to 1 µL pre-chilled templated DNA plasmid. The mix was allowed to equilibrate during a 10-minute incubation on ice, prior to heat shock treatment for 45 s at 42°C. The Mix was then chilled on ice, 100 µL lysogeny broth (LB) was added to feed the cells and cells were then incubated for 1 h at 37°C to both express the antibiotics resistance marker gene and multiply in number without antibiotic restriction before plating on LB-Agar containing kanamycin at 50 mg/mL. DNA of obtained colonies was purified using a standard MiniPrep protocol (QIAGEN). Cloning results were checked for the correct sequence via sequencing (Microsynth AG).

DNA for residues 18-317 or 19-313 of human STK10 (NCBI reference: NP_005981) was already available in the expression plasmid pNIC28-Bsa4 and pNIC-Bio3 respectively. These constructs expressed the STK10 truncations with an N-terminal hexahistidine tag and TEV (tobacco etch virus) protease tag cleavage site (extension MGSSHHHHHSQDPENLYFQ*GANS where * represents the TEV protease digestion site). The pNIC-Bio3 construct expressed the protein additionally to the above mentioned as a biotinylated protein using an Avi-Tag for *in vivo* BirA biotinylation (extension GLNDIFEAQKIEWHE on the C-terminus, where the lysine gets biotinylated by BirA). Point mutations were introduced to the expression plasmid of STK10 18-317 by PCR as described above. The mutated constructs were verified by DNA sequencing. Mutant STK10 proteins were produced from the modified plasmids using identical expression

8 Materials and Methods

and purification procedures as for the wild-type STK10 protein described below. Protein identities were confirmed by electrospray-ionisation mass spectrometry.

DNA for residues 19-320 of human SLK (NCBI reference: NP_001291672) was already available in the expression plasmid pNIC28-Bsa4 and pNIC-Bio3. These constructs expressed the STK10 truncations with an N-terminal hexahistidine tag and TEV (tobacco etch virus) protease tag cleavage site (extension MGSSHHHHHSQDPENLYFQ*GANS where * represents the TEV protease digestion site). The pNIC-Bio3 construct expressed the protein additionally to the above mentioned as a biotinylated protein using an Avi-Tag for BirA biotinylation (extension GLNDIFEAQKIEWHE on the C-terminus, where the lysine gets biotinylated by BirA).

Plasmids obtained by PROMEGA were point-mutated for mutagenesis studies using the standard method Quickchange Mutagenesis described above using HerclII polymerase (Agilent). PCR cycles were prolonged to 35 cycles to obtain sufficient amounts of plasmid. PCR products were then transformed into *E.coli* MACH1 and potential clones sequenced for positive DNA sequence. DNA obtained was then amplified and purified using Midi-Prep Kits (QIAGEN) and used in the NanoBRET experiments as described below.

8.2.2 Protein expression and purification

STK10 and SLK kinase domain proteins were expressed and purified from *E. coli* overexpression by standard methods: The constructs were transformed into BL21(DE3) cells that contained the pRARE2 plasmid that expressed rare tRNAs or for biotinylated proteins into BL21(DE3)-pRARE2-Bio3 that co-express the BirA enzyme. The resulting colonies were used to inoculate 50 mL of LB media containing 50 µg/mL kanamycin and 34 µg/mL chloramphenicol which was left shaking at 37 °C overnight. This culture was used to inoculate 1 L volumes of LB media containing 35 µg/mL kanamycin at a ratio of 10 mL culture to 1 L fresh media. The cultures were grown at 37 °C with shaking until an OD600 of 0.5 was reached. The temperature was reduced to 20 °C, and when the OD600 reached 0.7 isopropyl β-D-1-thiogalactopyranoside (IPTG) was added to a final concentration of 0.5 mM and the cultures were left overnight. For expression of biotinylated protein, Biotin was added to a final concentration of 0.5 mM. Cells were harvested by centrifugation and re-suspended in Binding Buffer (50 mM Hepes pH 7.5, 500 mM NaCl, 20 mM imidazole, 5% glycerol, 0.5 mM tris(2-carboxyethyl)phosphine

8 Materials and Methods

(TCEP). The re-suspended cells were lysed by sonication, polyethyleneimine (PEI) was added to a final concentration of 0.15%, and the insoluble debris was removed by centrifugation. The supernatant was passed through a column of 5 mL Ni-Sepharose resin (GE Healthcare). The resin was washed with Binding Buffer containing increasing amounts of imidazole before elution with Binding Buffer containing 250 mM imidazole. When the expression tag was removed, TEV protease was added to the eluate, which was dialyzed into 20 mM Hepes pH 7.5, 500 mM NaCl, 5 % glycerol, 0.5 mM TCEP (GF Buffer) overnight at 4 °C, and the protein complex was further purified by passing through a gravity column of 3 mL Ni-Sepharose. The flow-through was collected and the column was washed with GF Buffer containing 30, 60, 90, 120 and 250 mM imidazole. Proteins were further purified by size exclusion chromatography: the protein sample was concentrated to 5 mL and injected on a S75 16/60 gel filtration column (GE Healthcare) pre-equilibrated into GF Buffer. Fractions containing the desired protein were pooled and concentrated by ultrafiltration. Protein identities were confirmed by electrospray ionization mass spectrometry (ESI-MS).

Human FAK kinase domain was expressed and purified by Instituto de Biología Experimental e Tecnológica: The FAK catalytic domain used for crystallization experiments and SPR assays was expressed with an NH₂-terminal 6XHis-tag and comprises residues 410 to 689 after thrombin cleavage (FAK sequence with residue 410 changed from a Pro to a Gly). FAK was expressed in Hi5 insect cells using the Bac Magic kit (Invitrogen Corp.) Cells were harvested by centrifugation and resuspended in lysis buffer (20 mM Na-P, 500 mM NaCl, 0.1% NP 40, 5 mM MgCl₂, pH 7.5, 1 mM DTT, benzonase and protease inhibitor cocktail III). Cells were lysed by high pressure homogenization and cleared by centrifugation at 31.000x g for 40 min at 4 °C. The supernatant was loaded onto a Ni-NTA affinity column and the target protein was eluted in step gradient with buffer 20 mM Na-P, 500 mM NaCl, 500 mM Imidazole, 1 mM DTT, pH 7.5. Peak fractions were desalted and treated with hu-alpha Thrombin for histidine tag removal. The cleaved proteins were separated by passing through Ni-Sepharose resin and further purified using size-exclusion chromatography (Superdex 75 26/60). The resultant pure recombinant FAK was concentrated to 5.9 mg/mL and stored at -80 °C in a buffer containing 10 mM HEPES, 200 mM ammonium sulfate, and 0.1 mM TCEP, pH 7.5.

8 Materials and Methods

The human PYK2 kinase domain used for SPR measurements was expressed with an NH₂-terminal 6XHis-tag and comprised residues 420-691. PYK2 was cloned into pET28a including an N-terminal HIS-TEV-tag and expressed in *Escherichia coli* BL21 (DE3) cells. Cells were harvested by centrifugation and resuspended in lysis buffer (20 mM Na-P, 500 mM NaCl, 1 mM DTT, 20 mM Imidazole, 5 mM MgCl₂, pH 7.5, protease inhibitor cocktail III and Benzonase). Cells were lysed by high pressure homogenization and cleared by centrifugation at 20.400x g for 60 min at 4 °C. Subsequent steps were similar to previously described for FAK. The resultant pure recombinant PYK2 was concentrated to 10.7mg/mL and stored at -80 °C in a buffer containing 30 mM HEPES/NaOH, pH 7.5, 150 mM NaCl, 0.1 mM EGTA, 1 mM DTT.

8.2.3 TR-FRET assays

Time resolved fluorescence energy transfer (TR-FRET) is an effect used for ligand detection and describes a radiationless energy transfer between a TR-FRET donor and a TR-FRET acceptor when in close proximity. The assay performed here is a displacement assay in which a tracer molecule – an inhibitor coupled to a fluorophore – is competing for the targets binding site with the test compound resulting in an equilibrium signal. TR-FRET is a ratiometric method that is described as the ratio of A-Counts - the emission at 650 nm (binding molecule coupled to Alexa 647 fluorophore) - and the B-Counts - the emission at 622 nm (terbium-cryptate) - after excitation at 337 nm.

Equilibrium and kinetic HTRF (Cisbio) TR-FRET displacement assays were performed as described previously⁴⁴. In brief, a suitable system of tracer and N-terminally-biotinylated STK10 and SLK, respectively, was identified in an initial tracer titration showing a good signal for 500 pM STK10 or SLK and 12.5 pM Tracer 236 (Thermo Fisher Scientific) in the presence of 500 pM streptavidin-terbium (Thermo Fisher Scientific) in a standard buffer (150 mM NaCl, 20 mM HEPES pH 7.5, 0.01 % Tween 20, 0.01 % BSA, 2 mM DTT). The tracer K_D of the systems were determined performing an 8-point equilibrium titration in a range of 400 nM to 3125 pM which was allowed to incubate for 1 h and was then measured using the PHERAstar FS (BMG Labtech) for excitation at 337 nm, emission at 622 nm (terbium) and 650 nm (tracer) where the emission values were used for calculating the TR-FRET ratio. IC_{50} of the compounds were determined in a sixteen-point concentration curve in a range of 20 μ M to 610 pM in a two-times serial dilution in duplicates in the standard buffer with a final volume of 10 μ L

8 Materials and Methods

where preincubated 2x protein-terbium-solution (terbium-cryptate in same molarity as protein) was added first (5 μL) to the compounds (range of nL) dispensed using the ECHO and Access system (Labcyte), allowing the compound to be bound to the protein when adding the 2x tracer solution (5 μL). Data was measured after an incubation of 1 h as described above and evaluated using GraphPad Prism 6 software where background was reduced from the average ratios and a normalization in a range from 100 % to 0 % was done while the compound concentration values were logarithmised. Determined IC_{50} values were transformed to K_i values using the Cheng-Prusoff equation¹¹⁵.

The tracer binding kinetics were determined using a final tracer concentration range of 100 nM to 781 pM using a two-times serial dilution in sextuplicates (STK10) or duplicates (SLK) in standard buffer in a volume of 5 μL adding 5 μL of 2x preincubated protein-terbium-solution (same molarity of terbium-cryptate and protein) or terbium-solution (background) via the PHERAstar FS injector system and measure the signal for 10 minutes every 10 s. Data was evaluated using the in-build GraphPad 6 model "Association kinetics – two or more conc. of hot". Binding kinetics of the test compounds were determined using a final compound concentration range of 2.5 μM to 2.5 nM in a 4-point 10 times dilution experiment. Compounds were dispensed using the ECHO and Access system (Labcyte) in duplicates and 2x tracer solution and the background control (2x terbium-cryptate) was added into the measurement plates (black 384 small volume microplates (Greiner Bio-one)). For the measurement 5 μL 2x preincubated protein-terbium-solution was dispensed via the PHERAstar FS injector system giving a final volume of 10 μL and were measured for 6.5 minutes every 10 s. For high enough time resolution, the 384 plate was divided into octants for measurement as described before¹¹⁶. Background and no compound controls (DMSO) were included and the background was reduced from the average ratios. The resulting curves were evaluated using the in-built Motulsky-Mahan model¹¹⁷ of GraphPad Prism 6, determining the on-rate and off-rate of the compound and calculating the kinetic K_D .

8.2.4 DSF assay

Differential Scanning Fluorimetry (DSF) measurements were performed as described previously¹¹⁸. Using the Syproorange dye, in DSF, the protein denaturation process is monitored over a temperature increase from 25 $^{\circ}\text{C}$ to 95 $^{\circ}\text{C}$. A fluorescence enrichment is observed when the hydrophobic parts of the protein usually located in

8 Materials and Methods

the inside become solvent exposed due to protein denaturation. After denaturation the now hydrophobic solvent exposed protein molecules aggregate thereby reducing the fluorescence enrichment, which results in the well-known protein melting curve. A compound binding is believed to increase the melting temperature of a protein proportional to the binding affinity of the compound. The temperature shift is calculated by the difference in melting temperature of non-treated protein and compound treated protein and often used as an assay parameter to guide compound SAR. It is noteworthy, that comparisons for a single kinase to a set of inhibitors gives comparable results and serves as a ranking parameter, while the temperature shift is not suitable for comparisons across the kinome as each kinase has its own initial melting temperature and temperature range upon which it can be stabilized. Because of this different assay window comparisons are often to be discussed.

Here, a 2 μM solution of STK10 or SLK, respectively was tested with a compound concentration of 12.5 μM adding 2 μM of Sypro Orange to the solution. Measurements of the fluorescent curve was performed using a Stratagene Mx3005P (Agilent Technologies) in a temperature range from 25°C to 95°C. GraphPad Prism 6 was used for determination of the melting point which was then compared to the wild-type melting point of the individual protein as determined in an experiment without compound addition.

8.2.5 SPR assays

Surface Plasmon Resonance (SPR) is a surface-based technique that detects changes in the chemical environment of an immobilized analyte upon ligand binding via a change in the refractive index and hence a change in the reflection angle of polarized light applied through a prism in the detection device¹¹⁹. In a kinetic setup, the test compound is applied to the flow channel where it will associate to the immobilized target. After this dissociation phase, where an equilibrium should be reached, buffer is applied to determine the compounds dissociation time. Based on a titration of a range of different compound concentrations an equilibrium K_D , the inhibitors on-rate, off-rate and kinetic K_D can be obtained by data analysis.

For STK10, SPR measurements were performed on a Biacore T200 instrument from GE Healthcare. Recombinant Sf9 expressed STK10 [kinase domain (KD, M1-S348) and full-length (FL, M1-S968)] were immobilized on a Biacore SA chip at 15°C and 25°C,

8 Materials and Methods

respectively, at a flow rate of 10 $\mu\text{L}/\text{min}$ using SA coupling, according to Biacore's standard protocol. HBS-N (10 mM Hepes pH 7.40, 0.15 M NaCl, 0,05 % Tween-20) served as running buffer during immobilization. STK10-KD and -FL were applied at a concentration of 5 $\mu\text{g}/\text{mL}$ in a buffer containing a 60-fold excess of MSC1824740 and PF-431396 respectively. An unmodified SA matrix served as a reference surface. STK10 inhibitors stored as 10 mM stock solutions in 100% dimethyl sulfoxide (DMSO) were dissolved in running buffer (20 mM HEPES pH 7.50, 150 mM NaCl, 0.05% Tween 20, 1 mM DTT, 0.1 mM EDTA, 2% DMSO) and analyzed using 10-point two-fold dilution series. Kinetic titration experiments were performed at 15°C and 25°C for STK10-KD and -FL, respectively with a flow rate of 30 $\mu\text{L}/\text{min}$, a sample contact time of 120 s and a dissociation time of 300 s. Data sets were processed and analyzed using the Biacore T200 Evaluation software. Solvent corrected and double-referenced association and dissociation phase data were fitted to a simple 1:1 interaction model with mass transport limitations.

For FAK and PYK2, SPR measurements were performed on a Biacore 4000 instrument from GE Healthcare. Recombinant FAK [huFAK (410-689)] and PYK2 [huFAK (420-691)] were immobilized on a Biacore CM5 chip at 25°C at a flow rate of 10 $\mu\text{L}/\text{min}$ using amine coupling at pH 4.50 and pH 5.0 respectively, according to Biacore's standard protocol. HBS-N (10 mM Hepes pH 7.40, 0.15 M NaCl, 0,05 % Tween-20) served as running buffer during immobilization. FAK and PYK2 were applied at a concentration of 5 $\mu\text{g}/\text{mL}$ in a buffer containing a 60-fold excess of MSC1824740 and PF-431396 respectively. An unmodified carboxydextran matrix served as a reference surface. FAK and PYK2 inhibitors stored as 10 mM stock solutions in 100% dimethyl sulfoxide (DMSO) were dissolved in running buffer (20 mM HEPES pH 7.50, 150 mM NaCl, 0.05% Tween 20, 1 mM DTT, 0.1 mM EDTA, 2% DMSO) and analyzed using two-fold dilution series. Kinetic titration experiments were performed at 25°C with a flow rate of 30 $\mu\text{L}/\text{min}$, a sample contact time of 120 s and a dissociation time between 300 and 600 s. Data sets were processed and analyzed using the Biacore 4000 Evaluation software, version 1.1. Solvent corrected and double-referenced association and dissociation phase data were fitted to a simple 1:1 interaction model with mass transport limitations.

8 Materials and Methods

8.2.6 OMNIA assays

The OMNIA assay determines the test proteins activity based on the detection of a SOX-labeled peptide substrate that emits fluorescence at 485 nm after excitation with 385 nm¹²⁰. The fluorescent signal enriches upon substrate phosphorylation where the substrates phosphorylation is complexed by a magnesium ion to the fluorescent SOX moiety.

OMNIA enzymatic assays were performed as per the manufacturers indications (AssayQuandt). Recombinant Sf9 expressed STK10 [kinase domain (KD, M1-S348) and full-length (FL, M1-S968)] in standard buffer (10 mM MgCl₂, 50 mM HEPES pH 7.5, 0.01 % Tween 20, 0.2 mg/mL BSA, 1 mM DTT, 1% Glycerol) were both used at a concentration of 5 nM as a result from a kinase titration experiment. ATP titration in a range of 2,5 mM to 250 nM was performed at 1 μM STK10-SOX peptide (AssayQuandt) present. Following inhibitor titration experiments were performed at an ATP concentration of 60 μM, that was determined to be the K_M for both protein constructs, and 1 mM ATP (cellular conditions), respectively. Assay was performed in 20 μL reactions in white 384 plates (Greiner 784 074). After substrate addition, the reactions fluorescence after 360 nm excitation was monitored for 1 h at 487 nm emission in a PHERAstar platereader (BMG Labtech) and the linear partition of the curves (10% of maximum signal) was then fitted using GraphPad Prism 7 “straight line”-fit. The resulting slopes were plotted against the ATP or inhibitor concentration to provide a Michaelis-Menten-Diagram that was fitted using GraphPad Prism 7 Michaelis-Menten-Fit.

8.2.7 NanoBRET assays

The NanoBRET target engagement assay determines the binding potency of a test compound in the environment of a living cell¹²¹. For that, a full-length protein kinase is fused to a NanoLuc luciferase and that construct is transiently transfected into a suitable host cell for protein expression. In this setup, the kinase gets mildly overexpressed and will carry human post translational modifications. Usual binding partners are present in the cell as well as a cellular concentration of the kinases cosubstrate ATP. If a suitable tracer, here a promiscuous kinase inhibitor fused to a BODIPY fluorophore, is added to the cells a bioluminescence resonance energy transfer (BRET) can be observed for the luciferase and BODIPY upon coelenterazine substrate

8 Materials and Methods

addition¹²². Because of a competition for the binding site of both test compound and tracer, this BRET reduces in a dose-dependent manner when test compound is added.

The NanoBRET target engagement assay was performed as described previously¹²³. Full-length kinases (Table 4) plasmids containing N- or C-terminal placements of NanoLuc (Table 4) were obtained by the manufacturer (Promega) or point-mutated by QuickChange mutagenesis (see 8.2.1). To lower intracellular expression levels of the reporter fusion, the NanoLuc/kinase fusion constructs were diluted into carrier DNA (pGEM3ZF-, Promega) at a mass ratio of 1:10 (mass/mass), prior to forming FuGENE HD complexes according to the manufacturer's instructions (Promega). DNA:FuGENE complexes were formed at a ratio of 1:3 ($\mu\text{g DNA}/\mu\text{L FuGENE}$). 1 part of the transfection complexes was then mixed with 20 parts (v/v) of HEK293T cells suspended at a density of 2×10^5 /mL in DMEM (Gibco) + 10% FBS (GE Healthcare), seeded into T75 flasks and allowed to express for 20h.

For target engagement both serially diluted test compound and NanoBRET Kinase Tracer as specified in Table 4 (Promega) at the indicated final concentration were pipetted into white 384-well plates (Greiner 781 207). The corresponding transfected cells were added and reseeded at a density of 2×10^5 /mL after trypsinization and resuspending in Opti-MEM without phenol red (Life Technologies). The system was allowed to equilibrate for 2 hours at 37°C/5% CO₂ prior to BRET measurements.

For kinetic wash-out experiments the test compound at 10 times the IC_{50} determined in a target engagement experiment or at 10 μM maximum was incubated with transfected cells at a density of 2×10^5 /mL in Opti-MEM without phenol red (Life Technologies) for 2 hours at 37°C/5% CO₂. The medium was then exchanged to remove unbound test compound and the compound-incubated cells were pipetted into white 96-well plates (Corning 3600). Prior to BRET measurements NanoBRET Kinase Tracer as indicated in Table 4 (Promega) at the final concentration indicated was added.

To measure BRET, NanoBRET NanoGlo Substrate + Extracellular NanoLuc Inhibitor (Promega) was added as per the manufacturer's protocol, and filtered luminescence was measured on a PHERAstar plate reader (BMG Labtech) equipped with 450 nm BP filter (donor) and 610 nm LP filter (acceptor). For the kinetic wash-out experiment the luminescence was surveyed for two hours at 30°C.

8 Materials and Methods

Competitive displacement data was then graphed using GraphPad Prism 7 software using a 3-parameter curve fit with the following equation: $Y=100/(1+10^{((X-\text{Log}/C_{50}))})$ where data was normalized to background and tracer only control signal.

Kinetic wash-out data was graphed using GraphPad Prism 7 software and fitted using a one-phase association fit: $Y=Y_0 + (\text{Plateau}-Y_0)*(1-\exp(-K*x))$, where the plateau was set to be constant to the maximal signal of the DMSO control

Table 4: NanoBRET assay conditions.

Target	NLuc placement	Tracer	[Tracer], [M]
STK10	N	K10	1,00E-06
SLK	N	K10	1,00E-06
FAK	N	K5	5,00E-08
PYK2	C	K5	7,50E-08
STK10-S191A	N	K10	3,75E-07
SLK-T183A	N	K10	3,50E-07
SLK-S189A	N	K10	3,50E-07
FAK-R426S	N	K5	2,50E-08
FAK-R426A	N	K5	2,50E-08
FAK-L567A	N	K5	7,50E-08
FAK-E506Q	N	K5	2,50E-08
FAK-E506I	N	K5	2,50E-08
FAK-E430S	N	K5	2,50E-08
FAK-E430Q	N	K5	2,50E-08
FAK-Y576F+Y577F	N	K5	2,50E-08
PYK2-F435R	C	K5	2,50E-08
PYK2-N428G	C	K5	1,25E-07
PYK2-E474Q	C	K5	2,50E-08
PYK2-F435Q	C	K5	2,50E-08
PYK2-Y579F+Y580F	C	K5	2,50E-08

8.2.8 Protein crystallization and structure determination

Protein-ligand solution for crystallization was prepared adding 50 mM compound stock to a final concentration of 1 mM to 75 μL of concentrated purified protein at approximately 20 mg/mL, were incubated for 1 h on ice, spun down for 10 minutes at 4°C and transferred into a fresh tube for setting up two crystallization screen plates containing 25 μL of 96 different well conditions. Protein was dispensed by Mosquito robot (TTP Labtech) in a ratio of 1:1, 1:2 and 2:1 in comparison to well condition solution adding up to a final volume of 150 nL. Plates were sealed immediately after preparation and stored in a Minstrel imager (Rigaku) at 4°C. Pictures were automatically taken and drops were reviewed and ranked using TexRank software.

8 Materials and Methods

Crystals were mounted at 4°C using nylon loops at different sizes matching the crystal into the loop and sent for data collection at Diamond Synchrotron Beamline I04-1. One of the crystals sent initially diffracted to 2.2 Å and a data set was taken (1800 images with 0.1° rotation upon each image).

STK10 protein at a concentration of 20mg/mL was incubated for 1 h on ice with a 1:2 molar ratio of protein:compound solution. Precipitation was removed by centrifugation. Protein concentrations were measured by UV absorbance, using the calculated molecular weights and estimated extinction coefficients using a NanoDrop spectrophotometer (Thermo Scientific). Crystals were obtained using the sitting drop vapour diffusion method at 4°C using drops of a total volume of 150 nL pipetted using the Mosquito System (spt Labtech). Crystallisation conditions can be seen in Suppl. Table S 1. All data was collected at 100K at the Diamond Synchrotron. Data collection statistics can be found in Suppl. Table S 1. The diffraction data was indexed and integrated using MOSFLM¹²⁴ (Leslie and Powell, 2007) or XDS (Kabsch, 2010), and scaled using AIMLESS¹²⁵ (Evans, 2011) or SCALA (Evans, 2006). The structures were all solved by molecular replacement using PHASER¹²⁶ (McCoy et al., 2007) and a previous structure of STK10 as a search model. The models were built using Coot¹²⁷ (Emsley et al., 2010) and refined with REFMAC5¹²⁸ (Murshudov et al., 2011) or PHENIX (Adams et al., 2010). All models were validated using MOLPROBITY (Chen et al., 2010).

FAK was incubated for 2 hours with 2 mM adenosine 5'-triphosphate magnesium salt. Crystals were obtained using the hanging drop vapor diffusion method and equilibrating against 1 mL of the reservoir solution (0.2 M Magnesium formate dihydrate, 10-20% PEG 3350) at 20°C. The protein was mixed 1:1 with the reservoir solution. For complex formation with the inhibitor, the crystals were transferred to a stabilizing solution (0.2 M Magnesium formate dihydrate, 30% PEG 3350) containing 5 mM 1 and 5% DMSO and were soaked for 24 h. All data sets were collected at 100 K on beamline SLS X106 and processed with the XDS software package (Kabsch and XDS). The structures were solved by molecular replacement, using BUSTER (Bricogne et al., 2016). Model building was performed in Coot, with compounds and waters fitted into the initial $|F_o| - |F_c|$ map, and the structures were refined using BUSTER. The coordinates of the holo-structures of FAK have been deposited in the RCSB Protein Data Bank. The refinement statistics and PDB accession codes are given in **Suppl. Table S 4**.

8 Materials and Methods

9 RESULTS

In the following two studies on the protein kinases STK10/SLK and FAK/PYK2 we identified structural factors affecting the binding kinetics of the kinase inhibitors investigated.

9.1 STRUCTURAL FACTORS AFFECTING THE AFFINITY AND RESIDENCE TIME OF STK10 INHIBITORS

9.1.1 STK10 and SLK potently bind many clinically used kinase inhibitors *in vitro*

As it was previously described for STK10 to bind many diverse clinical kinase inhibitors we assessed how many kinase inhibitors are binding with a temperature shift (ΔT_m)¹¹⁸ screening campaign testing 352 clinical and preclinical kinase inhibitors on both STK10 and SLK. We found many of the inhibitors binding STK10 and SLK even stronger than erlotinib (**Fig. 6, Suppl. Table S 2**). To confirm our results, we performed a Time Resolved Fluorescence Resonance Energy Transfer (TR-FRET) tracer displacement equilibrium screen for the top 100 hits (**Suppl. Table S 2**) where we were able to confirm these hits and identified 35 clinically used inhibitors binding with less than 100 nM potency. The two methods showed a good correlation for both STK10 and SLK and resulted in a model for the convolution of ΔT_m data to TR-FRET IC_{50} s. As a general trend, most compounds bind more potent to STK10 than an SLK with the strongest inhibitor on STK10 being staurosporine showing a potency of 598 pM, where erlotinib shows an IC_{50} of 91 nM and gefitinib shows 315 nM. This shows that the potency between difference between erlotinib and gefitinib is only 3.5-fold and is unlikely to cause the differently observed skin-related side-effects for the two inhibitors. Our data agrees with literature reported IC_{50} s for STK10⁷⁵.

9 Results

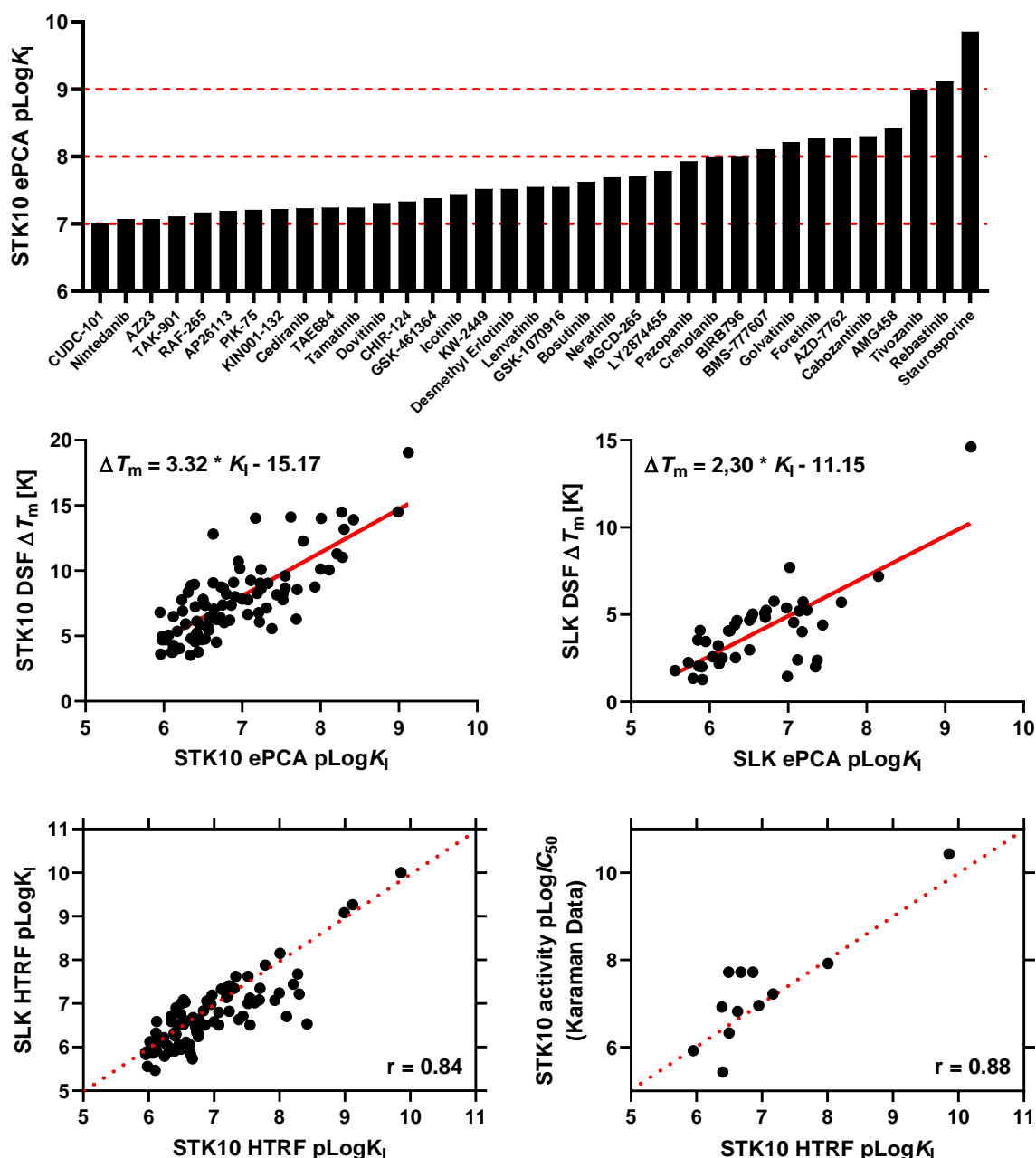


Fig. 6: STK10 and SLK bind many of the clinically used inhibitors potently *in vitro*. (a) TOP 35 hits of a clinical kinase inhibitor library for STK10 tested with a HTRF tracer displacement assay. Red line indicates a potency at 100 nM, 10 nM and 1 nM. The HTRF results are in good accordance with an orthogonal Thermal shift assay for STK10 (b) and SLK (c). The mathematical equation resulting from the linear fit of this large data comparison is given in the respective correlation. (d) The related STK10 and SLK kinase show comparable HTRF K₁s with STK10. (e) The screening results of this study correlated well with previously published results using Ambit technology by Karaman *et al*⁷⁵.

9.1.2 Intrinsic flexibility of the kinase domains of STK10 and SLK allows tight interaction with many diverse inhibitors

Next we asked why STK10 can bind so many diverse clinically used kinase inhibitors. To answer this question, we performed x-ray crystallography to obtain structural models for several inhibitors. We managed to resolve structures for bosutinib (PDB 5ajq), GW830263A (PDB 4aot), GW683134 (PDB 6eim), foretinib (PDB 6i2y), BIRB-

9 Results

796 (PDB 6gtt), dovitinib (PDB 5owq) and dasatinib (PDB 5owr). Strikingly, STK10 seems to be very flexible as it crystallized in 5 different space groups and a diversity of conformations for the different inhibitors (**Fig. 7, Suppl. Table S 1**). For both foretinib (PDB 6i2y) and GW683134 (6eim) we observed an activation segment exchange as observed with SU11274 (PDB 2j7t)⁸⁰. In a more close analysis, we found the α C of STK10 to show conformations within 8 Å, the activation loop DFG in both -in and -out positions and for the inhibitor SB-633825 we found two crystal forms showing a DFG-in confirmation in one structure (PDB 4usd) and a DFG-out in the other (PDB 4use). The R-spine residues were identified as L106, I82, L85, F176, H155 and D219 and we observed the typical break of the R-spine in type II inhibitors. Overall, the STK10 binding pocket can be described as very hydrophobic and opens a backpocket upon inhibitor binding.

9 Results

other inhibitors crystallized. The polar dichloromethoxyanilin moiety of bosutinib was perfectly surrounded by polar residues, closing the backpocket around the inhibitor.

For foretinib, a type II inhibitor for STK10, we observed the binding pocket to form a closed structure by hydrophobic interactions of the DFG F176, the core amino-fluoro-phenol of foretinib and an V50 located in β 2 flanking the P-Loop thereby forcing STK10 into an inactive DFG-out state. This forms a closed binding pocket where the P-Loop closes the binding site like a lid.

For BIRB-796, a type II inhibitor for STK10, we found a particularly stabilized DFG-out conformation, where the DFG-phenylalanine engages in a π -stacking with the naphthalene ring system of the inhibitor. Additionally, phenylalanine F47 engages in another π -stacking, sandwiching the naphthalene ring with the DFG F176 and stabilizing the otherwise most often flexible P-loop in a conformation clearly resolved in the structure. Whereas the mechanism of this binding remains unknown, we expect this structural rearrangement to happen in two steps, resulting in an induced fit conformation of STK10.

For dovitinib and dasatinib, two type I inhibitors for STK10, we mainly found the hinge and front pocket interactions of the type II inhibitors to be present as well. Both binding sites appear to be more open rather than enclosing the inhibitors. For dasatinib, however, we found the DFG-aspartate D175 interacting with E81 located in the α C unusually tightening the binding pocket and thereby potentially arresting the inhibitor.

9.1.3 Many STK10 inhibitors show only weak cellular potency

In the next step we asked whether the high potency of kinase inhibitors on STK10 translates into the cellular context. For that we used the NanoBRET cellular target engagement assay¹²⁹ that uses full length protein kinases and takes the cellular concentration of ATP into account. Surprisingly, we observed a shift to much less potent interactions in cells compared to *in vitro* (**Fig. 8, Suppl. Table S 2, Suppl. Fig. S 4, Suppl. Fig. S 5**). Noteworthy, the STK10 affinity was slightly more potent than that for SLK in cells - comparable to *in vitro*. Staurosporine remained the most potent compound as well in cells and showed an IC_{50} of 2 nM. While erlotinib was bound with 3 μ M, the potency of gefitinib was 15-fold lower (44 μ M) and hence showed a much wider window between the two inhibitors.

9 Results

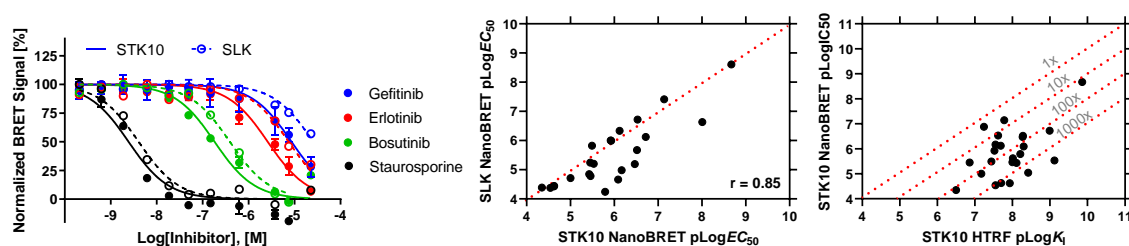


Fig. 8: Many of the inhibitors do not bind STK10 strongly in cells. (a) Representative titration of erlotinib, gefitinib, bosutinib and staurosporine for STK10 using NanoBRET target engagement assay. (b) STK10 and SLK NanoBRET data showed comparable albeit slightly less potent binding for SLK in comparison to STK10. Correlation coefficient is indicated in the figure. (c) In comparison to *in vitro* HTRF data, the cellular data showed significantly reduced potency in cells in the range of 100 to 1000 times for most inhibitors.

This relatively weak inhibition of cellular STK10 by erlotinib was observed previously⁷⁴ by Western Blot analysis in Jurkat cells which showed no effect on downstream phosphorylation of ERM, a known substrate of STK10 after treatment. However, the much lower potency of gefitinib in comparison to erlotinib is striking.

9.1.4 Reasons for the large decrease in STK10 affinity of inhibitors in cells

Logically, we were wondering about the causality of why the interaction of kinase inhibitors with STK10 is so weak in cells. To address this, we summarized the differences between the NanoBRET assay in cells and the *in vitro* methods: Firstly, in cells we have a very high ATP concentration of 1 mM which can shift inhibitor IC_{50} s due to competition for the active site. Secondly, the phosphorylation state of the kinase investigated might differ in a cellular system versus in a purified protein (E.coli). Thirdly, the protein state regarding domain organization is different in cells and can span more of the full-length protein than the kinase domain only in the purified protein. Lastly, the ability of the compounds across the cell membrane may be suboptimal.

First, we assessed the ATP K_M of STK10 using an OMNIA activity assay (**Fig. 9**) to investigate whether ATP binding to STK10 is potent and might be the reason for the shift in cells. Here we determined the K_M to be 60 μ M. We as well determined the IC_{50} s of a representative compound set of 8 compounds spanning different binding types in this assay and compared it to the IC_{50} s determined under high ATP conditions in the same assay. Using 1 mM ATP in our assay we simulated the ATP concentration present in cells. As expected, we found at least 10-fold shifts towards lower potency if more ATP is present which confirms the competitive binding mode of the inhibitors tested.

9 Results

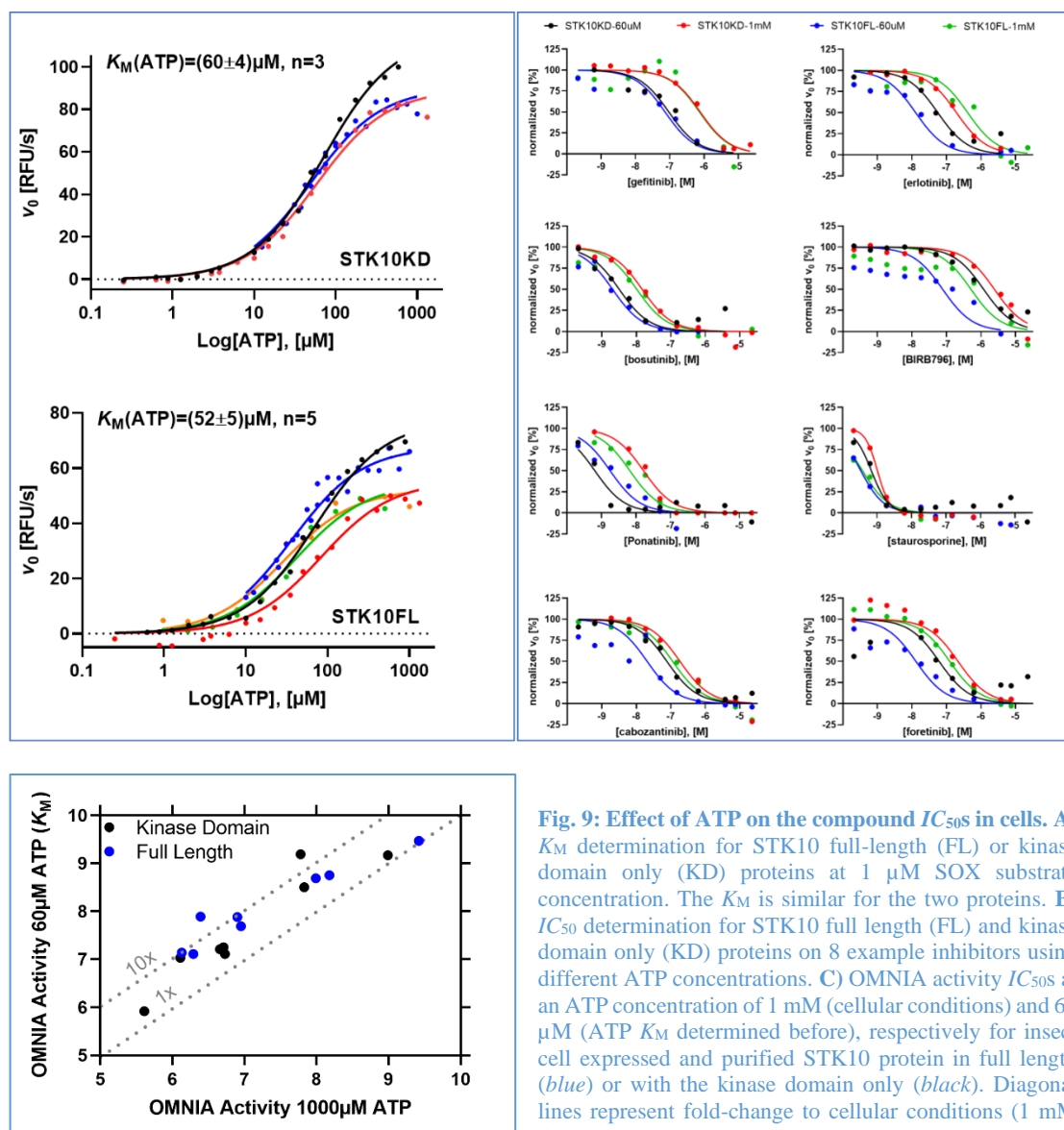


Fig. 9: Effect of ATP on the compound IC_{50} s in cells. **A)** K_M determination for STK10 full-length (FL) or kinase domain only (KD) proteins at 1 μM SOX substrate concentration. The K_M is similar for the two proteins. **B)** IC_{50} determination for STK10 full length (FL) and kinase domain only (KD) proteins on 8 example inhibitors using different ATP concentrations. **C)** OMNIA activity IC_{50} s at an ATP concentration of 1 mM (cellular conditions) and 60 μM (ATP K_M determined before), respectively for insect cell expressed and purified STK10 protein in full length (blue) or with the kinase domain only (black). Diagonal lines represent fold-change to cellular conditions (1 mM ATP).

Secondly, we investigated whether the use of a different construct would influence the IC_{50} s of the inhibitors. For that, we used two different constructs in the OMNIA assay: One containing the STK10 kinase domain only and the other containing a full-length STK10 protein. Interestingly, we did not see large differences in the binding behavior for the kinase domain and full-length construct. Also, the determined K_M for ATP is similar. To validate this, we used surface plasmon resonance (SPR) and determined the binding constants for the two constructs using an orthogonal method (Fig. 10). The binding to the kinase domain only was more potent than to the full length protein.

9 Results

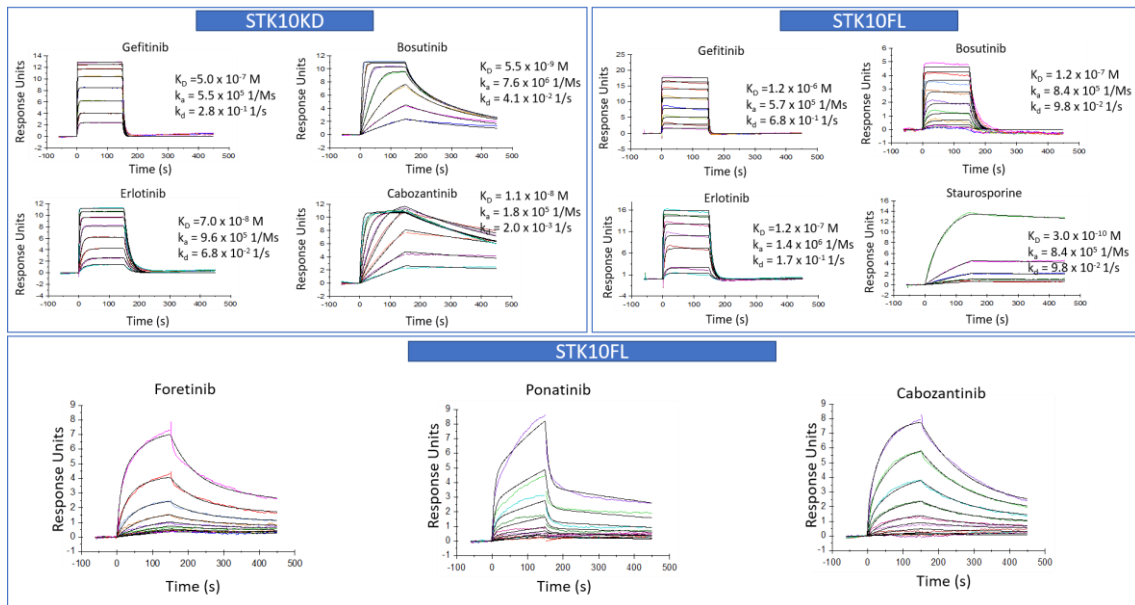


Fig. 10: SPR sensorgrams for STK10KD and STK10FL as indicated in the respective panel. The Compound Name and average results from three replicates of 1:1 Fits are included in the respective figure (upper panel). We observed two-step kinetics which did not result in conclusive on- and off-rates for the compounds (lower panel).

Thirdly, to investigate whether a different phosphorylation state of the proteins would impact inhibitor IC_{50} s, we point-mutated phosphorylation sites in the kinase domain activation loop of the respective protein and tested these constructs in the NanoBRET assay and determined the IC_{50} s for the 8 representative compounds (**Fig. 11**). Interestingly, for STK10 we did not observe a difference in the binding of wild type protein to phosphor-dead protein, however, for SLK we observed a 10-fold change for the compounds ponatinib, bosutinib, and erlotinib when comparing wild type to phosphor-dead mutant protein. Unfortunately, no trend for the often more affected type II inhibitors was observed here.

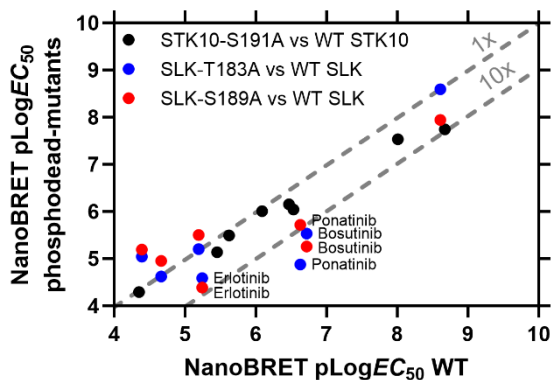


Fig. 11: Effect of STK10 and SLK phosphorylation on the compound potency shift in cells. NanoBRET cellular EC_{50} s in comparison of wild-type (WT) STK10 or SLK protein to respective phosphor-dead mutants. Diagonal lines represent fold-change to wild-type protein data

Lastly, we would expect the compound cell permeability to modulate the IC_{50} s of the inhibitors in the NanoBRET assay. As we only tested clinical kinase inhibitors that have been optimized for *in vivo* use, this possibility seems rather insignificant.

9 Results

In summary, we observed an up to 100-fold shift between *in vitro* and NanoBRET assays that can partly be explained by the high cellular ATP concentration. While both the phosphostate and the length of the protein did not yield reasonable conclusions, we suspect cellular binding partners present or the activation segment exchange producing autoinhibited kinases⁸⁰ to partly lower the IC_{50} s in cells.

9.1.5 Influence of residence time of the clinical kinase inhibitors

While we observed a weakened potency of erlotinib in cells, we wondered whether a slow residence time might cause the related side-effects. For assessing the binding kinetics of the compounds, we performed kinetic probe competition assays (kPCA) in the TR-FRET format we used for the equilibrium measurements (**Fig. 12, Suppl. Table S 2**). This assay format requires the tracer kinetics to be sufficiently fast in order to measure the displacement with the compound using the Mutulsky-Mahan-Model. In the kPCA assay we found a range of different binding kinetics. The slowest off-rates range from rebastinib ($1.18E-04 \text{ M}^{-1}\text{s}^{-1}$), ponatinib ($5.13E-04 \text{ M}^{-1}\text{s}^{-1}$), foretinib ($1.20E-03 \text{ M}^{-1}\text{s}^{-1}$) and BIRB796 ($1.74E-03 \text{ M}^{-1}\text{s}^{-1}$) to fast off-rates of bosutinib ($2.03E-02 \text{ M}^{-1}\text{s}^{-1}$), erlotinib ($2.12E-02 \text{ M}^{-1}\text{s}^{-1}$) and gefitinib ($1.15E-02 \text{ M}^{-1}\text{s}^{-1}$). However, the difference in potency for erlotinib and gefitinib (2-fold) seems to arise more from the on-rate that displays a 2.5-fold change than the contribution of the off-rate. Gratifyingly, the kinetically calculated kPCA K_{DS} ($K_D=k_{off}/k_{on}$) are in very good agreement with the equilibrium determined ePCA K_{IS} .

9 Results

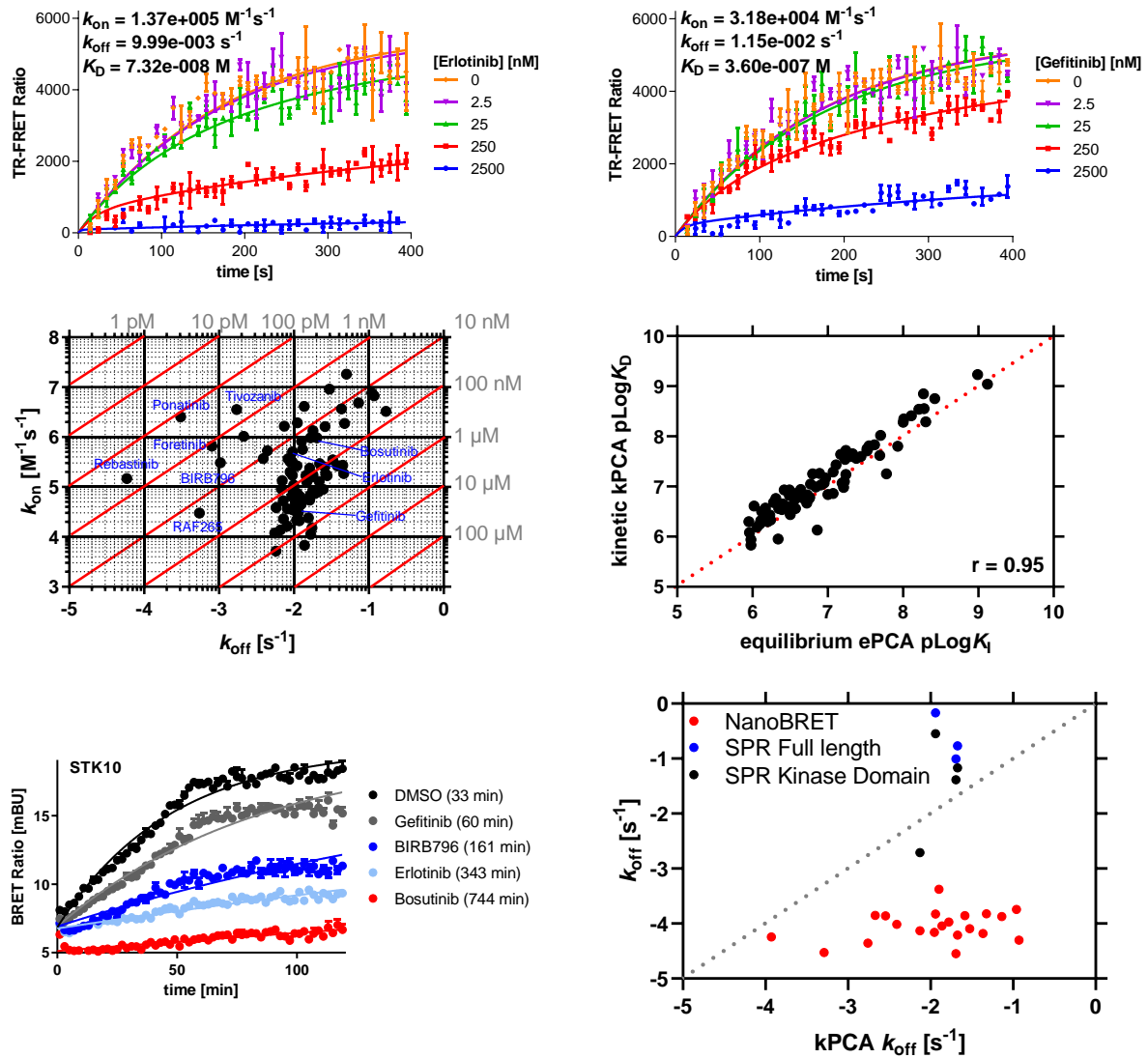


Fig. 12: Could residence time be important for achieving the observed physiological effects? Representative data from kPCA tracer assay for erlotinib (a) and gefitinib (b). (c) k_{on} - k_{off} -plot of the dataset generated for the inhibitors on STK10. Many compounds are on-rate limited, whereas only few compounds were detected showing slow on, slow off kinetics. (d) Nevertheless, the kinetically determined kPCA K_D correlates very well with the equilibrium determined ePCA K_I . (e) NanoBRET cellular wash-out data for erlotinib, gefitinib, bosutinib and BIRB-796. (f) Comparison of the kPCA data to SPR data generated using STK10 full-length or kinase domain protein, respectively and to the NanoBRET wash-out half-lives determined.

Next we wanted to know how the half-lives of the compound-STK10 complexes would be in cells and performed the NanoBRET assay in a wash-out format (**Fig. 12, Suppl. Fig. S 6**). Surprisingly, we found erlotinib to be much slower in cells compared to gefitinib with 6-fold. Clearly, the slowest compound among the 32 representative inhibitors tested in this format, bosutinib was the slowest which is contradictory to the kPCA result! However, BIRB796, which is among the slowest inhibitors in both the kPCA assay and the NanoBRET wash-out assay. Unfortunately, the SLK wash-out assay was of insufficient data quality and hence an assessment of the kinetic properties of the inhibitors on SLK in cells was not pursued (**Suppl. Fig. S 7**).

9 Results

We suspected, that the difference in the kinetics might result from the two different protein constructs used in kPCA and NanoBRET. Hence, we can compare the results to the previously discussed SPR results (**Fig. 10**). Here, we determined the binding kinetics for 3 compounds on both the STK10 kinase domain only and full-length construct and found the kinase domain only to show slower k_{off} s than the full-length construct. This however does not explain the fast off-rate of bosutinib in the kPCA versus the very slow half-live in the NanoBRET wash-out. Unfortunately, the SPR results do not in any way allow a correlation or statistical analysis with the NanoBRET data. We were only able to determine 3 out of 8 compound binding kinetics because of a mixed phosphorylation state of the proteins used, for which especially type II or bulky compounds will have a binding preference for one of the states.

9.2 STRUCTURE-KINETIC-RELATIONSHIP REVEALS THE MECHANISM OF THE SELECTIVITY OF FAK INHIBITORS OVER PYK2

9.2.1 A series of PF-562271-based inhibitors shows a range of binding kinetics on FAK and PYK2

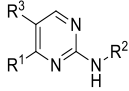
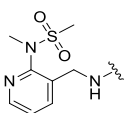
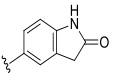
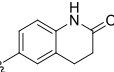
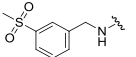
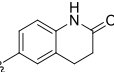
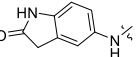
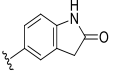
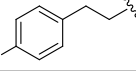
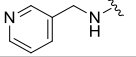
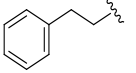
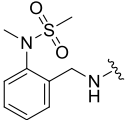
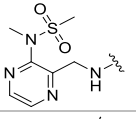
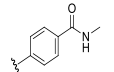
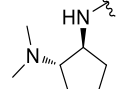
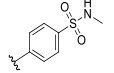
To better understand the reasons for the distinct selectivity profile of the selected inhibitor class for FAK and PYK2, we performed surface plasmon resonance (SPR) measurements on a series of 12 compounds (**Table 5**) that share the pyrimidine scaffold of PF-562271 (**1**) which provided a set of comparable affinity and binding kinetics data (**Fig. 13**).

Based on the alignment of the two crystal structures of **1** binding to FAK and PYK2, respectively (**Fig. 5**) we designed an inhibitor series that allowed studying the interactions observed for both FAK and PYK2 (**Table 5**).

We studied different observed interactions by varying three subsections of **1**. For investigating the role of the FAK-L567 hydrophobic interaction with **1** leading to a stabilized helical activation loop in FAK but not PYK2, we used additional published inhibitors that differ in the pyridyl-methansulfonamide moiety (**R**¹) to test for the interactions involvement based on polarity of the aromatic ring (phenyl- (PF-431396, **10**) and pyrazine-methansulfonamides (PF-4554878, defactinib, **11**)) and as well used different decorations of aromatic systems in **5**, **6**, **7**, **8** and **9**. The same changes in polarity in the aromatic ring system are suitable to test the interaction of PYK2-E509 which interacts with the pyridine nitrogen of **1** but is not present in FAK. Another promising interaction to FAK was a polar interaction of the **1** oxindole with FAK-R426, that was not present in the PYK2 binding mechanism although both proteins share an arginine in that position. To test this interaction, we changed this residue (**R**²) to a phenol (**3**) and a quinoline (**4**). As **1** - a dual FAK/PYK2 inhibitor - binds to PYK2 in a flipped way compared to FAK with the trifluoro moiety pointed towards the back of the pocket, we tested an absence of this decoration (**R**³) in **2**.

9 Results

Table 5: Chemical series based on PF-562271 investigated in this study. Three substituent sites on PF-562271 R¹, R² and R³ were considered to study the interactions in the kinase binding sites SPR= Surface Plasmon Resonance, k_{on} = association rate constant, k_{off} = dissociation rate constant, K_D = equilibrium dissociation constant, τ =residence time calculated as $1/k_{off}$

Cmpd No. (Name)				k_{on} [1/Ms]	k_{off} [1/s]	K_D [M]	τ [min]	k_{on} [1/Ms]	k_{off} [1/s]	K_D [M]	τ [min]
	R ¹	R ²	R ³	FAK (SPR)				PYK2 (SPR)			
1 PF-562271			-CF ₃	5.30 E+06	3.42 E-03	7.59 E-10	292.0	1.30 E+07	7.41 E-02	5.74 E-09	13.5
2			-H	8.81 E+05	2.92 E-01	3.29 E-07	3.4	8.98 E+05	7.50 E-01	8.22 E-07	1.3
3		-Phenyl	-CF ₃	8.72 E+04	6.22 E-03	7.06 E-08	160.6	3.72 E+04	1.75 E-02	4.74 E-07	57.2
4				-CF ₃	2.27 E+05	2.23 E+00	9.86 E-06	0.4	9.15 E+05	5.46 E-01	6.00 E-07
5 PF-573228			-CF ₃	7.02 E+06	8.16 E-03	1.32 E-09	122.5	1.33 E+06	3.34 E-01	2.52 E-07	3.0
6			-CF ₃	1.65 E+06	6.09 E-02	3.65 E-08	16.4	1.68 E+06	1.93 E-01	1.14 E-07	5.2
7			-CF ₃	1.42 E+05	1.35 E-01	1.00 E-06	7.4	No binding			
8			-CF ₃	4.79 E+06	7.14 E-02	1.52 E-08	14.0	1.27 E+06	2.53 E-01	2.38 E-07	4.0
9			-CF ₃	1.81 E+05	4.75 E-02	2.63 E-07	21.1	No binding			
10 PF-431396			-CF ₃	3.08 E+06	5.36 E-04	1.81 E-10	1864.2	5.76 E+06	4.04 E-02	6.92 E-09	24.7
11 PF-4554878 defactinib			-CF ₃	2.41 E+06	4.41 E-03	1.93 E-09	226.7	1.48 E+06	3.57 E-02	2.39 E-08	28.0
12 PF-719			-CF ₃	1.39 E+06	2.03 E-01	1.52 E-07	4.9	2.19 E+06	5.46 E-02	2.45 E-08	18.3

9.2.2 The hydrophobic L567-ligand interaction in FAK is crucial for high potency and long residence time inhibition

Within this subset, the phenylsulphonamide moiety of **10** at position **R**¹ showed the most potent binding followed by **1** containing a pyridyl-methansulphonamide with a 4-fold smaller potency. The benzene ring of **10** was thought to provide a more energetically favorable hydrophobic surrounding than the pyridine ring of **1** for the interaction with the DFG flanking L567. If this polarity of the ring system is increased with two nitrogens in **11** the affinity decreases. This change in affinity seems to be linked to a bigger amount to a change in the inhibitors off-rate as the on-rates of **1**, **10** and **11** are similar. For PYK2, we did not observe differences in the affinity and binding kinetics comparing **1**, **10** and **11**. Likely, the helical DFG-motif because of the leucine interaction does not form like in FAK as observed in the crystal structure (**Fig. 5**). We observed a decreased affinity compared to **1** for the phenylsulphodioxide in **5** at **R**¹ likely because of a shorter distance spanned by **5**. This as well leads to a more than 2-fold increase in the inhibitors off-rate. When removing the sulphur moiety we observed different binding affinities and kinetics. While methylaminoindoline (**6**) and N-methylpyridylmethane (**8**) showed a nanomolar potency because of a 10-fold increase in the off-rate, propylbenzene (**9**) and fluoro-propylbenzene (**7**) resulted in a 350-fold and 1300-fold loss in potency. The addition of the fluorine decoration (**7**) triggered a 2-fold drop in the inhibitors k_{off} when compared to the benzene (**9**). This was similar for PYK2. Moving the sulfur moiety to the **R**² position in **12** results in a 200-fold loss in activity on FAK compared to **1** triggered by a 60-fold higher off-rate while maintaining PYK2 potency, thereby creating a PYK2 selective inhibitor¹¹³.

The - from the DFG motif - more distant **R**² substituent, as well showed altered potency and binding kinetics. A phenyl in **3** results in a 93-fold drop in potency compared to the oxindole in **1** triggered by a 60-fold drop in the on-rate. This was expected, as a phenyl ring does not allow the formation of a hydrogen bond with R426. Unexpectedly, we determined a reduction in affinity with the quinoline **4** in **R**². However, determining an on-rate in the range of **4** is at the detection limit of SPR and the data might be unprecise. With PYK2, we observed the lowest off-rate with a phenyl (**5**) in **R**² although the affinity was decreased 82-fold compared to **1**. The quinoline derivative (**4**) resulted in a decreased affinity and increased off-rate compared to **1**.

9 Results

The absence of the trifluoromethyl R^3 group resulted in a 430-fold loss in potency in FAK and were as well lowered in PYK2. Binding kinetics were affected as expected but the difference results from a loss of both association kinetics and residence time here.

Comparing the sequence around these key interactions we identified, FAK-R426 is surrounded by a smaller FAK-C427 while the bulkier PYK2-I430 is following the PYK2-R429. This might restrict the arginine flexibility in FAK thereby preventing an interaction as seen in (Fig. 5). Overall, changes in R^1 resulted in larger differences of affinity for PYK2 compared to FAK. Compounds **6** and **8** contain an electron donor and preserved a potency in the nanomolar range. Compounds **7** and **9** however, did not show binding beyond the capacity of the techniques used here. Including the sulfonamide-moiety was most effective for PYK2 potency. Regarding a PYK2 SKR, we unfortunately only observed fast binding kinetics ($5.5E-01 \text{ mol}^{-1}\cdot\text{s}^{-1} - 1.75E-02 \text{ mol}^{-1}\cdot\text{s}^{-1}$) within this inhibitor set.

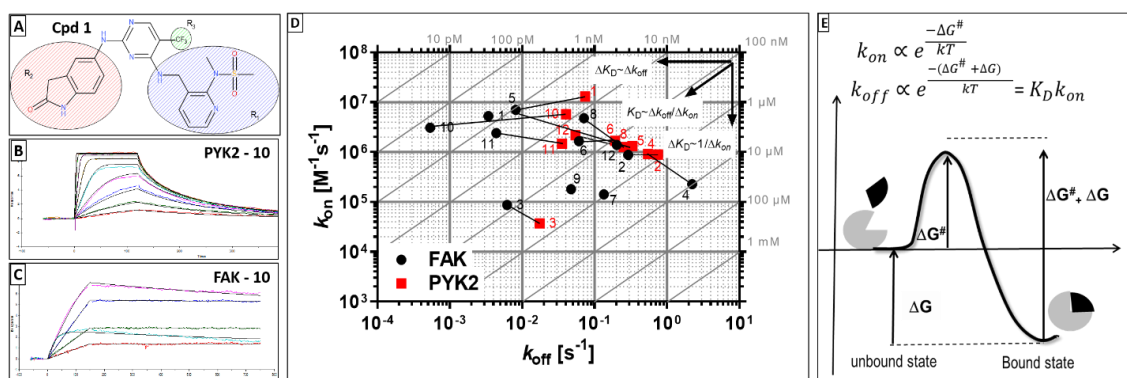


Fig. 13: Three substituent sites on PF-562271 R^1 , R^2 and R^3 were considered to study the interactions in the kinase binding sites (A). (B) SPR sensorgram of PF-431396 and PYK2. (C) SPR sensorgram of PF-431396 and FAK. (D) k_{on} - k_{off} -plot of the SPR-data. FAK is depicted in black circles and PYK2 in red squares. The Compound Name is indicated for each data point. (E) Schematic illustration of the binding free energy profile and relation between thermodynamic (K_D) and kinetic properties of the complex.

In the k_{on} - k_{off} -plot displayed in Fig. 13, we compared the selectivity profiles of both FAK and PYK2. Most inhibitors in this series have a similar on-rate in the range of less than 10-fold 10^6 - $10^7 \text{ mol}^{-1}\cdot\text{s}^{-1}$. However, the off-rates are more related to the change in the affinity (i.e. ΔG , see a schematic energy profile in Fig. 13). For PYK2, both association and dissociation rate constants are similar and no conclusions for a regulation in an SKR can be drawn from this inhibitor set.

9 Results

9.2.3 Slow off-rate inhibitors induce a helical conformation of the activation loop in FAK via a hydrophobic interaction with L567

To better understand the influence of the ligand scaffold on the binding mode and especially its involvement in the formation of the uncommon helical DFG motif on FAK, we have solved six crystal structures of FAK in complex with amino pyridine derivatives with different substitutions at the **R¹**, **R²** and **R³** position (**Fig. 14**).

9 Results

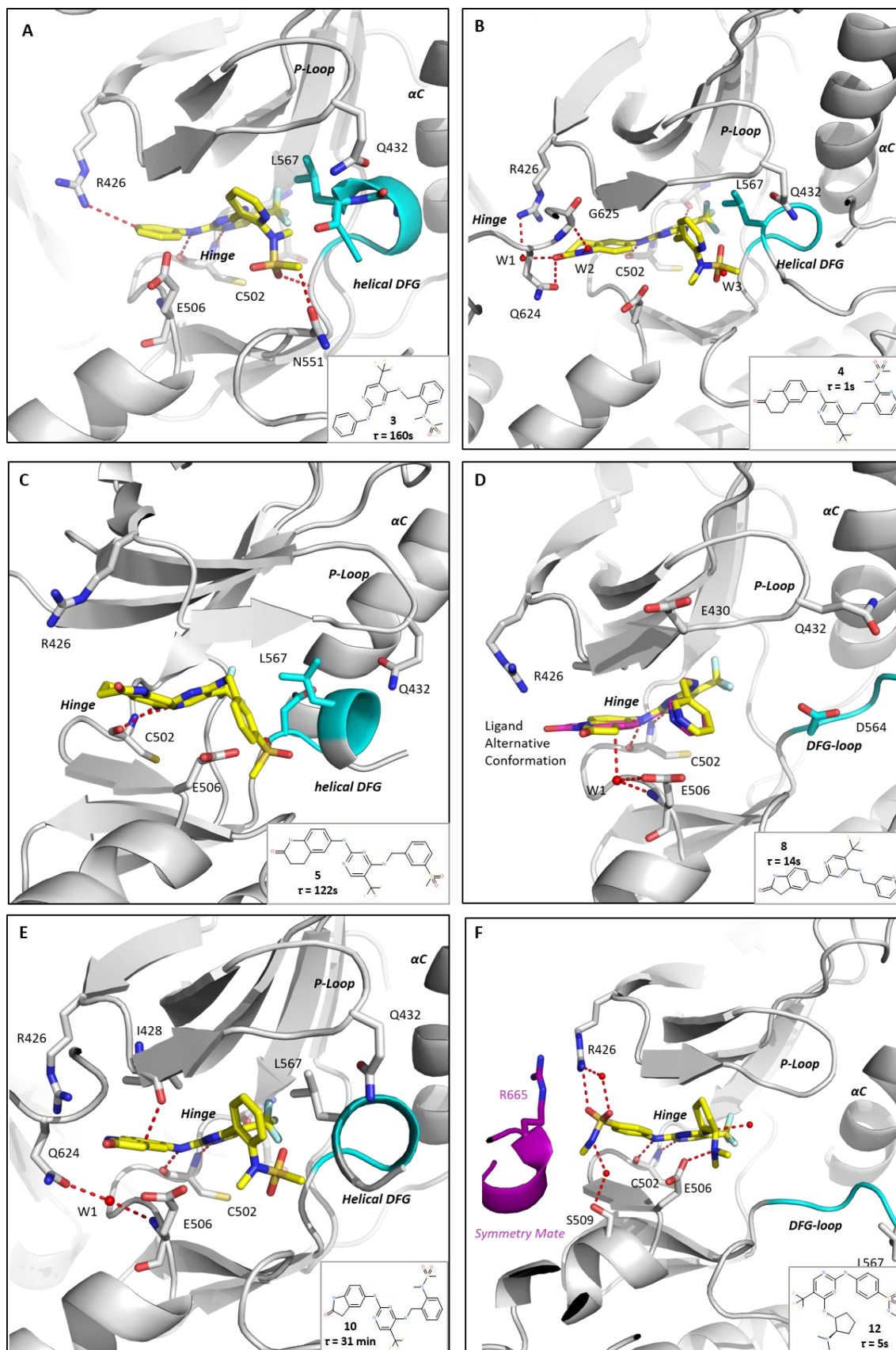


Fig. 14: Inhibitors with long residence times induce a helical conformation of the activation loop in FAK via a hydrophobic interaction with L567. Panels A-F show the interaction with FAK and the inhibitor indicated in each figure. For clarification, the respective residence time derived by SPR is shown with each inhibitor structure. Structural motifs are indicated in each structure distinguishing between a helical DFG-motif or a DFG-motif loop. P-Loop, hinge region and α C are labelled for orientation. Where indicated, crystallographic symmetry mates (F) or alternative inhibitor conformations (D) are shown. PDB IDs: 6yt6 (A), 6yq1 (B), 6yoj (C), 6yvs (D), 6yr9 (E), 6yvy (F).

9 Results

The binding mode of **10** is very similar to the binding mode of **1** published before¹¹⁰. **10** binds in the FAK ATP binding pocket and forms three hydrogen bonds with the FAK hinge region. Specifically, we observed interactions with the backbone of FAK-E500, and C502. When analyzing the residue of **R²**, we saw that the amino-oxindole oxygen atom is in proximity to FAK R-426. The Trifluoro-moiety in **R³** characteristically binds to the hydrophobic back of the pocket with interactions to M499, D564 and L567. This explains the significantly decreased potency on FAK when removing the trifluoro-moiety in **2**. Strikingly, the sulphonamide moiety **R¹** is involved in a hydrophobic interaction with FAK-L567 as discovered for **1** before as well as forming a hydrogen bond to the preceding D564, which in summary stabilized the DFG motif into a helical conformation. This binding mode is very similar to the FAK inhibitor TAE226^{130,131}.

Changes in **R¹** seem to be the major cause for the helical stabilization of the FAK DFG. The inhibitors containing a sulphonamide moiety in **R¹** – **3**, **4**, **5** and **10** – we observed the helical DFG formation. Strikingly, these inhibitors as well present the longest residence time within this inhibitor set. **4** interacted with FAK-L567, but our SPR data suggests a fast off-rate, which is not in agreement with our hypothesis. The on-rate determined for **4**, however, is at the detection limit of the SPR technique and a miscalculated on-rate and hence off-rate cannot be excluded. Nevertheless, **4** shows a helical stabilization for FAK. For **5**, the FAK-L567 interaction is rotated by 180° to form a T-like stacking because of the shorter distance spanned by the phenylsulphodioxide moiety. An absence of the **R¹** sulphonamide prevented the stabilization of a helical DFG in **8** and **12** and resulted in shortened off-rates in comparison to **1**.

12, which is structurally divergent and has **R¹** and **R²** moiety swapped, interestingly binds in a 'flipped' binding mode as compared to **1**. The sulphoxide-moiety interacts with the FAK-R426 here, while no interaction is observed with the DFG-Loop. The decrease in potency for FAK leads to a PYK2 selective inhibitor.

The oxindole ring of **1** and **10** in **R²** interacted with FAK-R426 via a hydrogen bond and showed hydrophobic interactions to the P-Loop preceding residues I428 and G505. Changes in **R²** generally did not alter the binding mode observed. A lack of the trifluoro-group resulted in a potency loss on FAK and in all structures the trifluoro-group pointed to the back of the FAK binding pocket.

9 Results

As expected from both SAR and SKR, the slowest off-rate inhibitors are **5** and **10**, which bound very similar to **1**. The DFG-motif is stabilized into a helical conformation upon hydrophobic interaction with FAK-L567. This generally shows the inhibitor binding conformation as a function of structural rearrangement of the DFG Loop. An interaction with FAK-R426 may alter the on-rate of this series. The slowest inhibitor among this set, **10**, shows both interactions.

9.2.4 The selectivity profile of FAK and PYK2 was dictated by the formation of a helical conformation of the DFG motif

We compared our structural data of FAK with published structures of PYK2 in complex with **1** (PDB 5tob) (**Fig. 5**), **10** (PDB 3fzr, **Fig. 15**) and **12** (PDB 3h3c, **Fig. 15**) to identify crucial interaction residues that are relevant for the selectivity for either FAK or PYK2. From our SPR analysis we observed that **10** showed a dissociation rate on FAK of $1.2 \times 10^{-4} \text{ s}^{-1}$ which is more than two orders of magnitude slower than that reported for PYK2¹³², despite the similar IC_{50} values.

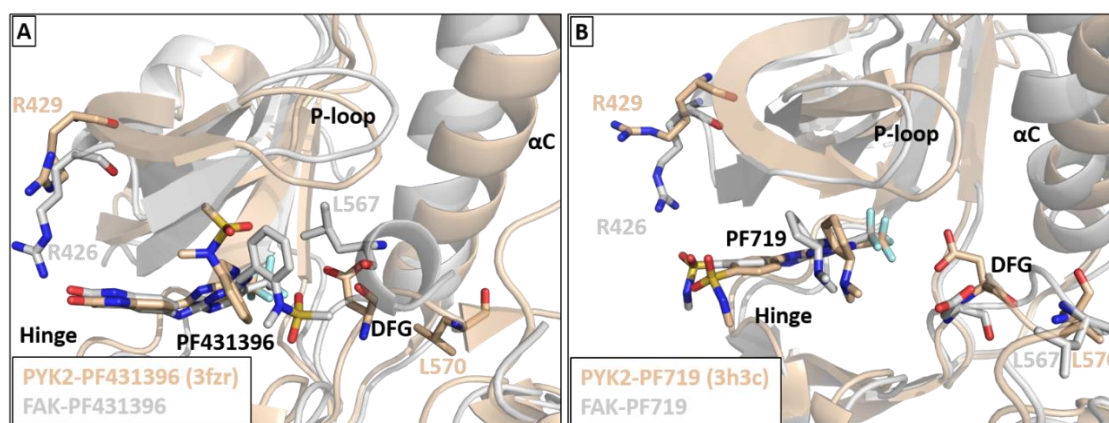


Fig. 15: The selectivity profile of FAK and PYK2 is dictated by the formation of a helical conformation of the DFG motif in FAK. FAK and its inhibitor are coloured grey and PYK2 and its inhibitor are coloured wheat. The inhibitor is indicated in the figure. A Structural alignment comparing the interaction of **10** on FAK (PDB 6yr9) with literature data for **10** on PYK2 (PDB 3fzr¹³²). B Structural alignment comparing the interaction of **12** on FAK (PDB 6yvy) with literature data for **12** on PYK2 (PDB 3h3c¹³³).

The superimposed crystal structures of FAK and PYK2 in complex with **10** show similar conformations as reported for **1**. However, we observed a 9-fold potency difference for FAK vs PYK2. Strikingly, the helical DFG-motif is missing in PYK2, as reported for **1**. The PYK2 interaction is characterized by an interaction with the P-Loop presiding residues L431, G432 and V439 and displayed a DFG-out conformation. We found differences in the P-Loop conformation and α C when comparing PYK2 to FAK. We found a striking sequence difference for PYK2 and FAK where in FAK we have a Q432 versus a F435 in PYK2 (**Fig. 5**) that may be involved in the stabilization of the DFG-Loop

9 Results

as Q432 interacts with the DFG glycine G566 in FAK but not in PYK2. Additionally, we observed the oxindole in FAK to interact with R426, but not with the corresponding PYK2-R429.

The superimposed crystal structures for **12** on both FAK and PYK2 show the mechanism for the 25-fold selectivity of **12** for PYK2 over FAK¹¹³. The sulphonamide position shifts from the DFG-Loop in **1** to the other side of the binding pocket and interacts with the FAK-R426 and PYK2-R429, respectively. No interaction of **12** with the DFG-Loop is observed, resulting in a type I interaction. **12** did not induce a helical DFG-Loop upon binding in support of the hypothesis that the FAK/PYK2 selectivity can be modulated via the induction of a helical DFG motif.

9.2.5 Binding potency and kinetics of FAK and PYK2 in living cells

Next, we wanted to both validate our findings, as well as investigating whether the effects observed *in vitro* translate to a cellular system. For that, we applied the NanoBRET target engagement assay¹²¹, using living cells under physiological conditions. The full-length expressed FAK and PYK2 proteins were analyzed in a tracer competition format with cellular substrate ATP present in cellular concentration⁹.

For the target engagement assay, the apparent tracer affinity was determined and used as an assay input parameter to later make determined affinities comparable. This apparent tracer K_D was found to be similar for both FAK and PYK2 (**Suppl. Fig. S 11**). The target engagement assay was performed with a fixed tracer concentration and resulting inhibitor IC_{50} values were converted to apparent K_I values using Cheng-Prusoff correction²⁸. Representative results for **1** and **10** can be seen in **Fig. 16** and **Suppl. Fig. S 12**. In comparison, the cellular affinity was 10-times higher than compared to SPR data *in vitro* for both FAK and PYK2, likely because of intracellular ATP present in the assay. However, we see an overall good correlation with our SPR data (**Fig. 16**). The *in vitro* selectivity was translated to cells, with **5** being most selective for FAK over PYK2 showing a 330-fold window and **12** being PYK2 selective with an 8-fold selectivity window.

The cell penetrant tracer for the NanoBRET assay as well allows for a kinetic assessment of inhibitor half-lives in a wash-out format. To investigate the binding kinetics, we hence performed wash-out experiments. The tracer used had sufficiently rapid kinetics (**Suppl. Fig. S 11**). The respective inhibitors were incubated at $10 \times IC_{50}$ to

9 Results

guarantee 90% target occupancy as a starting point and to make results comparable. We then diluted the samples 100-fold for the wash-out and tracer association upon inhibitor dissociation was measured. From the resulting curves we fitted the half-live (Table 6, Fig. 16, Suppl. Fig. S 16). We observed remarkably slow off-rates for **10** on FAK and distinguishable slower kinetics for **1** on FAK while other inhibitors were within the assay tracer association noise. We did not observe any slow compounds for PYK2 in cells which is in agreement with our SPR data.

Table 6: NanoBRET target engagement and wash-out data. The *in cellulo* potency and kinetics of a series of inhibitors based on **1** were determined using NanoBRET target engagement and wash-out assays. $K_{i, app}$ = Cheng-Prusoff corrected Inhibitory Concentration for 50% (IC_{50}) observed under cellular conditions, k_{obs} = observed kinetic constant, $t_{1/2}$ = half-life calculated as $\ln(2)/k_{obs}$

NanoBRET, <i>in cellulo</i>	FAK			PYK2		
	$K_{i, app}$ [M]	k_{obs} [1/min]	$t_{1/2}$ [min]	$K_{i, app}$ [M]	k_{obs} [1/s]	$t_{1/2}$ [min]
1	(9.3±1.2)E-09	(5.9±0.2)E-02	11,8	(1.5±0.2)E-07	(5.1±3.0)E-01	1,4
2	(4.1±1.3)E-06	n.d.	n.d.	(2.3±0.4)E-05	n.d.	n.d.
3	(1.2±0.1)E-08	(2.2±0.7)E-01	3,1	(1.2±0.1)E-7	(6.3±5.3)E-01	1,1
4	(3.2±0.3)E-09	(4.0±0.8)E-02	17,5	(8.4±0.7)E-08	(2.7±0.2)E-01	2,6
5	(1.1±0.1)E-08	(2.7±0.6)E-01	2,6	(3.6±0.3)E-06	(7.3±3.9)E-01	1,0
8	(7.6±1.4)E-06	> 1	0,7	(2.6±1.2)E-05	> 1	0,7
10	(8.7±1.0)E-10	(1.2±0.8)E-02	57,3	(8.0±0.4)E-08	(4.9±3.0)E-01	1,4
11	(1.0±0.2)E-09	(1.3±0.2)E-01	5,4	(6.3±1.1)E-07	(5.5±2.2)E-01	1,3
12	(7.8±0.3)E-06	> 1	0,7	(9.7±1.6)E-07	(5.3±1.0)E-01	0,7

In summary, we confirmed that **10** and **1** which had the longest residence time within this series are as well slow in cells. As expected from the SPR data we only observed fast binding rates for PYK2. Gratifyingly, the observed rank order for the kinetics is in agreement with the SPR data on FAK. Inhibitor **5** showed cellular selectivity for FAK via a more potent affinity, while **10** may show kinetic selectivity for FAK over PYK2. We demonstrated, that the residence time can be used as a parameter for determining cellular selectivity. Hence, the NanoBRET technique proved useful in determining both cellular potency and binding kinetics.

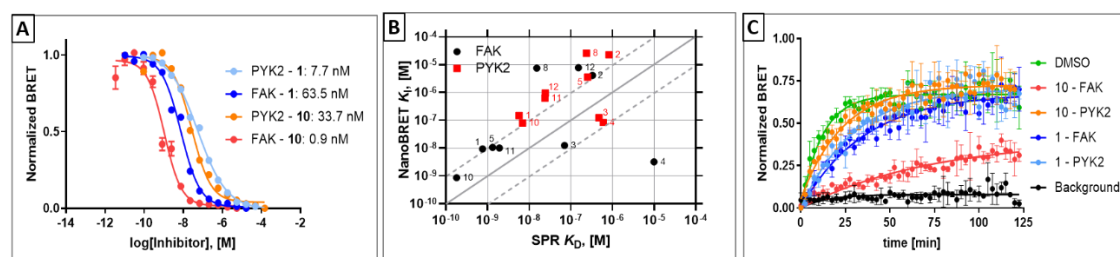


Fig. 16: Both binding potency and kinetics translate from *in vitro* into the cellular system. (A) Target engagement assays for FAK and PYK2 for **1** and **10** as indicated in the figure legend. (B) Correlation of the *in cellulo* potency with the potency determined *in vitro* by SPR for entire inhibitor series as indicated in the figure. (C) NanoBRET wash-out experiments for **10** and **1** in comparison to background data and tracer only (DMSO added instead of test compound).

9 Results

9.2.6 Structural mechanisms affecting the protein binding site flexibility in FAK and PYK2

Lastly in this study, we wanted to investigate structural differences in FAK and PYK2 on the inhibitor binding behavior and both answer whether PYK2 can assume a helical DFG-motif or show slow off-rate kinetics and if the FAK slow kinetics could be reversed by mutagenesis. Hence, we made 12 mutant constructs and tested them in both NanoBRET target engagement (Table 7, Suppl. Fig. S 13, Suppl. Fig. S 14, Suppl. Fig. S 15) and wash-out (Table 8, Suppl. Fig. S 17, Suppl. Fig. S 18) assays (Fig. 17).

Table 7: NanoBRET site directed mutagenesis to validate FAK-L567 as the driver of slow off-rate inhibition of FAK. Depicted is the fold-change to FAK and PYK2 wild type protein IC_{50} s for the FAK and PYK2 mutants, respectively, determined using NanoBRET target engagement assay. Blue indicates a fold-change of more than 2, indicating the potency decreased for the mutant in comparison to the WT while red indicates a fold change of less than 0.5, indicating the potency increased for the mutant compared to the WT. This table is graphically displayed in Suppl. Fig. S 15.

Cpd	FAK									PYK2				
	WT	R426S	R426A	L567A	E506Q	E506I	E430S	E430Q	Y576F+Y577F	WT	F435R	E474Q	F435Q	Y579F+Y580F
1	1,0	1,0	0,91	13	1,6	19	1,3	0,90	1,0	1,0	1,8	8,8	1,4	1,1
3	1,0	1,7	1,4	28	2,3	2,1	2,0	1,9	1,5	1,0	1,4	5,1	1,1	1,4
4	1,0	1,2	1,0	42	2,4	1,5	1,4	1,3	1,2	1,0	1,6	6,2	0,8	0,7
5	1,0	1,4	1,2	3,2	6,6	1,9	1,3	1,2	1,2	1,0	1,2	2,1	0,5	0,5
8	1,0	1,6	1,2	1,6	3,4	2,0	2,5	1,5	1,7	1,0	1,4	4,9	0,7	0,7
10	1,0	1,6	1,3	46	1,8	2,3	1,6	1,5	1,3	1,0	1,9	5,4	0,9	0,8
11	1,0	1,6	1,7	98	3,4	2,2	1,8	1,4	1,5	1,0	1,6	3,1	0,8	0,7
12	1,0	0,68	1,6	0,38	19	0,00038	3,4	0,65	1,0	1,0	1,4	9,5	0,7	0,9

Table 8: NanoBRET site directed mutagenesis to validate FAK-L567 as the driver of slow off-rate inhibition of FAK. Depicted is the fold-change to FAK and PYK2 wild type protein k_{obs} for the FAK and PYK2 mutants, respectively, determined using NanoBRET wash-out assay. Blue indicates a fold-change of more than 2, indicating the k_{obs} increased for the mutant in comparison to the WT (overall faster kinetics). A fold change of less than 0.5 is marked in red, indicating the k_{obs} decreased for the mutant compared to the WT (overall slower kinetics).

Normalized k_{obs} Ratio	Mutant / WT							
	1	3	4	5	8	10	11	12
FAK	1.0	1.0	1.0	1.0	1.0	1.0	1.0	1.0
FAK-R426S	0.9	0.8	13.2	0.7	1.0	1.0	0.8	1.0
FAK-R426A	1.0	0.8	1.6	0.7	1.0	1.4	1.0	1.0
FAK-L567A	5.0	3.2	7.9	0.7	0.6	22.7	6.0	0.6
FAK-E506Q	2.2	2.5	2.1	1.1	1.0	1.9	3.8	1.0
FAK-E506I	1.4	1.7	1.6	3.0	1.0	1.1	2.1	1.0
FAK-E430S	0.9	1.4	1.0	0.6	1.0	1.1	1.1	1.0
FAK-E430Q	0.8	1.0	0.9	0.7	1.0	0.8	0.9	1.0
FAK-Y576F+Y577F	1.0	1.1	1.0	0.5	1.0	1.2	0.7	1.0
PYK2	1.0	1.0	1.0	1.0	1.0	1.0	1.0	1.0
PYK2-F435R	2.0	1.6	3.8	1.4	1.0	2.0	1.8	1.9
PYK2-F435Q	0.2	0.6	0.9	0.3	0.1	0.4	0.5	0.3
PYK2-E474Q	0.8	0.8	1.3	1.1	0.9	1.1	1.4	1.6
PYK2-Y579F+Y580F	0.4	0.3	0.8	0.4	0.3	0.4	0.5	0.3

9 Results

First, we tested the FAK-L567 interaction by mutagenesis to alanine (FAK-L567A). Gratifyingly, we observed a large decrease in potency for the inhibitors involved in FAK-L567 interactions – **1**, **3**, **4**, **5** and **10** - as judged by the crystal structures (**Fig. 5**, **Fig. 14**, **Fig. 15**), but an increase in potency for **12** which did not show a crystal contact to FAK-L567. More interestingly, we were able to demonstrate a reversed binding kinetic effect, where the half-lives for the inhibitors **1**, **3**, **4**, **10** and **11** reversed from a slow binding for FAK wildtype to a fast binding for FAK-L567A (**Fig. 17**). For **11**, where we did not obtain crystallographic information, the FAK-L567A shows very strong effects, indicating a similar binding mode as to the other slow off-rate inhibitors **1**, **3**, **4**, **5** and **10**. For **5**, the hydrophobic interaction to FAK-L567 seems to only be affected in potency, but not in kinetics which fits the FAK wild-type NanoBRET results that showed high selectivity for FAK versus PYK2, but no prolonged kinetic selectivity.

To investigate the polar interaction of the inhibitors oxindole moiety in **R²** with FAK-R426, we mutated to alanine (FAK-R426A). We observed no change in potency nor binding kinetics for the inhibitor series, suggesting that the involvement of FAK-R426 in the binding behavior as observed by crystal structure interactions seems to have no impact. Indeed, crystallographic analysis showed that the interaction with FAK-R426 is only present in half of the molecules in the asymmetric unit cell. Otherwise the interaction was observed to be unstable and mediated by water. For **4**, we observed similar potency for the FAK-R426S mutant but did interestingly observe a largely faster kinetics. As judged from the crystal structure (**Fig. 14**) the FAK-R426 interaction is mediated by a water molecule here and the replacement of water may be connected to the faster kinetics here, as the binding of the water cannot happen with the hydroxyl group of the serine residue in the mutant. It can be hypothesized, that the incorporation of a water into the wild-type binding interface happens as an induced fit mechanism.

In **1**, we observed an interaction of PYK2-E509 with the pyridine nitrogen (**Fig. 5**) but not for FAK-E506. To test whether this rigidifies the PYK2 protein binding site we mutated FAK-E506 to E506Q to test different electrostatics and E506I to add more hydrophobicity to the binding site. Both showed a decreased potency indicating that a change is unfavored in FAK. Specifically, for FAK-E506Q we observed less potency for all

9 Results

inhibitors but **1** and **10**, indicating this interaction does not play a role in their binding interfaced supporting what was seen in the crystal structures. **12** on the other hand was largely affected and showed decreased potency because of a main interaction with FAK-E506. Changing the electrostatics is hence unfavored for FAK. The binding kinetics were changed for **1**, **3**, **4** and **11**. For **4** and **11** we saw a water mediated bond. Changing the electrostatics may influence the corporation of this water and hence change the kinetics to more fast kinetics. When making the residue more hydrophobic as in FAK-E506I, we observed a large decrease in potency for **1**. This is in accordance with the pyridine ring being more polar than the phenyl in **10**, suggesting more hydrophobicity is unfavored for **1**. For **12** on the other hand we observed a large increase in potency, which makes sense as judged from the crystal structure, where the hydrophobic five membered ring of **12** is now in a more hydrophobic surrounding. The kinetics did change for **5** and **11** when more hydrophobic, suggesting a potential water displacement here. Altogether, this may indicate an interaction of E506 with the binding site when mutated and this residue to make the protein more rigid and potentially prevent a helix formation in PYK2.

The PYK2 P-Loop was observed to be stabilized by polar interactions of the PYK2-E432 sidechain with the PYK2-G347 backbone. In FAK FAK-E430 is oriented towards the solvent and does not stabilize the P-Loop. Hence, the PYK2 active site might be limited in flexibility to not be able to form the helical DFG needed for slow off-rates. We prepared two mutants, FAK-E430S and FAK-E430Q to try to establish a similar rigid FAK P-Loop, potentially preventing the helical DFG. The potency was decreased for **3**, **8** and **12** indicating a P-Loop interaction lost here, but the kinetics were similar to wild-type FAK. The slow off-rate inhibitors still were able to induce the helix and P-Loop rigidity may not be a part of the helix prevention in PYK2. We as well prepared a mutant for PYK2-F435 which was a glutamine in FAK. PYK2-F435Q and PYK2-F435R did not show a change in potency for the series, and an even reduced binding kinetics for PYK2-F435R. Gratifyingly, we observed a shift to slower kinetics for the FAK-like PYK2-F435Q mutant which indicates this residue is crucial for the low off-rate kinetics. Whether PYK2 could form a helix in this construct can only be speculated on, as no crystal structure was obtained.

Next, we observed that PYK2-E474 located in the α C might contribute to less flexibility in PYK2 and hence we mutated it to PYK2-E474Q. We observed a decreased

potency but similar binding kinetics as for PYK2 WT. This may support the hypothesis that the interaction increases PYK2 rigidity.

Lastly, we tested whether protein phosphorylation in the cell may impact binding properties for this series and prepared phosphodead mutants for both FAK and PYK2, mutating FAK-Y576+Y577 and the respective PYK2-Y579+Y580 to phenylalanine. In FAK we did not observe a difference in potency, while in PYK2 there was 2-fold increase in potency. We did not observe an impact on the binding kinetics for the FAK phosphodead mutant but observed shifts to slower kinetics for the PYK2 phosphodead mutant, indicating a phosphorylated version in the in-cell NanoBRET wild type experiments.

The SPR *in vitro* data suggested FAK-R426 might impact the binding kinetics, specifically the inhibitors on-rate. Comparing the mutagenesis and NanoBRET data to the SPR data, we could not confirm this behavior. Likewise, for **4**, where we observed an on-rate at the SPR detection limit, we can report slower kinetics on FAK in support of our hypothesis in the cellular system. In conclusion, the SPR data may be miscalculated here.

In summary, for PYK2 no mutants showed slower binding kinetics. As a representative we chose **10**, that only shows fast kinetics for PYK2. Basted on crystal structures and mutagenesis, we hypothesize it is the overall reduced mobility of PYK2 as compared to FAK that prevents the helical DFG and hence slow kinetics. Likewise, the mutagenesis analysis showed that the FAK-L567 interaction is crucial for slow off-rate kinetics in FAK and proves to be targeted for slow off-rates and avoided in order to yield fast binding kinetics.

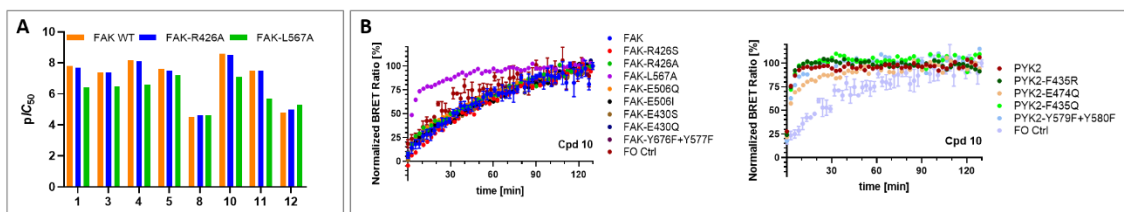


Fig. 17: Structural stability of the ligand binding sites in FAK and PYK2 explored by site-directed mutagenesis: A) Mutant potency determined by NanoBRET for the inhibitors indicated in the figure. B) Representative wash-out experiment for **10** on the mutants tested on FAK and PYK2 respectively. The signal was normalised to the tracer control and fitted using a one phase exponential decay. FO Ctrl=Full occupancy control (no wash-out performed).

9 Results

10 DISCUSSION

10.1 THE IMPORTANCE OF CELLULAR CHARACTERIZATION OF INHIBITOR POTENCY FOR INHIBITOR SELECTIVITY

10.1.1 The presence of ATP changes inhibitor potency and selectivity in cells

Most inhibitors target the ATP binding site either directly or allosterically. As a consequence, cellular ATP directly competes with inhibitor binding and the K_M for this co-factor therefore influences the inhibitor potency. The concentration of ATP in cells is estimated to be in the range of 1 to 3 mM and typical K_M s are in the micromolar range and hence very potent inhibitors are needed for a full inhibition of the targets in competition with ATP. Recently, we compared the activity of the approved drug crizotinib for its designated targets ALK and MET and its off targets measured in enzyme kinetic assays and in cells using NanoBRET assays⁹ (**Fig. 18**). The results of the cellular NanoBRET assay correlate with traditional in cell ELISA IC_{50} s. In order to deconvolute the effect of compound cell penetrance and the effect of the cellular ATP present, we studied inhibitor potency in both permeabilized cells and ATP depleted cells (after addition of an ATP-pump inhibitor). This comparison revealed the influence of cell penetration and the presence of high ATP concentration on inhibitor potency for individual kinase targets and inhibitor tested (**Fig. 18D**). As the K_M s for ATP differ for each kinase but the ATP concentration remains similar, inhibitor potencies are affected based on the individual kinases K_M s, which led to a much narrower selectivity profile for the kinome when comparing *in vitro* KinomeScan binding data with in-cell NanoBRET data (**Fig. 18C**). In our study, kinases which have a higher K_M did not shift to lower potencies as much as kinases showing a low K_M for ATP in cells. Furthermore, the K_M for ATP for individual kinases is dependent on kinase activation states¹³⁴ and interaction partners. These influences need to be addressed in future studies.

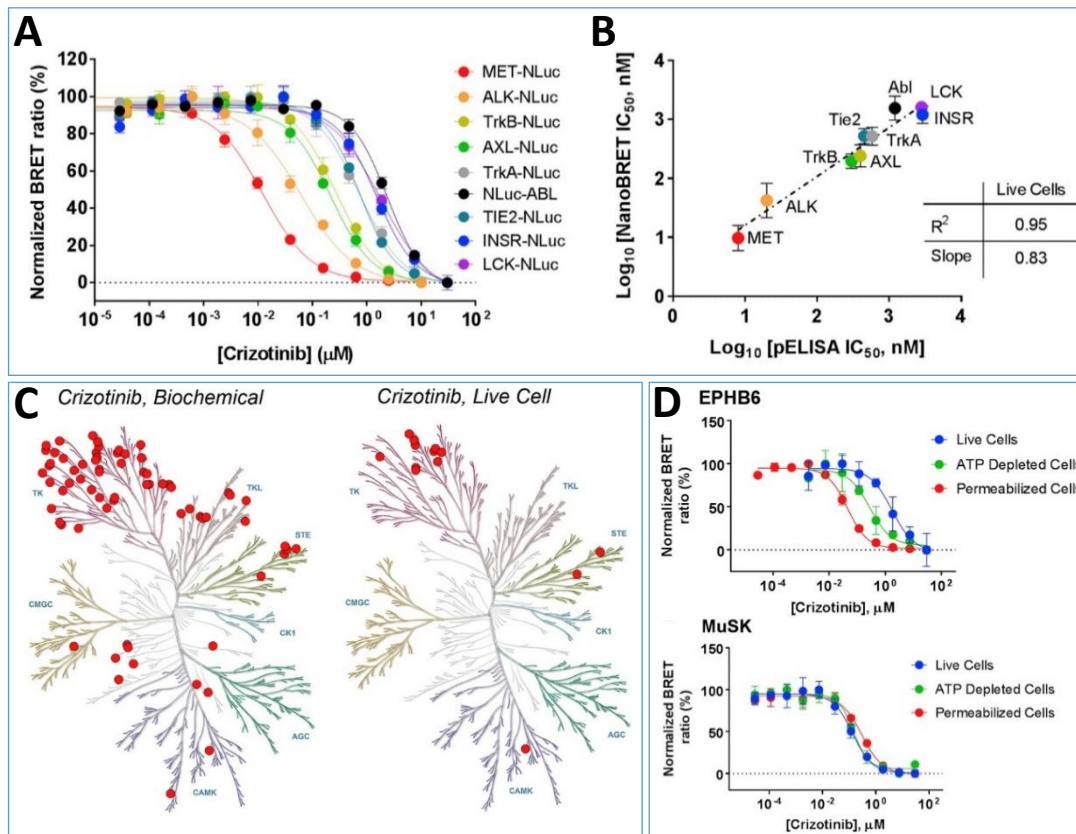


Fig. 18 *In cellulo* profiling of the approved drug crizotinib⁹. Literature known biochemical hits of crizotinib were determined in cells and compared to *in vitro* biochemical data (C). The hits were validated in a follow up titration (A) and this data correlated well with an *in vitro* ELISA (B). However, differences between cellular and *in vitro* data were observed, which we investigated further. We found the K_M for ATP and hence the competition of the compound against ATP to be a main reason for differences (D). This behavior was not observed for all kinases tested but differs for each individual kinase.

10.1.2 Examples of unexpected cellular selectivity

During my thesis, I contributed to the characterization of several chemical probes, which are tool compounds used to question a specific targets biology and therefore have several very tight criteria: A chemical probe needs to be very potent both *in vitro* (< 50 nM) and in cells (< 1 μM) and show a very narrow selectivity profile where the closest off-target needs to show an at least 30-fold window. Additionally, a chemically related negative control compound with a potency window of at least 100-fold needs to be developed. Within these projects, we frequently investigated the selectivity profile derived from *in vitro* assays for their effect in live cells. Some of these are presented here:

In a first project, we developed a chemical probe for Cyclin-G associated kinase (GAK)¹. The probe candidate presented a very narrow selectivity with very potent IC_{50} values for GAK and the closest off-target as the related kinase RIPK2 with a 50-fold window. When testing the compound in cells, we observed a complete shift to lower

10 Discussion

potency for the target GAK but a near 1:1 correspondence of the potency of the off-target RIPK2 in cells – shrinking the selectivity window to only 3-fold. This led us to propose the compound as a dual GAK/RIPK2 probe molecule which we supplemented with both a negative control compound and a control for RIPK2 that was very potent in cells, but not probe material for RIPK2. Likewise, the chemical probe PF-04554878 was suggested as a dual FAK/PYK2 probe based on *in vitro* IC_{50} s (0.2 nM/0.1 nM, respectively), but the potency in cells shows it was more potent on FAK versus PYK2 (IC_{50} = 36 nM/820 nM) giving opportunity to unravel FAK biology as a tool compound¹³⁵.

In another project, we aimed to develop a probe molecule for ALK4 and ALK5, two closely related kinases involved in TGF- β signalling⁴. Our probe candidate was observed to have some off-targets *in vitro*, which we could clear using NanoBRET, where we observed potency shifts to lower potency for the off-targets. This was as well seen for our p38 α/β probe⁷.

In different projects, we observed cellular potency to be different from *in vitro* determined potencies. These include a study on the ephrin receptors⁸, a study on JAK3² and a project for CLK3⁶.

10.1.3 Comparison of the different techniques used in this study: A typical screening cascade

Within this study, we used different techniques to assess the potency of the inhibitors. The choice of our assays resembles a more classical screening cascade: With the differential scanning fluorimetry assays we have a very cost effective and fast primary assay available, that only delivers a ranking of compounds for a target kinase, but not in between different target kinases, as only nominal values are obtained. This ranking however can be confirmed with a more accurate tracer displacement assay such as homogenous TR-FRET used here for STK10/SLK. As the tracer binding properties influence the IC_{50} determined, a Cheng-Prusoff correction can be performed taking the individual tracer concentration used into account with the individual tracer K_D determined in that assay system which delivers inter-target comparable values.

As a more direct assay system, surface plasmon resonance has proven helpful in determining a binders K_D for its target. As this assay is lower in throughput it usually is used for closely characterizing a representative set of compounds. The only problem is

the immobilization of the target, which can happen in different conformations with a resulting binding preference of the compound for one target conformation. We observed this for STK10 when comparing different protein constructs with SPR.

A more functional readout is an activity assay. Here, the OMNIA assay¹²⁰ has proven helpful, which enables a kinetic readout of the phosphorylation of a substrate based on the artificial SOX amino acid that enriches fluorescence upon forming a complex of the phosphorylation in proximity with a chelating magnesium ion. With this assay, a functional inhibition of the target can be confirmed, as well as the K_M can be accurately determined as we did here for STK10 (see **Fig. 9**).

Lastly, to investigate the cellular potency of an inhibitor, the NanoBRET target engagement assay has proven very helpful. As a tracer competition assay, we can observe the inhibitors effect in living cells. This adds information about a compounds ability to cross the cell membrane and to inhibit its target with cellular ATP present.

A next step would be an *in cellulo* functional assay which utilizes a phenotypic readout. We applied such assay in a different study, where we discovered that dasatinib inhibits the cell migration of AGP01 gastric cancer cells using a cell migration scratch wound assay.

In this cascade, the assays offer increasing information with increasing cost in time, money and know-how. However, to investigate a compounds effect, several additional experiments must be done *in vivo*, before testing in clinical studies.

10.2 THE IMPORTANCE OF CELLULAR CHARACTERIZATION OF INHIBITOR KINETICS

The kinetics of binding have only recently emerged as an important but largely neglected factor of kinase inhibitor efficacy³³. To efficiently suppress a signaling pathway, the targeted kinase needs to be continuously inhibited. Thus, it has been hypothesized that fast binding on-rates and slow off-rates would be the preferred property of an efficacious inhibitor. Despite optimizing the potency of kinase inhibitors, in the past decade optimization of kinetic selectivity has therefore gained interest as a molecule cannot be active unless it is bound, as Paul Ehrlich once stated. The IMI campaign 'kinetics for drug discovery', where we had a project, has proven the concept helpful in many cases⁶⁷ and has shown, that the limited information of an enzymatic

10 Discussion

assay often is not capturing the complexity of the interaction of a target with a compound. Additionally, we have shown, that with increasing clinical stages, we observe an enrichment in high residence time inhibitors³.

10.2.1 The prolonged target residence time of erlotinib but not gefitinib might be the cause for STK10-related off target toxicity

In the STK10 study, we confirmed that STK10 and SLK are potently inhibited by clinical kinase inhibitors. However, we found this potency to be decreasing in cells. Investigating the potential reasons for this shift in potency, we found the cellular concentration of ATP to be a main competitor for the STK10 active site that shifted compound IC_{50} s at least 10-times. Other factors not investigated could be STK10 autoinhibited states that were reported previously⁸⁰, other intracellular factors competing for the binding site such as protein-protein interactions or the compounds ability to cross the cell membrane.

To confirm the effect of cellular ATP we compared literature values in different assays to our *in vitro* data (**Fig. 19**). We observed a good correlation with literature reported *in vitro* values (Ambit³²), but observed a 10- to 100-fold shift when comparing our results to the cell lysate assay Kinobeads¹³⁶ and a shift of 100-1000-times when comparing to our cellular data. Strikingly, this staged shift of the potency correlates with increasing ATP concentrations in these assays. While the HTRF assay does not use ATP (but a tracer at K_i determined before) and the Ambit assay (an immobilized probe competition assay) used ATP at its K_M for STK10, the Kinobeads assay shows elevated ATP concentrations. However, it becomes clear that not only the ATP concentration, but as well other factors included in cell lysates right-shift the compound potency as different shift from 10-100-fold can be observed. The NanoBRET assay uses cellular ATP concentrations and hence a concentration in the millimolar range.

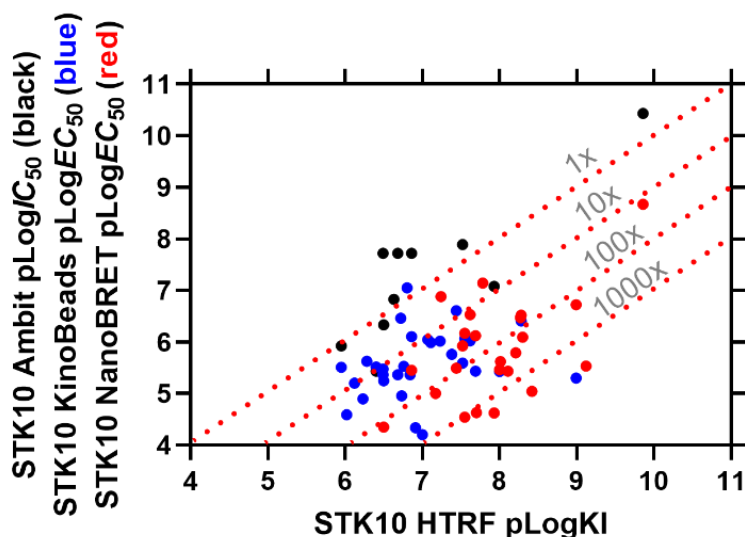


Fig. 19: Dependence of the IC_{50} determined on the concentration of ATP. *In vitro* HTRF K_{is} in comparison to literature activity IC_{50} s (Ambit³⁰, black), cell-lysate EC_{50} s (Kinobeads¹³⁷, blue) and cellular EC_{50} s (NanoBRET, red). Diagonal lines represent fold-change to *in vitro* HTRF data.

After having shown that the clinical compounds potency is much weaker in cells, including that of erlotinib, which was reported to cause skin-related side-effects because of its inhibition of STK10. Nevertheless, we observed a 15-fold lower potency for gefitinib, which was not reported to cause the side-effects. After we investigated cellular binding kinetics behavior of erlotinib and gefitinib on STK10, we observed a much longer inhibition of STK10 by erlotinib than by gefitinib. As the binding kinetics was reported to be related to the drug's efficacy *in vivo*, we think the long residence time of erlotinib on STK10 might be an explanation for the side-effects. The plasma concentration after oral administration of erlotinib was reported to be 2.8 μ M and decreases to 1.5 μ M within 12 hours¹³⁸. Therefore, it is likely that the prolonged residence time of erlotinib in cells may be responsible for the observed skin rash side effect of this drug. Also, the slowest compound, bosutinib, was reported to show rash as a common side-effect. The severity of the skin-rash of EGFR targeting drugs like erlotinib is not reported for bosutinib¹³⁹. This shows, that not only affinity but as well binding kinetics should be investigated in pre-clinical stages of drug development as an optimization parameter of drug safety.

10.2.2 Structural elements affecting inhibitor residence time on STK10

Based on the analysis of the STK10 structures with different inhibitors bound, we found structural rearrangements of the protein to be a good explanation for the prolonged residence times. In particular, we found BIRB-796 and foretinib, two type II kinase inhibitors, to be effectively trapped by a folded and stabilized P-Loop. We assume

10 Discussion

a two-step mechanism, that was described as induced fit before⁵⁶. The two-step binding might happen less fast resulting in a reduced on-rate.

Additionally, we found hydrophobic interactions, in particular with bosutinib and BIRB-796, to be an explanation for prolonged residence times. The sandwiched π -stacking was linked to prolonged residence times before¹⁴⁰.

10.2.3 The design of slow off-rate inhibitors on FAK for improved pharmacological properties

In this study, we investigated the inhibitor binding of Amino-pyrimidines and confirmed existing FAK SARs. With our SPR data, we provided the first SKR study for FAK. Essentially, the induction of a helical DFG-motif that was proposed as a selectivity mechanism for selectivity over PYK2 was shown to be a cause for a kinetic selectivity and proved to be a general mechanism for the design of slow off-rate inhibitors on FAK. We as well showed that PYK2 is not able to form this helical motif despite the high sequence similarity between FAK and PYK2. The SPR data translated into the cellular context of a NanoBRET wash-out assay and proved PF-431396 (**10**) to be as well the slowest inhibitor in this set in cells. Nevertheless, PF-431396 was not used in clinical trials due to a lack of efficacy in phenotypical assays¹⁴¹. The half-life in NanoBRET was determined to be 1 h which was rather short in clinical contexts, highlighting that future drug discovery efforts should optimize for prolonged residence times to improve clinical efficacy. To improve the inhibitor behavior, the Amino-pyrimidine-series was developed into a macrocyclic compound¹⁴² and as well the development of covalent inhibitors¹⁴³ was shown to have an impact on the effectiveness of a drug. Future efforts should include the knowledge about the stabilization of the helical activation loop in FAK and be combined with prolonging the residence time on FAK.

This study highlights, that minor changes in the sequence between related proteins can result in different mechanisms of protein-ligand interactions and result in distinct protein conformations.

10.2.4 Structural elements affecting FAK and PYK2 kinetics

As a major indicator for a slow off-rate inhibitor for FAK, we observed the structural stabilization of an induced helical structure of the DFG-motif. We believe that this structural rearrangement happened in a two-step mechanism, highlighting the

10 Discussion

importance of the induced-fit model. Inhibitors of the amino-pyrimidine series not inducing this structural rearrangement were not observed to be slow off-rate binders. The rearrangement was based on the hydrophobic interaction of L567 with the inhibitors hydrophobic core, resulting in a very stable conformation. Increased hydrophobicity of the compound correlated with increased residence time for FAK. For PYK2, we did not observe this interaction.

10.2.5 Using the NanoBRET cellular wash-out assay for a kinetic compound characterization in cells.

In vivo the lifetime of a drug-target complex is an important parameter for later efficacy and in many cases, cellular and *in vivo* pharmacological activity and duration correlate³³.

Hence, we want to assess whether the NanoBRET cellular wash-out assay used in both case studies for STK10/SLK and FAK/PYK2 is a suitable assay for assessing the cellular binding kinetics of a compound and what potential limitations the assay has.

First, the NanoBRET wash-out assay relies on the availability of a suitable tracer molecule. The wash-out assay starting point is typically set at high target occupancy. Then, unbound compound is removed and the wash-out starts by tracer and substrate addition and subsequent luminescence measurement.

As an initial input we hence require the NanoBRET IC_{50} of the compound for its target. However, this value typically shows an error in the range of 2-3 times, which means in the worst-case scenario we may have one inhibitor 1 at not 10-fold IC_{50} as desired, but at 30-fold, while the other inhibitor 2 is at 3-fold IC_{50} . This means, the occupancy of inhibitor 1 would likely be 95%, while the occupancy of inhibitor 2 would start at approximately 75%. Subsequently, inhibitor 2 would appear to be washed-out much faster than inhibitor 1, even when having similar IC_{50} s and in reality, similar half-lives. When comparing the two, the determination of an accurate half-life will be difficult and hence only sufficient replication may result in a half-life with sufficient accuracy.

Next, we have seen, that a use of a fast kinetics tracer will result in more accurate half-lives as more information can be captured. If suitable tracers are available, the tracer with the fastest kinetics should be chosen.

10 Discussion

As this assay is a luciferase assay, the assay quality will decrease upon substrate consumption and hence a reduction in luciferase signal produced to be used in the BRET to the tracer molecule. We found a detection of up to 2 h to be optimal which can be expanded to 4 h with good quality. Longer measurements will result in very inaccurate signals and high error bars between replicates. The manufacturer (Promega) developed a new substrate with improved stability, that enables measurements up to 24 h. This substrate however was not tested in the studies presented here and the improved substrate should be tested in future kinetic studies.

Using the normal substrate and tracer kinetics, we found the determination of half-lives in the range of 0.5 h to 5 h to be most accurate, regarding measurement times of up to 4 h. We observed curves showing plateaus that do not reach the expected 100% mark of the tracer. Here, an insufficient wash-out lead to an insufficient removal of unbound inhibitor, allowing it to rebind to the target establishing an equilibrium that did not result in the complete wash-out expected by a 100-fold dilution of the sample. Therefore, a sufficient wash-out is necessary to get accurate half-lives in the NanoBRET assay. Similarly, it might be that the previously determined IC_{50} was not accurate enough to allow the system to start at 10-times IC_{50} , or 90% occupancy.

Especially with STK10, we observed potentially different kinetic stages of the reaction where an initial compound wash-out might be faster for a subpopulation of STK10 to be not fully bound and a section to be correctly kinetically trapped as expected from the crystal structures which results in a two-step kinetic mechanism. This is what we as well observed in the SPR data. As we use a cellular system, not all proteins might be in the same conformation despite equilibrating the inhibitor and cells for 2 h prior to the wash-out. Unfortunately, there was no two-step kinetic fit identified to confront this problem, nor would be clear which kinetic half-live is the resemblance of the true state. Likely, depending on the protein population different half-lives will be determined and the usual fit will deliver a mix of these populations.

Additionally, in an open system, we do observe drug rebinding. Although the tracer is used between IC_{50} or $10 \times IC_{50}$, depending on the tracer IC_{50} determined and the upper tracer toxicity limit of $1 \mu\text{M}$, drug rebinding could occur. In an open system as *in vivo* however, drug rebinding has been invoked as a major mechanism for higher efficacy of slow kinetics inhibitors and hence may be both desired and consequently considered

as a global wash-out system in NanoBRET. As this global system, the NanoBRET wash-out assay delivers a ranking of the half-lives of inhibitors for a given target. It is designed to take several obstacles into account with defined starting point and endpoint of the assay. I believe that NanoBRET might serve as a useful model for *in vivo* blood wash-out experiments although the validation of this hypothesis is out of the scope of our standard laboratory techniques. We however think, that the NanoBRET cellular wash-out assay is a useful technique to determine cellular half-lives in a more global context.

10.3 ELUCIDATION OF STRUCTURAL MECHANISMS FOR IMPROVING BINDING KINETICS

Based on the two case studies investigated here, STK10/SLK and FAK/PYK2, it can be emphasized that two underlying mechanisms were the most likely interactions promoting slower residence times.

Firstly, we saw that hydrophobic interactions prolong the drug target residence time. For STK10 it was the largely hydrophobic backpocket, which offered hydrophobic interactions to the type II inhibitors foretinib and BIRB796, while in FAK it was a specific hydrophobic interaction with L567 that triggered the stabilization of the activation loop upon inhibitor binding. This is in good agreement with the hydrophobic effect. Desolvation of the hydrophobic pocket to allow inhibitor association presents an energy barrier, which – if overcome by the system – will result in a prolonged residence time because of a kinetically more stable complex^{61,144}.

Secondly, protein flexibility allows for more interactions conformationally locking the inhibitor as seen especially with the clearly resolved P-Loop folding over the pocket in STK10 and bosutinib or in the stabilization of the helical DFG-Loop in FAK upon inhibitor binding which was not possible in the very related PYK2 protein. Ordering otherwise flexible loops is known as a cause for prolonged residence times and is in agreement with the findings for e.g. DOT1L⁶⁸.

In conclusion, in the case studies of STK10/SLK and FAK/PYK2 we found new examples supporting existing hypothesis for prolonging drug-target residence times. In the future, more structure-kinetic-relationships are necessary to both understand how to modulate a specific targets kinetic properties to design a molecule with the required binding kinetic behavior and to consider slow binding kinetics a factor for the

10 Discussion

development of unwanted off-target effects – even if affinity assays suggest a selectivity window.

10 Discussion

11 SUPPLEMENTAL INFORMATION

Suppl. Table S 1: Data collection and refinement statistics for STK10 structures.

	Bosutinib	Bosutinib isomer	GW830263A	GW683134	Foretinib	BIRB-796 (Doramapimod)	Dovitinib	Dasatinib
Crystallization condition	0.1M TRIS PH 8.1, 0.1M MAGNESIUM CHLORIDE, 30%(W/V) PEG 10000	0.1M SPG PH 7.0; 60% MPD	0.2M NAI, 0.1M BISTRISPROPANE PH 6.5, 20% PEG3350, 10% ETHYLENE GLYCOL	10% PEG1000, 10% PEG8000	0.2M sodium chloride -- 25% PEG3350 -- 0.1M bis-tris pH 5.5	20% PEG6000, 10% ethylene glycol, 0.1M MES pH 6.0, 0.1M magnesium chloride	0.1M sodium formate, 15%(w/v) PEG 3350	40% PEG 300, 0.20M Ca(ac)2, 0.1M cacodylate pH 6.5
Inhibitor Type	Type I		Type II		Type II	Type II	Type I	Type I
PDB ID	5AJQ	4BC6	4AOT	6eim	6i2y	6GTT	5OWQ	5OWR
Space group	<i>P22₁2₁</i>	<i>I222</i>	<i>P2₁2₁2₁</i>	<i>P2₁2₁2₁</i>	<i>P2₁2₁2₁</i>	<i>P6₄22</i>	<i>P2₁</i>	<i>I222</i>
No. of molecules in the asymmetric unit	2	1	2	2	2	1	2	1
Unit cell dimensions <i>a, b, c</i> (Å), α, β, γ (°)	41.2, 108.1, 144.3 90, 90, 90	51.2, 114.0, 134.3, 90, 90, 90	55.7, 87.5, 148.6, 90, 90,90	49.5, 99.8, 125.8, 90, 90, 90	50.9, 95.2, 132.8 90, 90, 120	100.7, 100.7, 145.8, 90, 90, 120	57.6, 50.4, 114.6, 90.0, 96.6, 90.0	49.7, 111.7, 133.2, 90, 90, 90
Data collection								
Resolution range (Å) ^a	86.51-2.20 (2.27-2.20)	19.18-2.20 (2.32-2.20)	56.64-2.33 (2.42-2.33)	46.39-1.43 (1.48-1.43)	95.20-2.40 (2.63-2.56)	87.18-2.25 (2.32-25)	57.19-2.70 (2.86-2.70)	85.58-2.30 (2.38-2.30)
Unique observations ^a	33518 (2809)	20251 (2949)	31773 (3276)	46390 (1430)	21389 (1011)	21422 (1920)	16619 (2672)	16890 (1643)
Average multiplicity ^a	4.1 (3.4)	4.4 (4.5)	6.1 (6.4)	4.1 (3.9)	6.3 (5.8)	17.7 (18.3)	2.8 (2.7)	4.3 (4.3)
Completeness (%) ^a	99.6 (98.3)	99.9 (99.8)	99.8 (99.9)	96 (94.8)	99.9 (100.0)	100.0 (100.0)	91.4 (91.8)	99.9 (100.0)
<i>R</i> _{merge} ^a	0.05 (0.62)	0.04 (0.72)	0.14 (1.19)	0.05 (0.84)	0.11 (1.12)	0.07 (1.70)	0.14 (0.61)	0.10 (1.03)
Mean (<i>I</i>)/σ(<i>I</i>) ^a	12.0 (1.9)	16.3 (1.9)	9.8 (2.1)	12.6 (n/a)	5.8 (1.1)	22.8 (2.1)	4.7 (1.3)	37.2 (1.7)

11 Supplemental Information

	Bosutinib	Bosutinib isomer	GW830263A	GW683134	Foretinib	BIRB-796 (Doramapimod)	Dovitinib	Dasatinib
Mean CC(1/2) ^a	0.988 (0.665)	n/a	0.996 (0.523)	0.999 (0.535)	0.996 (0.534)	0.999 (0.589)	0.984 (0.692)	0.997 (0.667)
Refinement								
Resolution range (Å)	86.51-2.20	19.18-2.20	75.40-2.33	41.81-1.43	54.50-2.56	87.18-2.25	113.81-2.70	85.58-2.30
R-value, <i>R</i> _{free}	0.22, 0.26	0.21, 0.25	0.22, 0.25	0.16, 0.17	0.26, 0.28	0.24, 0.30	0.27, 0.30	0.22, 0.25
r.m.s. deviation from ideal bond length (Å)	0.010	0.010	0.014	0.004	0.003	n/a	0.014	0.008
r.m.s. deviation from ideal bond angle (°)	1.42	1.08	1.59	0.68	0.67	n/a	1.69	1.18

^a Values within parentheses refer to the highest resolution shell.

11 Supplemental Information

Suppl. Table S 2: kPCA, ePCA, DSF and NanoBRET data for STK10 and ePCA, DSF and NanoBRET data for SLK. kPCA= kinetic probe competition assay, ePCA= equilibrium probe competition assay, SD= standard deviation, SEM= standard error of the mean, k_{on} =association kinetic constant, k_{off} =dissociation kinetic constant, K_D =dissociation constant, K_I =dissociation constant, DSF=Differential Scanning Fluorimetry

Cpd Name	STK10														SLK										
	kPCA k_{on} [1/Ms]	kPCA SD [1/Ms]	kPCA k_{on} (1/s)	kPCA k_{off} [1/s]	kPCA SD [M]	kPCA K_D [M]	kPCA K_D [M]	kPCA SD [M]	ePCA K_I [M]	ePCA SD [M]	DSF K_I [K]	DSF ΔT_m [K]	NanoBR ET [M]	NanoBRET IC_{50} [M]	NanoBRET SEM [M]	NanoBRET kinetics [min]	NanoBRET Halflife [min]	NanoBRET kinetics [min]	NanoBRET SD	ePCA K_I [M]	ePCA SD [M]	ePCA K_I [M]	DSF SLK ΔT_m [K]	NanoBRET potency [M]	NanoBRET IC_{50} [M]
Staurosporine	7,64E+06	6,16E+05							5,98				2,16E-09							1,00				2,43	3,71
	+06	5							E-10	n=1			09	3,15E-10	360,50		277,79			E-10	n=1			E-09	E-10
Ponatinib	2,55E+06	1,80E+05	5,13E-04	3,04E-04	1,44	8,57E-11	7,68	4,12E-11	E-10	10			9,86E-09	8,49E-10	389,20		97,18			4,72	5,52E-11			2,32	4,86
	+06	5	-04	04	E-10	11	E-10	10	09				09	8,49E-10	389,20		97,18			E-10	11	14,62		E-07	E-08
Rebastinib	1,47E+05	2,15E+04	1,18E-04	9,18E-04	9,14	7,00E-09	9,76	3,70E-09	E-10	10	5	06	2,88E-06	202,90			155,00			5,34	7,10E-11			6,33	8,59
	+05	4	-04	04	E-10	09	E-10	10	09				2,88E-06	202,90			155,00			E-10	11			E-06	E-07
Tivozanib	3,56E+06	2,65E+05	2,85E-03	4,41E-04	5,85	5,83E-11	1,85	2,07E-10	E-09	10	0	07	3,79E-08	83,90			4,75			8,25				7,63	1,42
	+06	5	-03	04	E-10	11	E-09	10	07				3,79E-08	83,90			4,75			E-10	n=1			E-07	E-07
LY2874455	3,66E+06	1,16E+05	4,31E-02	2,43E-02	5,59	3,69E-09	1,29	4,02E-09	E-08	09	8	08	1,10E-08	175,33			30,58			8,50				3,92	1,09
	+06	6	-02	02	E-08	09	E-08	09	08				1,10E-08	175,33			30,58			E-10	n=1			E-08	E-08
AZD7762	4,13E+06	1,25E+05	1,37E-02	4,95E-03	2,82	2,27E-10	4,43			11,0			3,04E-07							1,35				2,12	5,55
	+06	6	-02	03	E-09	10	E-09	n=1	2	07			4,61E-08	128,30						E-09	n=1	5,70		E-06	E-07
CHIR-124	5,67E+05	1,42E+04	1,30E-02	4,10E-03	2,23	1,90E-09	4,27													1,56					
	+05	5	-02	03	E-08	09	E-08	n=1	9,04											E-09	n=1				
KW-2449 Foretinib (GSK1363089)	1,87E+06	1,71E+05	4,76E-02	4,60E-02	1,96	1,11E-09	2,82						1,20E-06							1,58				9,92	6,12
	+06	6	-02	02	E-08	09	E-08	n=1	7,77	06			2,26E-07	76,88			25,91			E-09	n=1			E-07	E-08
Golvatinib (E7050)	6,56E+05	4,64E+04	1,20E-03	4,11E-04	1,41	6,25E-10	3,58	1,40E-09	14,4	3,41E-09	14,4	07	8,15E-08	n.d.			n.d.			2,21				6,51	4,12
	+05	4	-03	04	E-09	10	E-09	09	9	07			8,15E-08	n.d.			n.d.			E-09	n=1			E-06	E-07
Tamatinib	1,82E+06	7,73E+05	5,03E-02	2,24E-02	2,87	1,81E-09	6,39			11,2			1,63E-06							2,38				5,70	5,40
	+07	6	-02	02	E-09	10	E-09	n=1	9	06			7,43E-07	n.d.			n.d.			E-09	n=1	4,40		E-05	E-06
KIN001-132	3,26E+06	9,27E+05	1,69E-01	4,80E-01	5,80	4,82E-09	4,41	1,15E-09			8,61									2,59					
	+06	6	-01	01	E-08	09	E-08	09												E-09	n=1				
TAE684	2,52E+05	1,41E+04	2,57E-02	1,67E-02	7,95	6,70E-09	4,74													2,60					
	+05	5	-02	02	E-08	09	E-08	n=1	6,07											E-09	n=1				
MGCD-265	6,73E+06	1,16E+05	1,18E-01	2,04E-01	1,91	1,95E-09	4,61			10,0			1,31E-08							2,75					
	+06	7	-01	01	E-08	09	E-08	n=1	9	07			1,35E-08	231,90			78,21			E-09	n=1	2,38			
Dovitinib	3,69E+06	3,86E+05	3,89E-03	8,46E-04	9,57	2,40E-09	1,73	2,06E-09					2,33E-05							2,93				3,60	5,61
	+05	4	-03	04	E-09	09	E-08	09	8,55	05			3,24E-06	120,01			66,34			E-09	n=1	2,01		E-05	E-06
Dovitinib	3,67E+06	7,34E+05	8,31E-03	2,49E-03	2,53	2,07E-09	3,75													2,94					
	+05	4	-03	03	E-08	09	E-08	n=1	7,14											E-09	n=1				

11 Supplemental Information

Cpd Name	STK10															SLK							
	kPCA <i>K_{on}</i> [1/Ms]	kPCA <i>k_{on}</i> SD [1/Ms]	kPCA <i>k_{off}</i> [1/s]	kPCA <i>k_{off}</i> SD [1/s]	kPCA <i>K_D</i> [M]	kPCA <i>K_D</i> SD [M]	ePCA <i>K_i</i> [M]	ePCA <i>SD</i> [M]	<i>K_i</i> [M]	DSF ΔT_m [K]	NanoBR ET [M]	<i>IC₅₀</i> [M]	NanoBRET <i>IC₅₀</i> SEM [M]	NanoBRET kinetics [min]	NanoBRET Halflife [min]	SD	ePCA <i>K_i</i> [M]	ePCA <i>SD</i> [M]	<i>K_i</i> [M]	DSF SLK ΔT_m [K]	NanoBRET potency [M]	<i>IC₅₀</i> [M]	
TAK-901	2,01E+05	4,48E+04	8,88E-03	2,78E-03	3,68E-08	3,44E-09	5,67E-08	1,99E-08		9,25							3,03E-09		n=1				
Crenolanib	1,93E+06	4,28E+05	1,11E-02	3,23E-03	5,23E-09	3,91E-10	9,03E-09	n=1	2	06		4,31E-07	166,90	53,17			3,73E-09		n=1	5,26E-05	1,68E-05	6,82E-07	
Cabozantini b	1,65E+06	1,95E+05	7,42E-03	2,03E-03	5,16E-09	5,15E-10	5,19E-09	1,28E-09	13,1	8,18E-07							3,92E-09	2,23E-10		2,19E-05	1,87E-06		
pf234	2,38E+05	6,91E+04	1,62E-03	5,61E-03	6,80E-08	5,31E-09	7,09E-08	4,86E-08	10,1	8							4,22E-09		n=1	5,73E-05			
PIK-75	1,77E+05	4,90E+04	1,51E-02	5,39E-03	1,05E-07	7,79E-09	8,73E-08	4,33E-08		6,78							4,33E-09		n=1	4,02E-04			
AP26113	1,92E+05	5,45E+04	1,62E-03	6,59E-03	8,54E-08	6,36E-09	1,10E-07	8,24E-08	8,26								4,75E-09		n=1	5,20E-05			
GSK107091 6	4,86E+06	5,34E+06	7,27E-02	8,07E-02	1,55E-08	1,28E-09	2,92E-08	n=1	8,67	05	2,89E-05	2,70E-06	86,22	7,61			4,94E-09		n=1	2,41E-05	4,21E-05	6,62E-06	
Neratinib	8,20E+05	1,85E+05	1,26E-02	3,57E-03	2,39E-08	1,39E-09	2,12E-08	n=1	6,29	07	7,59E-07	1,87E-07	27,65	9,91			5,37E-09		n=1	E-07	4,66E-07	3,86E-08	
AZ 960	5,26E+04	1,02E+04	7,18E-03	2,14E-03	1,36E-07	1,66E-08	2,03E-07	n=1	7,34								5,37E-09		n=1				
Pazopanib	9,65E+05	2,78E+05	1,66E-02	5,48E-03	1,57E-08	1,11E-09	1,91E-07	7,70E-07		2,40E-05							5,58E-09		n=1	4,56E-05	3,70E-05	1,61E-06	
AEE-788	3,50E+05	1,95E+05	3,29E-02	2,00E-02	9,41E-08	7,00E-09	1,26E-07	n=1	8,01								5,64E-09		n=1				
AZD3463	1,72E+05	4,62E+04	9,54E-03	3,48E-03	5,53E-08	6,78E-09	1,08E-08	n=1	9,11								5,72E-09		n=1				
PF-562271	6,52E+04	1,77E+04	1,19E-03	4,12E-03	1,82E-07	1,82E-08	2,37E-07	n=1	5,79								6,10E-09		n=1				
Bosutinib	9,69E+05	2,88E+05	2,03E-02	7,38E-03	1,48E-08	8,43E-09	2,06E-08	1,91E-08	14,1	2,93E-07							6,20E-09		n=1	7,70E-07	1,92E-07	2,90E-08	
Desmethyl Erlotinib	5,08E+05	1,13E+05	9,61E-03	2,90E-03	1,76E-08	1,55E-09	2,46E-08	n=1	8,22								6,58E-09		n=1				
Danusertib	3,85E+04	7,26E+03	5,77E-03	1,85E-03	1,50E-07	2,25E-08	3,14E-07	n=1	4,73								6,70E-09		n=1	1,46E-05			
JNJ- 7706621	1,68E+05	4,39E+04	1,44E-02	4,61E-03	8,60E-08	6,75E-09	1,06E-07	n=1	10,7								6,83E-09		n=1	5,38E-05			

11 Supplemental Information

Cpd Name	STK10														SLK									
	kPCA K _{on} [1/Ms]	kPCA SD [1/Ms]	kPCA k _{on} [1/s]	kPCA k _{off} [1/s]	kPCA SD [M]	kPCA K _D [M]	kPCA K _D [M]	ePCA K _i [M]	ePCA SD [M]	SD K _i [M]	DSF ΔT _m [K]	NanoBR ET [M]	NanoBRET IC ₅₀ [M]	NanoBRET SEM [M]	NanoBRET kinetics [min]	NanoBRET Halflife [min]	NanoBRET kinetics Halflife [min]	SD	ePCA K _i [M]	ePCA SD [M]	K _i	DSF SLK ΔT _m [K]	NanoBRET potency [M]	IC ₅₀
BIRB 796 (Doramapi mod)	3,06E+05	2,42E+04	1,74E-03	4,08E-04	4,42E-09	7,73E-10	9,58E-09	1,95E-09	14,00	2,37E-06									7,12E-09	n=1		7,19		
PF-562271	4,23E+04	9,82E+03	1,02E-02	3,17E-03	2,40E-07	2,41E-08	2,51E-07	n=1	5,23										8,13E-09	n=1				
CYC-116	1,73E+05	5,40E+04	1,80E-02	6,55E-03	1,04E-07	7,80E-09	1,26E-07	1,36E-07		6,21									9,73E-09	n=1				
Cediranib	3,19E+05	7,16E+04	9,51E-02	2,90E-03	2,88E-07	2,62E-09	4,19E-08	2,04E-08		9,04									9,82E-09	n=1		5,77		
AZ23	1,34E+05	2,74E+04	6,96E-03	2,18E-03	5,18E-08	6,69E-09	6,08E-08	2,47E-08		7,77									1,02E-08	n=1				
Sunitinib	1,25E+05	3,45E+04	1,48E-02	4,96E-03	1,18E-07	9,56E-09	3,17E-07	n=1											1,12E-08	n=1				
PF 431396	4,45E+04	1,34E+04	1,24E-02	4,72E-03	2,78E-07	2,96E-08	3,02E-07	2,56E-07		8,87									1,25E-08	n=1		5,24		
Icotinib	1,62E+05	4,56E+04	2,61E-02	8,01E-03	2,49E-08	2,47E-09	2,52E-09	7,57E-09		8,16	3,24E-06								1,26E-08	n=1		4,85	1,51E-06	4,93E-09
BMS777607	9,10E+04	2,36E+04	2,97E-02	8,27E-03	3,88E-09	2,82E-10	8,08E-09	n=1	10,0	3,72E-05									1,29E-08	n=1		5,08	1,41E-05	1,20E-06
Sunitinib	6,29E+04	1,43E+04	1,02E-02	3,11E-03	1,63E-07	1,58E-08	1,71E-07	4,59E-08		6,26									1,35E-08	n=1				
BMS-582664	1,10E+05	2,60E+04	9,93E-03	3,16E-03	9,00E-08	9,31E-09	1,47E-07	n=1	6,03										1,49E-08	n=1				
GSK-461364	3,20E+05	7,38E+04	8,89E-03	2,86E-03	2,78E-08	3,18E-09	3,60E-08	n=1	5,56										1,53E-08	n=1				
Sotrastaurin	1,69E+05	7,08E+04	2,78E-02	1,28E-02	1,65E-07	1,08E-08	1,51E-07	7,92E-08		6,41									1,65E-08	n=1				
Gandotinib	1,64E+05	4,75E+04	8,17E-03	3,42E-03	4,98E-07	7,78E-08	4,39E-07	1,51E-07		6,49									1,66E-08	n=1				
SB1518	5,23E+04	1,40E+04	1,17E-02	4,02E-03	2,23E-07	2,24E-08	2,70E-07	n=1	4,80										1,67E-08	n=1				
CUDC-101	2,65E+05	1,69E+04	3,80E-02	2,60E-02	1,43E-07	1,05E-08	8,18E-08	n=1	7,83										1,73E-08	n=1				

11 Supplemental Information

Cpd Name	STK10														SLK							
	kPCA <i>K_{on}</i> [1/Ms]	kPCA <i>k_{on}</i> SD [1/Ms]	kPCA <i>k_{off}</i> [1/s]	kPCA <i>k_{off}</i> SD [1/s]	kPCA <i>K_D</i> [M]	kPCA <i>K_D</i> SD [M]	ePCA <i>K_i</i> [M]	ePCA <i>SD</i> [M]	<i>K_i</i> [M]	DSF ΔT_m [K]	NanoBR ET [M]	<i>IC₅₀</i> [M]	NanoBRET <i>IC₅₀</i> SEM [M]	NanoBRET kinetics [min]	NanoBRET Halflife [min]	SD	ePCA <i>K_i</i> [M]	ePCA <i>SD</i> [M]	<i>K_i</i> [M]	DSF SLK ΔT_m [K]	NanoBRET potency [M]	<i>IC₅₀</i> [M]
AT-9283	1,34E+06	3,74E+05	1,79E-02	5,94E-03	5,62E-08	4,72E-09	9,79E-08	4,02E-08	8,21								1,83E-08	n=1		5,03		
AMG458	1,03E+06	8,53E+04	2,14E-03	4,75E-04	1,76E-09	3,67E-10	4,54E-09	4,77E-09	13,9	9,17E-06		1,18E-06	82,78	24,54			1,94E-08	2,21E-10			>1,0	
ENMD-2076	1,86E+05	1,33E+05	4,62E-02	3,51E-02	2,49E-07	1,70E-08	3,09E-07	n=1	3,78								1,95E-08	n=1				
BX-912	5,20E+04	1,31E+05	1,29E-02	4,12E-03	2,45E-07	2,13E-08	2,01E-07	1,31E-07	4,78								1,96E-08	n=1				
Lenvatinib	7,69E+06	9,81E+05	1,10E-01	1,37E-01	1,63E-08	1,16E-09	2,03E-08	3,97E-10	9,60	6,83E-07		8,97E-08	64,33	11,24			2,01E-08	n=1		4,68	1,04E-05	9,99E-07
Erlotinib	7,97E+04	2,20E+05	2,12E-02	1,02E-02	7,47E-07	5,00E-08	9,13E-08	4,02E-08	7,36	3,59E-06		1,68E-07	188,03	73,81			2,01E-08	n=1			5,81E-06	6,15E-07
Nintedanib	2,69E+05	2,15E+05	4,62E-02	4,41E-02	1,39E-07	1,09E-08	9,86E-08	2,96E-08	6,65								2,02E-08	n=1		2,98		
GSK-1059615	5,00E+04	1,24E+05	1,07E-02	3,51E-03	2,15E-07	2,18E-08	1,19E-07	n=1	6,40								2,28E-08	n=1				
Brivanib	7,49E+04	1,76E+05	1,11E-02	3,42E-03	1,49E-07	1,37E-08	1,97E-07	n=1	8,75								2,88E-08	n=1		4,66		
AC-480	6,46E+04	1,59E+05	1,12E-02	3,58E-03	1,73E-07	1,66E-08	1,67E-07	n=1	7,37								3,04E-08	n=1		2,53		
P505-15								n=1									3,08E-08	n=1				
VX-680	5,60E+04	1,85E+05	1,60E-02	6,32E-03	2,86E-07	2,57E-08	3,44E-07	n=1	8,95								3,12E-08	n=1		4,40		
LY2835219	1,38E+04	3,14E+05	6,61E-03	2,37E-03	4,79E-07	7,34E-08	6,33E-07	n=1	3,75								3,14E-08	n=1				
BMS-754807	9,10E+04	1,88E+05	6,77E-03	2,26E-03	1,18E-07	2,10E-08	2,36E-07	5,06E-08	6,13								3,25E-08	n=1				
Ruboxistaurin	5,15E+04	1,29E+05	1,16E-02	3,75E-03	2,25E-07	2,13E-08	2,01E-07	1,87E-07	7,24								3,54E-08	n=1		4,07		
Axitinib	2,73E+05	1,70E+05	4,49E-02	2,96E-02	1,66E-07	9,92E-08	1,57E-07	4,53E-08	8,69								3,74E-08	n=1		4,07		
Saracatinib	3,03E+04	9,05E+05	1,14E-02	4,40E-03	3,75E-07	4,29E-08	3,11E-07	1,04E-07	7,75								3,89E-08	n=1				

11 Supplemental Information

Cpd Name	STK10														SLK							
	kPCA K _{on} [1/Ms]	kPCA SD [1/Ms]	kPCA K _{on} [1/s]	kPCA K _{off} [1/s]	kPCA SD [M]	kPCA K _D [M]	kPCA K _D [M]	ePCA K _i [M]	ePCA SD [M]	DSF K _i [K]	NanoBR ET [M]	NanoBRET IC ₅₀ [M]	NanoBRET SEM [M]	NanoBRET kinetics [min]	NanoBRET Halflife [min]	SD	ePCA K _i [M]	ePCA SD [M]	SLK K _i [M]	DSF SLK ΔT _m [K]	NanoBRET potency [M]	IC ₅₀ [M]
PF-477736	3,51E+04	8,54E+03	9,51E-03	3,18E+03	2,71E-07	3,07E-08	2,87E-07	1,20E-07		4,01							4,49E-08	n=1	2,50			
Motesanib	2,17E+04	5,66E+03	1,08E-02	3,71E+03	4,97E-07	5,24E-08	4,99E-07	n=1	4,04								4,83E-08	n=1				
PF-477736	2,93E+04	7,85E+03	1,11E-02	3,88E+03	3,77E-07	4,00E-08	5,55E-07	n=1	5,36								4,88E-08	n=1				
ASP-3026	5,34E+05	4,86E+04	4,42E-03	1,55E+03	2,43E-07	4,00E-08	3,99E-07	2,27E-07	4,71								4,91E-08	n=1	2,18			
Alisertib	8,99E+04	3,84E+04	2,46E-02	1,17E+02	2,73E-07	2,08E-08	2,49E-07	4,46E-07		5,44							5,11E-08	n=1	3,22			
RAF265 (CHIR-265)	2,99E+04	2,44E+03	8,17E-04	5,07E+04	2,30E-08	1,50E-08	5,12E-08	3,75E-09	14,0	9,97E-06	2,47E-06	n.d.	n.d.				5,22E-08	n=1		1,94E-05	3,14E-06	
VX-689	6,45E+04	1,46E+04	9,37E-03	2,92E+03	1,45E-07	1,55E-08	2,03E-07	n=1	9,07								5,71E-08	n=1				
OSI-930	7,37E+04	2,47E+04	1,90E-02	7,38E+03	2,58E-07	1,98E-08	2,48E-07	n=1	5,85								5,81E-08	n=1				
SGI-1776	8,54E+04	2,76E+04	1,78E-02	6,70E+03	2,10E-07	1,71E-08	2,33E-07	1,54E-07	5,93								5,95E-08	n=1	2,58			
Linifanib	1,58E+05	5,36E+04	1,73E-02	6,52E+03	1,72E-07	1,87E-08	2,41E-07	7,12E-08	8,36								6,75E-08	n=1				
Gefitinib	3,18E+04	8,29E+03	1,15E-02	3,87E+03	3,60E-07	3,58E-08	3,15E-07	n=1	7,80	4,44E-05	6,46E-06	77,67	29,72				7,35E-08	n=1	3,45	4,03E-05	6,70E-06	
MLN-8054	3,62E+04	7,44E+03	8,18E-03	2,44E+02	2,26E-07	2,53E-08	2,97E-07	n=1	4,55								8,00E-08	n=1	1,28			
SU5416	5,17E+03	1,14E+03	5,74E-03	2,17E+03	1,11E-06	1,98E-07	4,07E-07	n=1	3,52								8,04E-08	n=1				
Canertinib	2,29E+04	5,07E+03	7,22E-03	2,44E+03	3,16E-07	4,34E-08	4,70E-07	n=1	4,27								8,10E-08	n=1				
AVL-292	1,52E+04	5,33E+03	1,74E-02	7,17E+03	1,14E-06	9,91E-08	8,40E-07	n=1	4,95								8,12E-08	n=1	2,01			
Sorafenib	1,82E+05	7,40E+04	2,65E-02	1,23E+02	1,46E-07	9,87E-09	1,43E-06	6,65E-08	12,8	1							8,29E-08	n=1				
Dasatinib	6,80E+04	1,96E+04	1,64E-02	5,72E+03	4,99E-07	4,30E-08	7,05E-07	2,08E-07	6,80								8,66E-08	n=1	4,10			

11 Supplemental Information

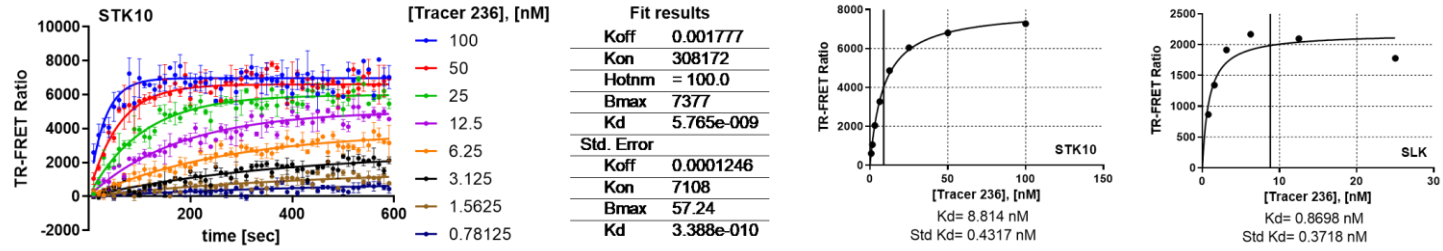
Cpd Name	STK10														SLK							
	kPCA <i>k_{on}</i> [1/Ms]	kPCA SD [1/Ms]	<i>k_{on}</i> kPCA <i>k_{off}</i> [1/s]	kPCA <i>k_{off}</i> SD [1/s]	kPCA <i>K_D</i> [M]	kPCA <i>K_D</i> SD [M]	ePCA <i>K_i</i> [M]	ePCA SD [M]	<i>K_i</i> SD [M]	DSF ΔT_m [K]	NanoBR ET [M]	NanoBRET <i>IC₅₀</i> [M]	NanoBRET SEM [M]	NanoBRET kinetics Halflife [min]	NanoBRET kinetics Halflife [min]	SD	ePCA <i>K_i</i> [M]	ePCA SD [M]	<i>K_i</i> SD [M]	DSF SLK ΔT_m [K]	NanoBRET potency [M]	<i>IC₅₀</i> [M]
Ibrutinib	2,40E+04	8,12E+03	1,56E-02	6,33E-03	6,47E-07	6,06E-08	5,13E-07	3,95E-07		5,06							9,04E-08			2,04		
PF299804							3,26E-07	n=1									9,25E-08	n=1		3,33		
Dabrafenib	2,95E+05	1,42E+05	2,20E-02	1,12E-02	1,15E-07	1,40E-08	1,52E-07	4,51E-08		7,05							9,27E-08	n=1		3,55		
Momelotini b	5,46E+04	2,03E+04	1,62E-02	6,70E-03	8,24E-07	1,18E-07	5,39E-07	3,66E-07		3,61							9,58E-08	1,31E-08				
ARRY33454 3	1,19E+04	2,72E+03	5,53E-03	2,17E-03	4,63E-07	8,64E-08	3,86E-07	n=1		6,90							1,05E-07	n=1		1,34		
NVP- BGJ398	1,29E+05	4,95E+04	2,18E-02	9,47E-03	1,68E-07	1,29E-08	1,72E-07	n=1		4,52							1,20E-07	n=1		2,25		
MK-2461	6,79E+03	2,52E+03	1,38E-02	6,33E-03	2,04E-06	2,39E-07	1,34E-06	n=1									1,37E-07	n=1				
CP-724714	1,13E+04	3,98E+03	1,67E-02	6,97E-03	1,48E-06	1,35E-07	7,25E-07	n=1		4,70							1,81E-07	n=1		1,79		
OSI-027	2,10E+04	6,08E+03	1,18E-02	4,38E-03	5,61E-07	5,96E-08	4,12E-07	n=1		3,75							2,19E-07	n=1				
Lapatinib Fostamatini b	1,02E+02	5,17E+01																				
Vandetanib	1,66E+05	4,82E+04	1,95E-02	6,56E-03	1,18E-07	7,64E-09														4,29		
KX2-391																				1,81		
Regorafeni b	5,28E+05	1,87E+05	2,20E-02	8,83E-03	4,17E-08	2,99E-09																
OSI-420											1,16E-06	1,35E-07	61,23	0,71							1,02E-06	1,04E-07

11 Supplemental Information

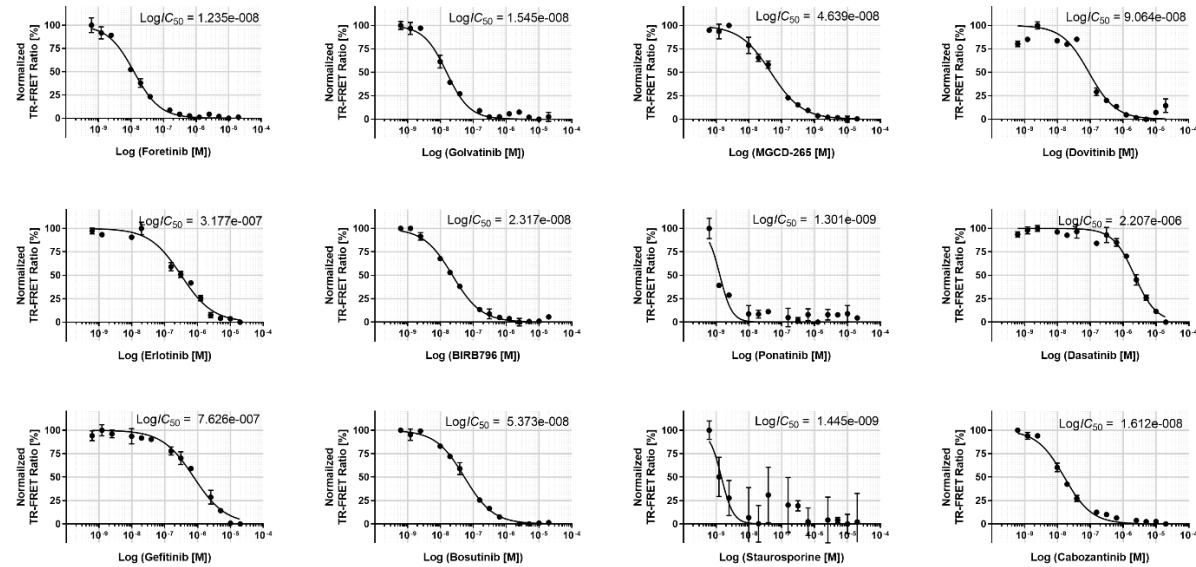
Suppl. Table S 3: Comparison of the Omnia activity, NanoBRET potency, SPR potency, kPCA kinetics, SPR kinetics and the NanoBRET half-lives for 8 representative compounds.

what to determine		potency	potency	potency	potency	potency	potency	potency	potency	potency	kinetics	kinetics	kinetics	kinetics	kinetics	kinetics	kinetics	kinetics	kinetics			
[Protein]		[STK10]=5 nM	[STK10]=5 nM	[STK10]=5 nM	[STK10]=5 nM	[STK10]~pM	[STK10]~pM	[STK10]=500 pM	[STK10]=2 μM	[STK10]~pM	[STK10]=500 pM	[STK10]=500 pM	[STK10]=500 pM	[STK10]~pM	[STK10]~pM	[STK10]~pM	[STK10]~pM	[STK10]~pM	[STK10]~pM	[STK10]~pM		
assay used		OMNIA Activity	OMNIA Activity	OMNIA Activity	OMNIA Activity	NanoBRET	NanoBRET	HTRF ePCA	DSF Tm	SPR K_i	SPR K_i	HTRF kPCA	HTRF kPCA	HTRF kPCA	SPR k_{on}	SPR k_{off}	SPR K_D	SPR k_{on}	SPR k_{off}	SPR K_D	NanoBRET wash-out	
Protein used		STK10-FL	STK10-KD	STK10-FL	STK10-KD	STK10-FL	STK10-FL	STK10-KD	STK10-KD	STK10-KD	STK10-FL	STK10-KD	STK10-KD	STK10-KD	STK10-KD	STK10-KD	STK10-KD	STK10-FL	STK10-FL	STK10-FL	STK10-FL	
Phospho-State		multiple	2 Phosphorylations	multiple	2 Phosphorylations	multiple	multiple	2 Phosphorylations	2 Phosphorylations	2 Phosphorylations	multiple	2 Phosphorylations	2 Phosphorylations	2 Phosphorylations	2 Phosphorylations	2 Phosphorylations	2 Phosphorylations	multiple	multiple	multiple	multiple	
[ATP]		60 μM ATP	60 μM ATP	1000 μM ATP	1000 μM ATP	cellular	cellular, low tracer	0 ATP	0 ATP	0 ATP	0 ATP	0 ATP	0 ATP	0 ATP	0 ATP	0 ATP	0 ATP	0 ATP	0 ATP	0 ATP	0 ATP	cellular
Cpd	Binding mode	IC_{50} , [M]	IC_{50} , [M]	IC_{50} , [M]	IC_{50} , [M]	IC_{50} , [M]	IC_{50} , [M]	K_i , [M]	T_m , [K]	K_D , [M]	K_D , [M]	k_{on} [1/mol*s]	k_{off} [1/s]	K_D , [M]	k_{on} [1/mol*s]	k_{off} [1/s]	K_D , [M]	k_{on} [1/mol*s]	k_{off} [1/s]	K_D , [M]	Half-life [min]	
Gefitinib	type I	7,30E-08	9,41E-08	7,36E-07	7,78E-07	4,44E-05	3,80E-06	3,16E-07	7,80	5,70E-07	1,68E-06	3,18E+04	1,15E-02	3,60E-07	5,54E+05	2,82E-01	4,97E-07	5,74E+05	6,80E-01	1,16E-06	102,95	
Erlotinib	type I	1,28E-08	5,60E-08	4,11E-07	1,95E-07	3,59E-06	2,31E-06	1,37E-07	7,36	8,36E-08	2,36E-07	7,97E+04	2,12E-02	7,47E-07	9,58E+05	6,77E-02	6,99E-08	1,44E+06	1,70E-01	1,17E-07	307,45	
Bosutinib	type I	2,04E-09	3,20E-09	1,03E-08	1,48E-08	2,93E-07	9,78E-08	2,39E-08	14,10	1,18E-08	3,09E-07	9,69E+05	2,03E-02	1,48E-08	7,58E+06	4,13E-02	5,48E-09	8,40E+05	9,82E-02	1,16E-07	819,9	
BIRB796	type II	7,77E-08	1,20E-06	5,14E-07	2,45E-06	2,37E-06	2,69E-07	9,73E-09	14,00	6,39E-06		3,06E+05	1,74E-03	4,42E-09							205,35	
AP24534	type II	1,78E-09	6,42E-10	6,65E-09	1,66E-08	9,86E-09	<200 pM					2,55E+06	5,13E-04	1,44E-10							1155,7	
Staurosporine	type I	3,38E-10	6,82E-10	3,79E-10	1,03E-09	2,16E-09	<200 pM	1,36E-10				7,64E+06						7,25E+05	2,08E-04	2,97E-10	134,21	
Cabozantinib	type II	2,06E-08	7,70E-08	1,13E-07	1,84E-07	8,18E-07	9,09E-09	5,01E-09	13,18	2,41E-08		1,65E+06	7,42E-03	5,16E-09	1,79E+05	1,95E-03	1,11E-08				419,1	
Foretinib	type II	1,31E-08	6,14E-08	1,25E-07	2,17E-07	3,41E-07	7,84E-09	5,39E-09	14,49	3,66E-08		6,56E+05	1,20E-03	1,41E-09							371,7	

11 Supplemental Information

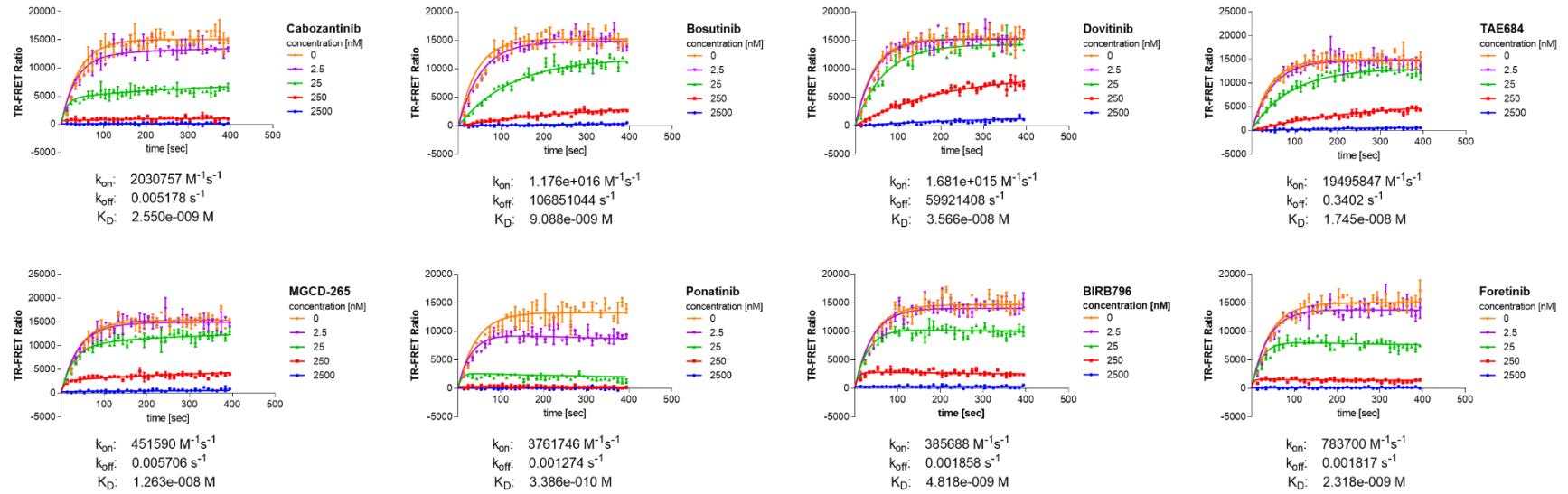


Suppl. Fig. S 1: HTRF tracer 236 properties for STK10 (association kinetics and potency) and SLK (potency only). Results are indicated in the figures.



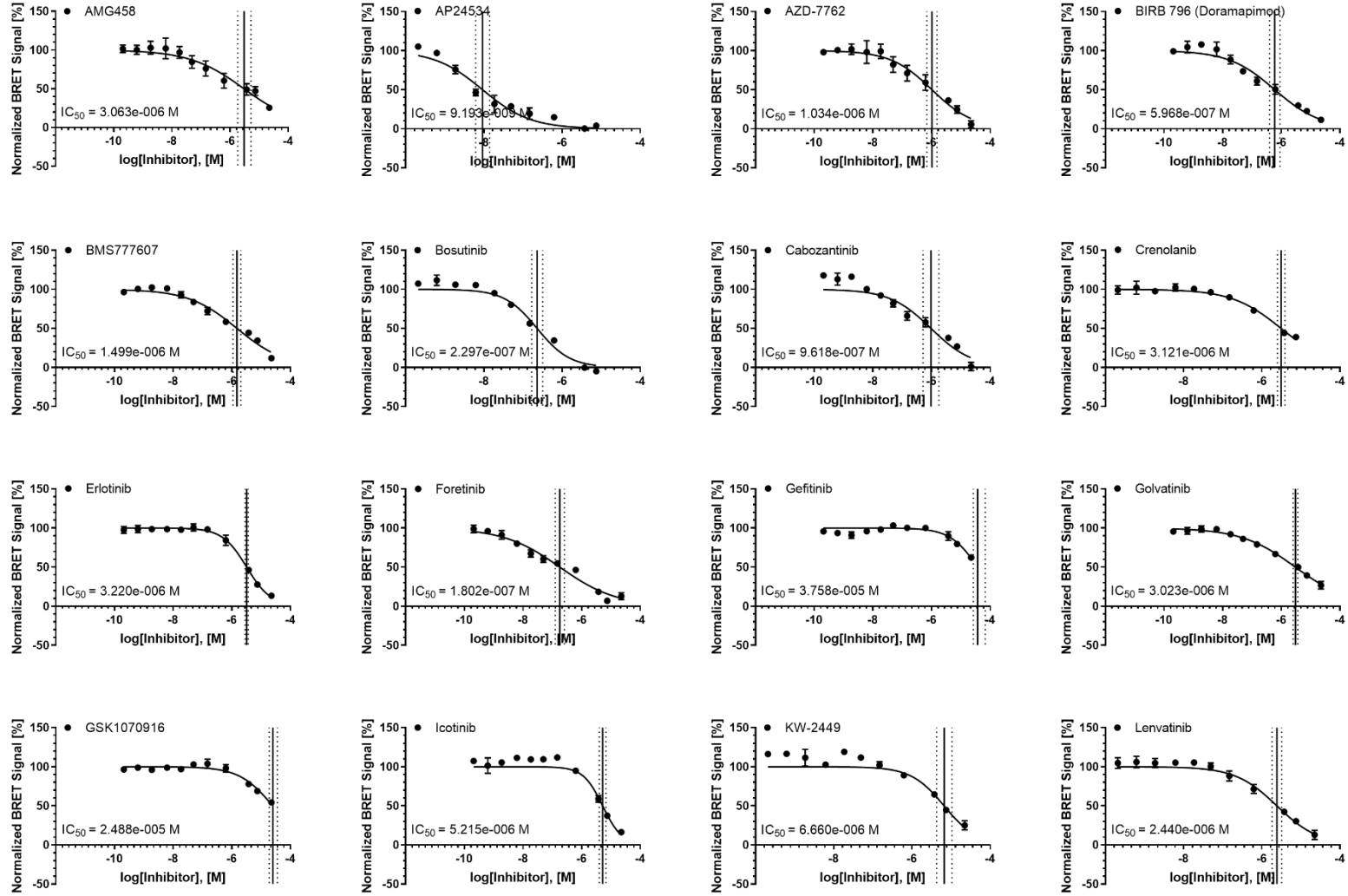
Suppl. Fig. S 2: Examples of ePCA compound titrations and resulting fits. Compound name and IC₅₀ are indicated in each respective graph.

11 Supplemental Information



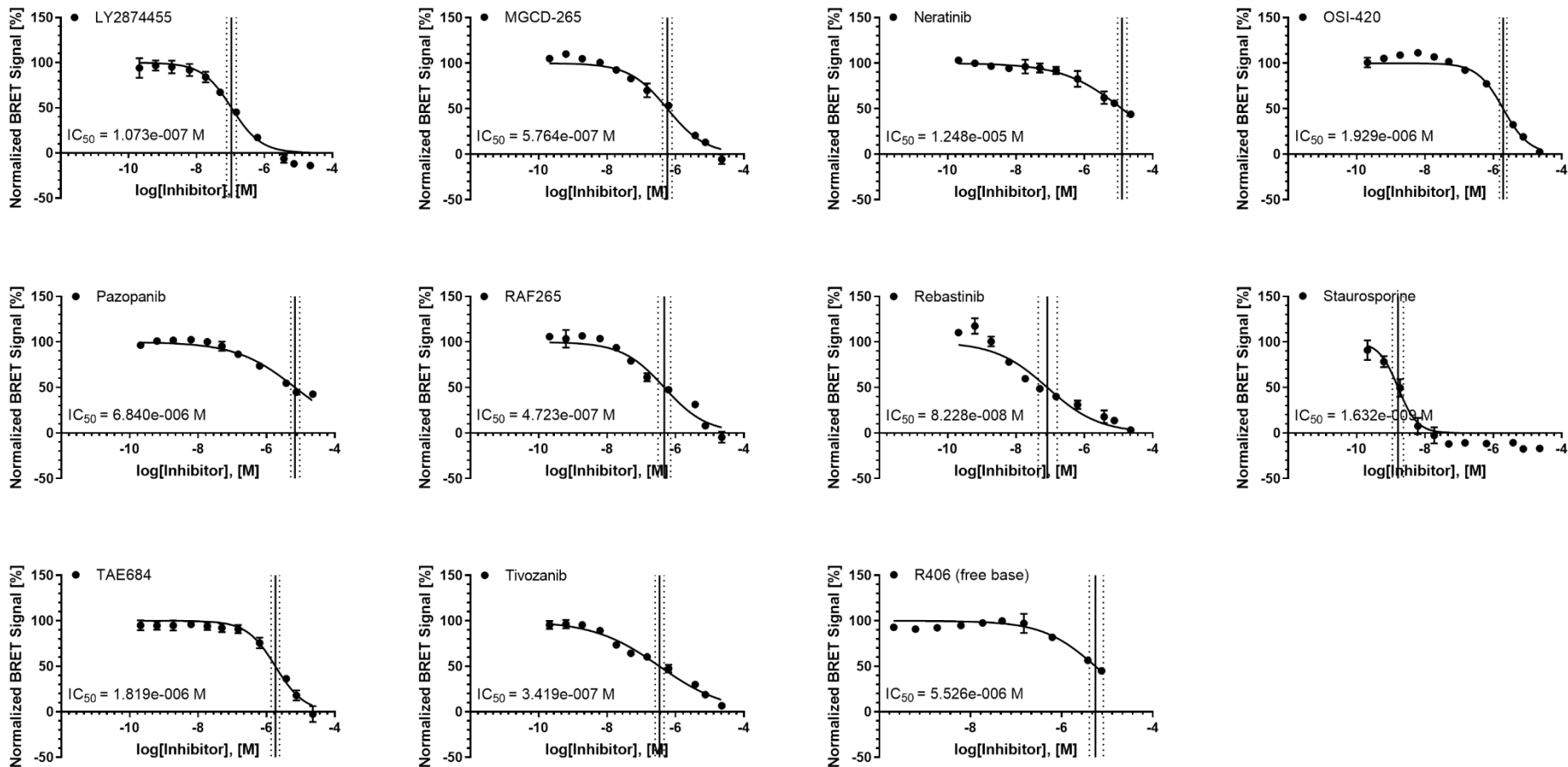
Suppl. Fig. S 3: Examples of kPCA data curves and resulting fits. Compound name, k_{on} and k_{off} as well as the calculated kinetic K_D ($K_D=k_{on}/k_{off}$) are indicated in each respective graph.

11 Supplemental Information



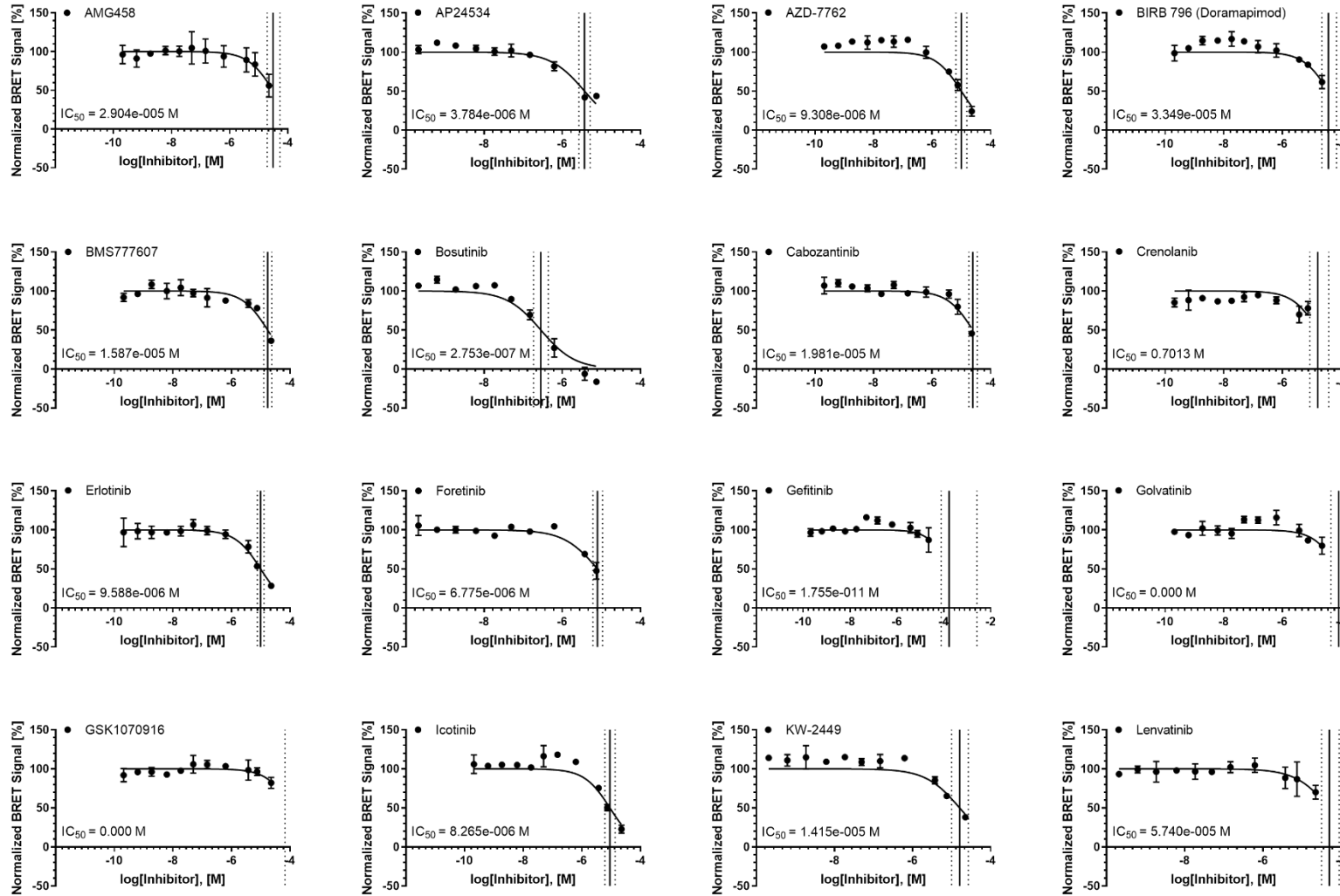
Suppl. Fig. S 4: Representative NanoBRET potency of inhibitors on STK10. IC_{50} of this single run is indicated in the figure.

11 Supplemental Information



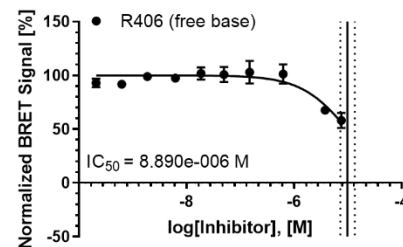
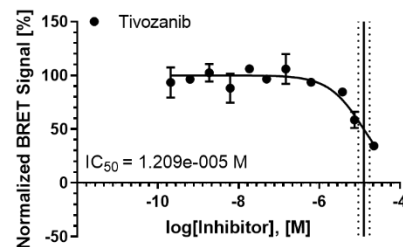
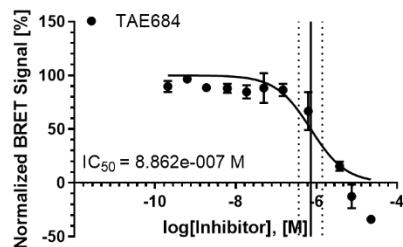
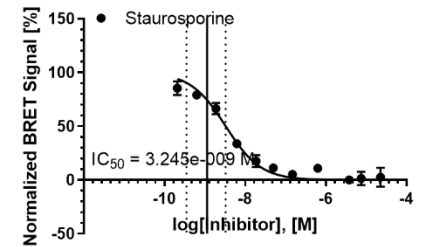
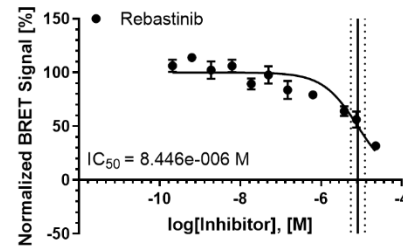
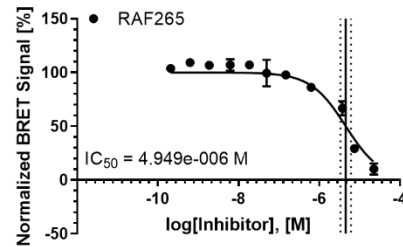
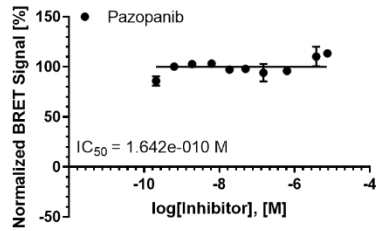
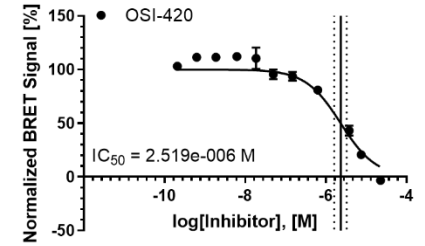
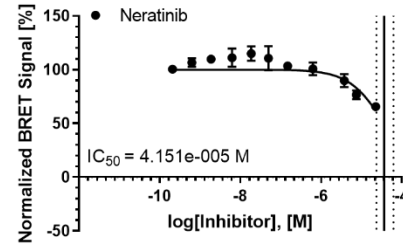
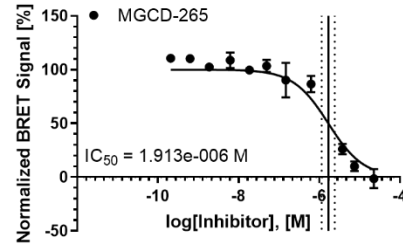
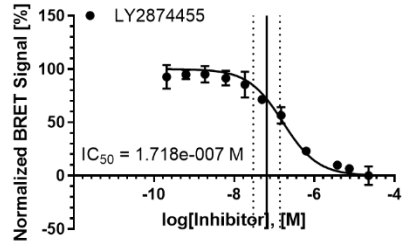
Suppl. Fig. S 4: Representative NanoBRET potency of inhibitors on STK10. IC₅₀ of this single run is indicated in the figure.

11 Supplemental Information



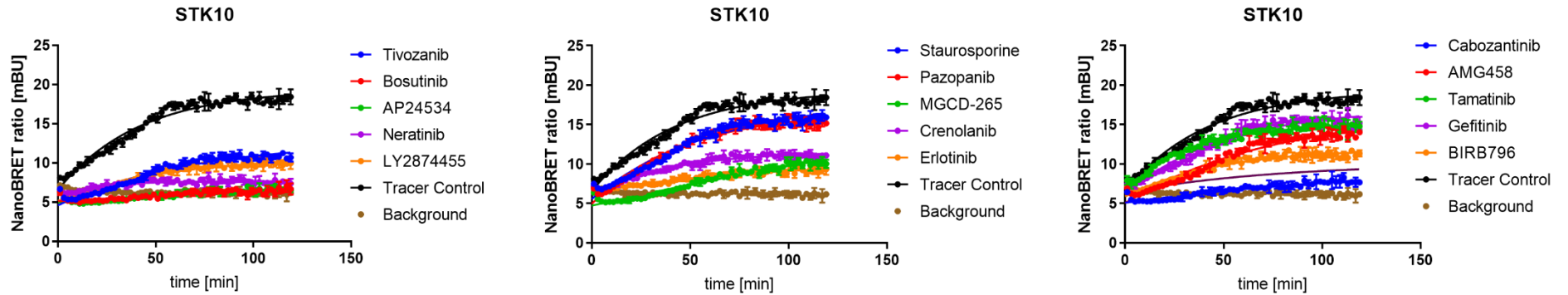
Suppl. Fig. S 5: Representative NanoBRET potency of inhibitors on SLK. IC_{50} of this single run is indicated in the figure.

11 Supplemental Information

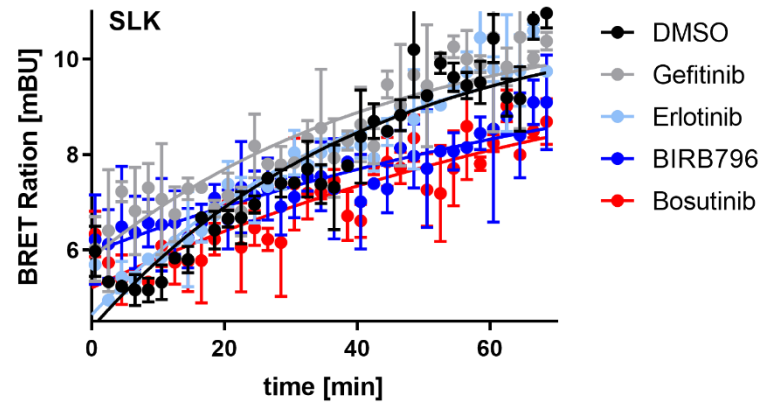


Suppl. Fig. S 5: Representative NanoBRET potency of inhibitors on SLK. IC₅₀ of this single run is indicated in the figure.

11 Supplemental Information

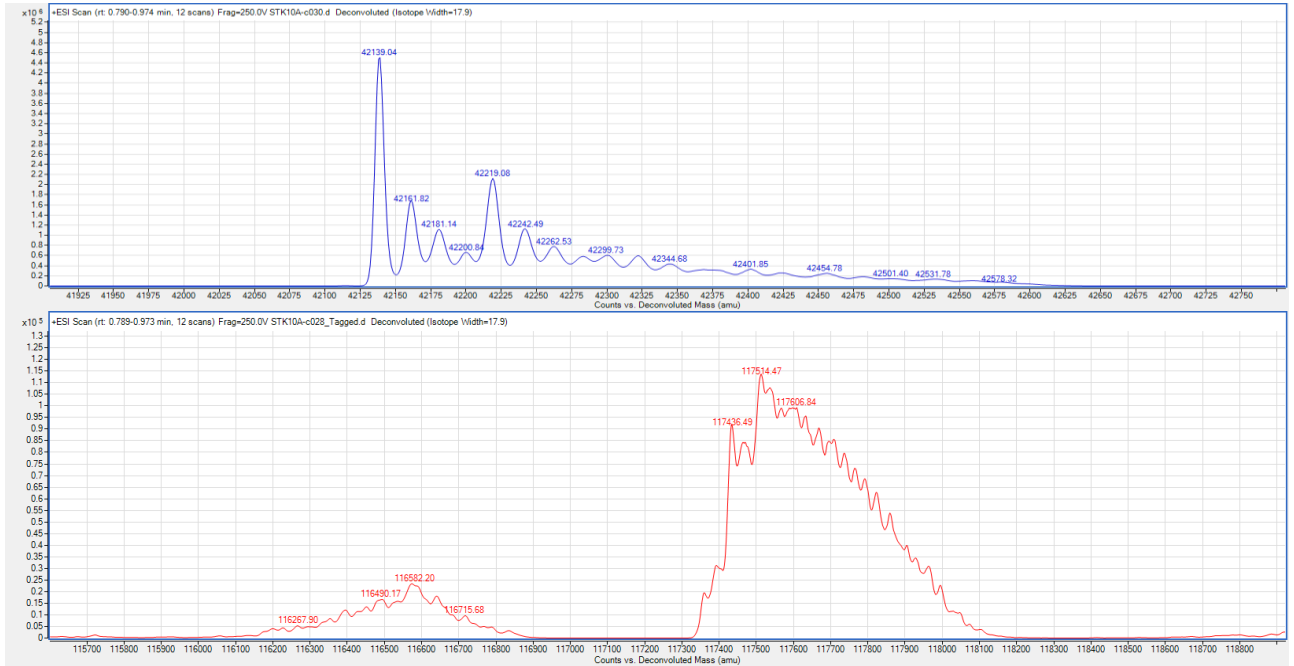


Suppl. Fig. S 6: Representative NanoBRET wash-out data for STK10.

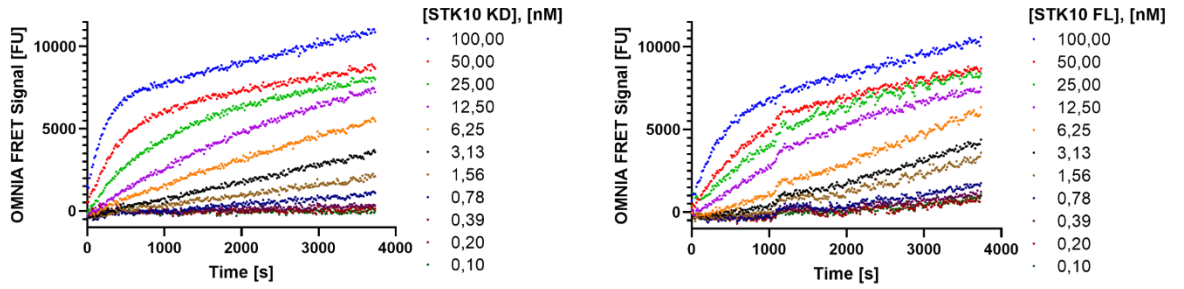


Suppl. Fig. S 7: Representative NanoBRET wash-out data for SLK. The assay was of insufficient data quality and not further pursued.

11 Supplemental Information

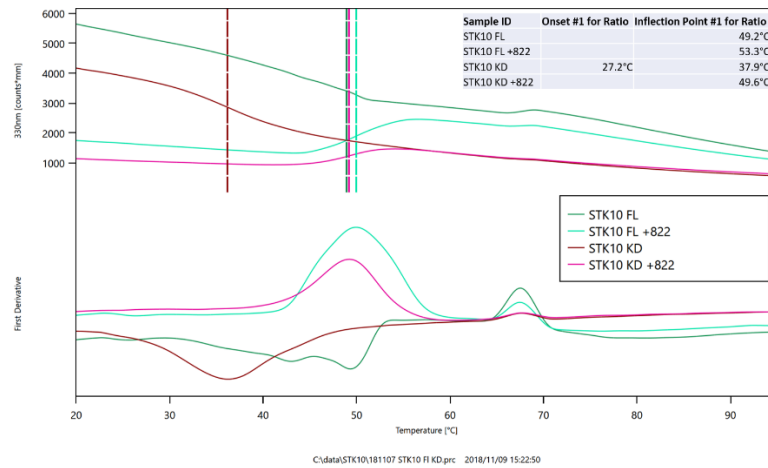


Suppl. Fig. S 8: Mass Spec analysis of STK10 KD (a) and STK10 FL (b).



Suppl. Fig. S 9: Titration of STK10 full-length (FL) or kinase domain only (KD) proteins using 1 mM ATP and 1 mM SOX substrate in the OMNIA assay. We decided to use 5 nM final STK10 concentration in following assays.

11 Supplemental Information



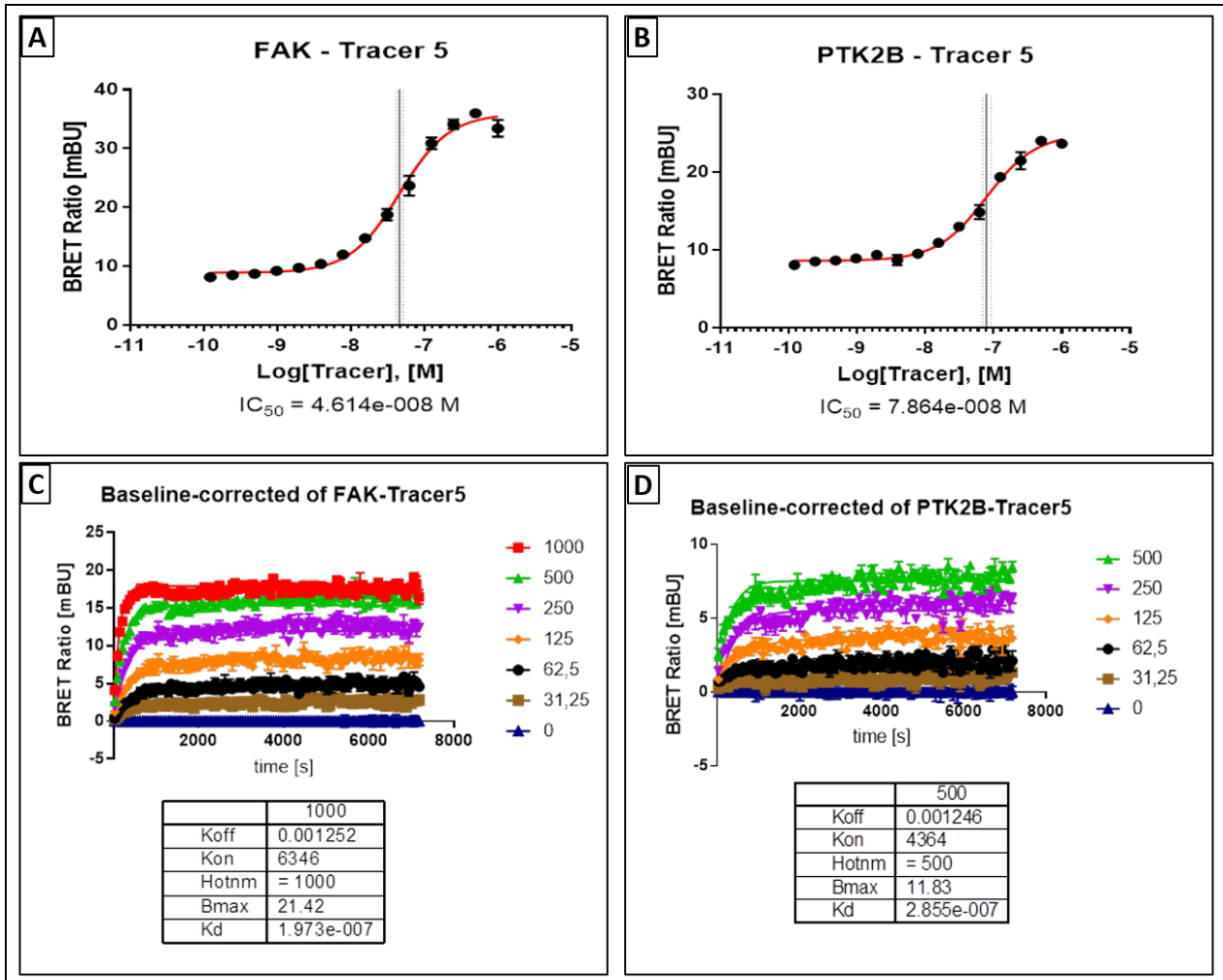
Suppl. Fig. S 10: Stability of insect cell expressed STK10 proteins. NanoDSF experiments for STK10 full-length (=STK10 FL) and STK10 kinase domain only (STK10 KD) constructs show a high stability of STK10 FL but a low window for stabilization. It shows low stability of STK10 KD, which starts denaturing at 27 °C. Upon ligand addition the Kinase domain is stabilized to 49 °C creating a good assay window.

11 Supplemental Information

Suppl. Table S 4: Data collection and refinement statistics for FAK structures.

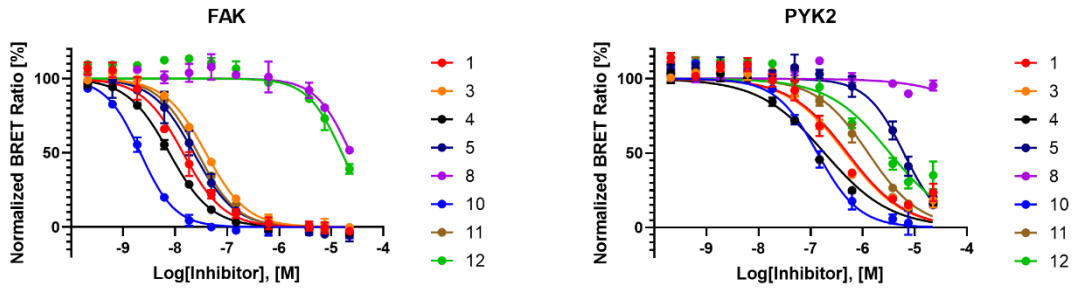
Structure	2	3	4	5 (PF-573228)	8	10 (PF431396)	12 (PF-719)
<i>Data Collection</i>							
Space Group	<i>P1</i>	<i>C2</i>	<i>C2</i>	<i>P212121</i>	<i>C2</i>	<i>C2</i>	<i>C2</i>
cell parameters (Å)	45.35, 51.35, 67.07	118.05, 77.13, 174.93	112.53, 75.75, 173.27	42.53, 48.40, 129.33	114.17, 76.08, 172.85	110.22 74.54 172.55	113.97, 75.86, 172.64
cell angles (°)	99.36, 102.89, 92.51	90.00, 101.34, 90.00	90.00, 102.37, 90.00	90.00, 90.00, 90.00	90.00, 102.53, 90.00	90.00 103.11 90.00	90.00, 102.66, 90.00
Molecules/AU	2	4	4	1	4	4	4
Resolution (Å) ^a	64.35-1.54 (1.64-1.54)	171.52-2.30 (2.57-2.30)	62.37-1.78 (2.02-1.78)	45.33-1.36 (1.44-1.36)	84..37-1.81 (2.035-1.81)	84.03-1.93 (2.17-1.93)	56.49-1.92 (1.98-1.92)
Unique reflections	56803	44522	82421	47762	81043	48069	88953
Completeness (%) ^a	82.7 (64.9)	92.6 (64.7)	93.2 (67.9)	89.8 (51.7)	92.0 (69.5)	88.0 (72.8)	85.6 (71.7)
Multiplicity ^a	1.9 (1.9)	3.3 (3.4)	4.1 (3.8)	7.6 (5.1)	3.4 (3.4)	3.4 (3.5)	4.9 (5.1)
<i>R</i> _{pim} (%) ^a	2.8 (57.0)	3.5 (42.7)	4.2 (34.4)	3.2 (58.1)	3.5 (39.2)	3.4 (40.7)	3.5 (36.6)
CC(1/2) ^a	0.999 (0.522)	0.999 (0.710)	0.998 (0.786)	0.999 (0.387)	0.999 (0.728)	0.999 (0.670)	0.997 (0.730)
Mean <i>I</i> / <i>s(I)</i> ^a	10.5 (1.2)	12.3 (1.9)	10.5 (2.2)	16.0 (1.2)	11.7 (1.8)	14.3 (1.9)	11.9 (1.7)
<i>Refinement</i>							
<i>R</i> _{work} , (%) ^b	19.0	23.2	18.3	17.1	19.2	19.2	21.4
<i>R</i> _{free} , (%) ^b	21.2	20.2	21.4	19.8	21.5	21.8	23.5
No. of atoms	4553	8654	9648	2479	8983	8664	8960
Protein ^c	4125	8387	8576	2081	8244	8349	8323
Water	360	138	922	364	622	175	508
Ligands	67	124	144	34	116	140	124
other solvent molecules	1	5	6	0	5	0	5
RMSD bonds (Å)	0.008	0.008	0.008	0.008	0.008	0.008	0.008
RMSD angles (°)	0.88	0.98	0.89	0.95	0.85	0.86	0.91
Mean <i>B</i> (Å ²)	32.9	60.78S	31.0	17.0	39.2	38.4	39.2
Ramachandran (%)							
Favoured	92	93	92	94	93	93	93
Allowed	8	7	8	6	6	7	7
Outliers	0	0	0	0	0.1	0.1	0
PDB entry	6YT6	6YXV	6YQ1	6YOJ	6YVS	6YR9	6YVY

11 Supplemental Information

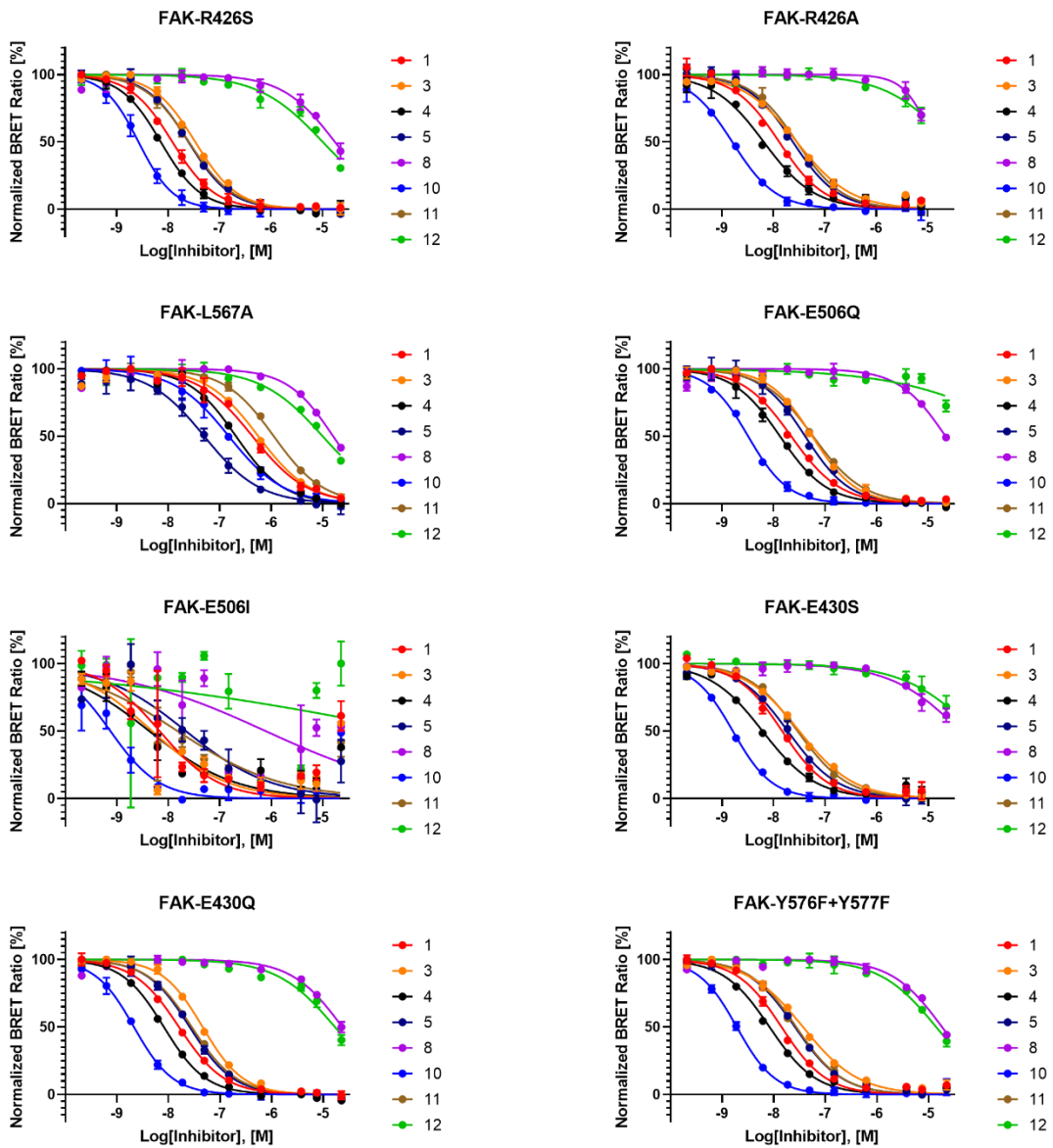


Suppl. Fig. S 11: Tracer parameters determined in NanoBRET for FAK and PYK2. NanoBRET tracer potency were determined for FAK (A) and PYK2 (B), respectively. The tracer kinetics of FAK (C) and PYK2 (D) were determined using intact cells.

11 Supplemental Information

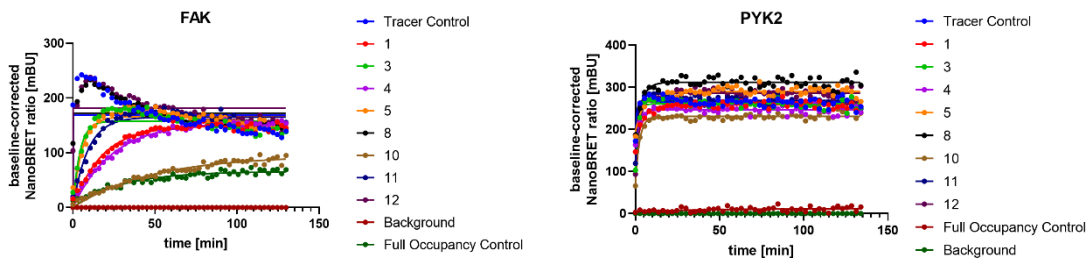
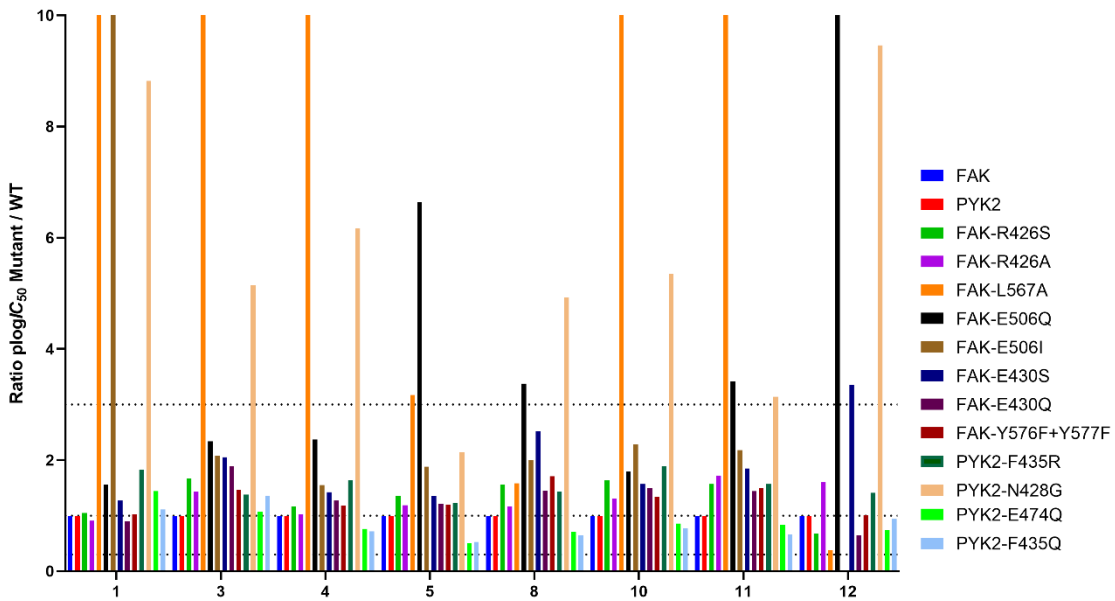
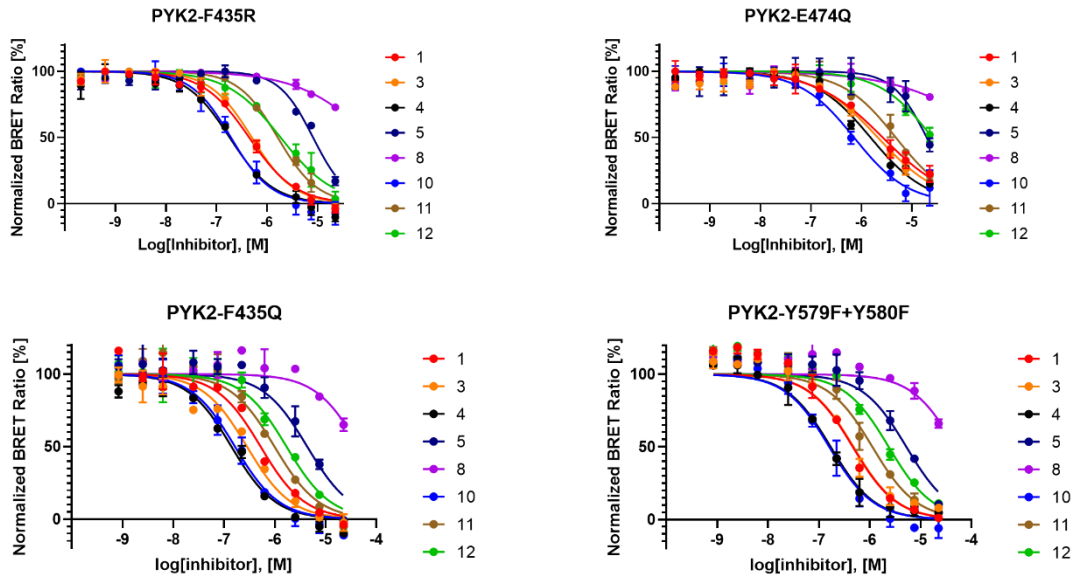


Suppl. Fig. S 12: NanoBRET potency for the inhibitor series on FAK and PYK2 as indicated in the figure.

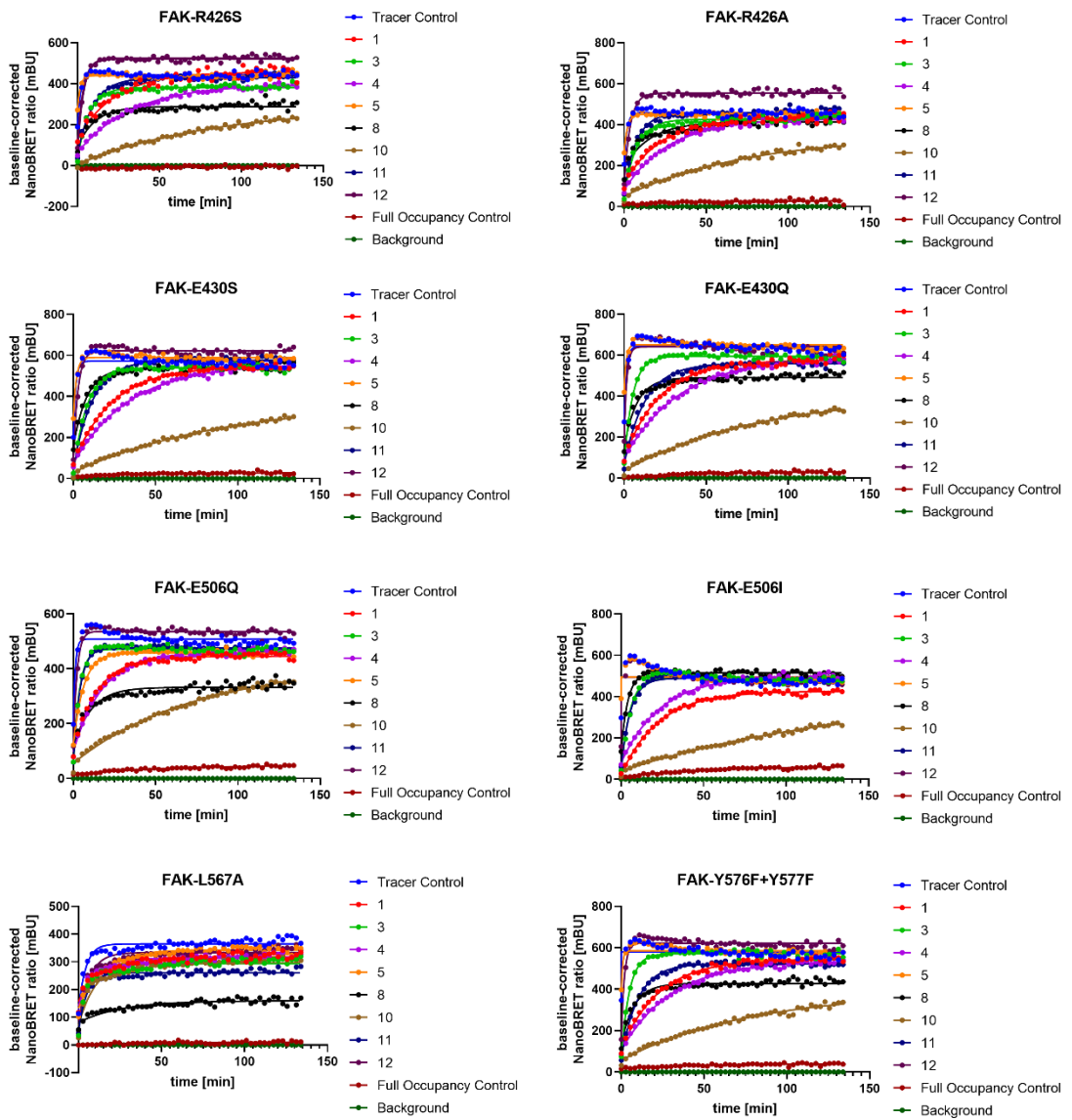


Suppl. Fig. S 13: NanoBRET potency for the inhibitor series on FAK mutants as indicated in the figure.

11 Supplemental Information

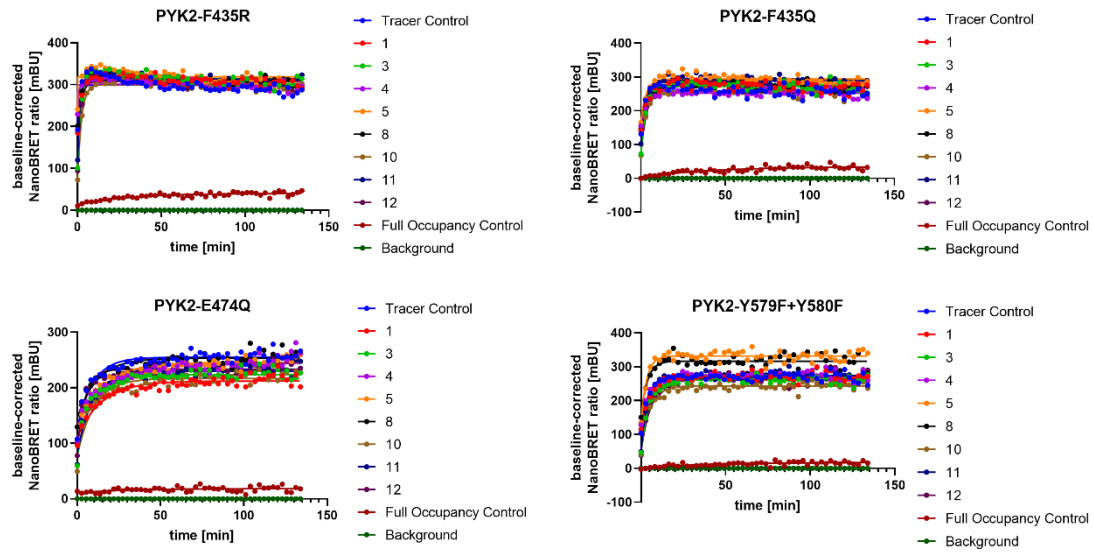


11 Supplemental Information



Suppl. Fig. S 17: NanoBRET wash-out data on FAK mutants as indicated in the figure for the inhibitor series investigated here.

11 Supplemental Information



Suppl. Fig. S 18: NanoBRET wash-out data on PYK2 mutants as indicated in the figure for the inhibitor series investigated here.

12 ABBREVIATIONS

ABL	<i>Abelson murine leukemia viral oncogene homolog 1</i>
Akt	<i>Protein kinase B synonym</i>
APE	<i>Aspartate-Proline-Glutamate</i>
ATP	<i>Adenosine Triphosphate</i>
BCR	<i>breakpoint cluster region</i>
BRET	<i>Bioluminescence resonance energy transfer</i>
BSA	<i>Bovine Serum Albumin</i>
CAMK	<i>calcium/calmodulin dependent protein kinases</i>
CDK	<i>Cyclin dependent kinase</i>
CK1	<i>Casein Kinase 1</i>
CLK	<i>CDC-like kinase</i>
DFG	<i>Aspartate-Phenylalanine-Glycin</i>
DMEM	<i>Dulbecco's modified eagles medium</i>
DMSO	<i>Dimethylsulfoxide</i>
DSF	<i>Differential Scanning Fluorimetry, Differential Scanning Fluorimetry</i>
EGFR	<i>Epidermal Growth Factor Receptor</i>
ELISA	<i>Enzyme linked Immuno Sorbent Assay</i>
ePCA	<i>equilibrium probe competition assay</i>
ERM	<i>ezrin, radixin, moesin</i>
FAK	<i>Focal Adhesion Kinase</i>
FAT	<i>focal adhesion targeting</i>
FBS	<i>Fetal Bovine Serum</i>
FDA	<i>Food and drug administration</i>
FERM	<i>4.1 protein, ezrin, radixin, moesin</i>
FGFR	<i>fibroblast growth factor receptor</i>
FL	<i>full-length</i>
FRET	<i>Fluorescence resonance energy transfer</i>
GAK	<i>Cyclin G associated kinase, Cyclin-G associated kinase</i>
GSK3	<i>Glycogen synthase kinase 3</i>
HBS	<i>HEPES buffered saline</i>
HEK293T	<i>Human embrionic kidney</i>
HEPES	<i>N-2-hydroxyethylpiperazine-N-ethanesulfonic acid</i>
HTRF	<i>homogenous TR-FRET</i>
IC₅₀	<i>inhibitory concentration for 50%</i>
IMI	<i>Innovative Medicines initiative</i>
ITC	<i>Isothermal Titration Calorimetry, Isothermal titration calorimetry</i>
K_D	<i>dissociation constant, Kinase Domain</i>
K _i	<i>dissociation constant</i>
k _{off}	<i>kinetic dissociation constant</i>
k _{on}	<i>kinetic association constant</i>
kPCA	<i>kinetic probe competition assay</i>
LB	<i>Laurea Bertani</i>
LOK	<i>lymphocyte oriented kinase</i>
MAP	<i>Mitogen activated protein</i>

12 Abbreviations

MAPK	<i>mitogen activated protein kinase</i>
MEK1	<i>MAPK kinase 1</i>
MEK2	<i>MAPK kinase 2</i>
MEM	<i>Minimal essential medium</i>
MET	<i>Synonym of hepatocyte growth factor receptor</i>
MOPS	<i>3-(N-morpholino)propanesulfonic acid</i>
mTOR	<i>mammalian target of rapamycin</i>
NLuc	<i>Nanoluciferase</i>
NTA	<i>nitrilotriacetic acid</i>
PBS	<i>Phosphate Buffered Saline</i>
PDB	<i>Protein Databank</i>
PEG	<i>Polyethyenglycole</i>
PEI	<i>Polyethylenimine</i>
PenStrep	<i>Penicillin Streptomycin</i>
PI3K	<i>Phosphoinositide 3-kinase</i>
PKA	<i>Protein Kinase A</i>
PKC	<i>Protein Kinase C</i>
PKG	<i>Protein Kinase G</i>
PLK	<i>Polo-like Kinase</i>
PYK2	<i>Proline-rich tyrosine kinase 2</i>
RL	<i>Receptor Ligand complex</i>
RL*	<i>high affinity receptor ligand complex</i>
RSK	<i>ribosomal s6 kinase</i>
SA	<i>Streptavidin</i>
SAR	<i>structure activity relationship</i>
SGC	<i>Structural Genomics Consortium</i>
SKR	<i>structure-kinetic-relationship</i>
SLK	<i>STE20 like kinase</i>
SPR	<i>Surface Plasmon Resonance</i>
STK10	<i>Serine/Threonine kinase 10</i>
TCEP	<i>tris(2-carboxyethyl)phosphine</i>
TEV	<i>tobacco etch virus</i>
TK	<i>Tyrosine kinase</i>
TKL	<i>tyrosine kinase-like</i>
TR	<i>time-resolved</i>
TRIS	<i>tris(hydroxymethyl)aminomethane</i>
WNK	<i>with no lysine kinases</i>

13 REFERENCES

- 1 Asquith, C. R. *et al.* SGC-GAK-1: a chemical probe for cyclin G associated kinase (GAK). *Journal of medicinal chemistry* **62**, 2830-2836 (2019).
- 2 Forster, M. *et al.* Development, optimization, and structure–activity relationships of covalent-reversible JAK3 inhibitors based on a tricyclic imidazo [5, 4-d] pyrrolo [2, 3-b] pyridine scaffold. *Journal of medicinal chemistry* **61**, 5350-5366 (2018).
- 3 Georgi, V. *et al.* Binding Kinetics Survey of the Drugged Kinome. *J Am Chem Soc* **140**, 15774-15782, doi:10.1021/jacs.8b08048 (2018).
- 4 Hanke, T. *et al.* A Highly Selective Chemical Probe for Activin Receptor-like Kinases ALK4 and ALK5. *ACS Chemical Biology* (2020).
- 5 Montenegro, R. C. *et al.* Identification of molecular targets for the targeted treatment of gastric cancer using dasatinib. *Oncotarget* **11**, 535 (2020).
- 6 Němec, V. *et al.* Furo [3, 2-b] pyridine: A Privileged Scaffold for Highly Selective Kinase Inhibitors and Effective Modulators of the Hedgehog Pathway. *Angewandte Chemie* **131**, 1074-1078 (2019).
- 7 Röhm, S. *et al.* Fast Iterative Synthetic Approach toward Identification of Novel Highly Selective p38 MAP Kinase Inhibitors. *Journal of medicinal chemistry* **62**, 10757-10782 (2019).
- 8 Tröster, A. *et al.* NVP-BHG712: Effects of Regioisomers on the Affinity and Selectivity toward the EPHrin Family. *ChemMedChem* **13**, 1629-1633 (2018).
- 9 Vasta, J. D. *et al.* Quantitative, Wide-Spectrum Kinase Profiling in Live Cells for Assessing the Effect of Cellular ATP on Target Engagement. *Cell Chem Biol* **25**, 206-214 e211, doi:10.1016/j.chembiol.2017.10.010 (2018).
- 10 Robers, M. B. *et al.* Quantifying Target Occupancy of Small Molecules Within Living Cells. *Annu Rev Biochem*, doi:10.1146/annurev-biochem-011420-092302 (2020).
- 11 Siegel, R. L., Miller, K. D. & Jemal, A. Cancer statistics, 2020. *CA: A Cancer Journal for Clinicians* **70**, 7-30 (2020).
- 12 Hanahan, D. & Weinberg, R. A. Hallmarks of cancer: the next generation. *Cell* **144**, 646-674, doi:10.1016/j.cell.2011.02.013 (2011).
- 13 Fouad, Y. A. & Aanei, C. Revisiting the hallmarks of cancer. *American journal of cancer research* **7**, 1016 (2017).
- 14 Adams, J. L., Veal, J. & Shewchuk, L. Kinases. *Protein Crystallography in Drug Discovery*, 47-81 (2003).
- 15 Manning, G., Whyte, D. B., Martinez, R., Hunter, T. & Sudarsanam, S. The protein kinase complement of the human genome. *Science* **298**, 1912-1934, doi:10.1126/science.1075762 (2002).
- 16 Chartier, M., Chenard, T., Barker, J. & Najmanovich, R. Kinome Render: a stand-alone and web-accessible tool to annotate the human protein kinome tree. *PeerJ* **1**, e126, doi:10.7717/peerj.126 (2013).
- 17 Noble, M. E. M., Endicott, J. A. & Johnson, L. N. Protein kinase inhibitors: Insights into drug design from structure. *Science* **303**, 1800-1805, doi:DOI 10.1126/science.1095920 (2004).
- 18 Zhang, J., Yang, P. L. & Gray, N. S. Targeting cancer with small molecule kinase inhibitors. *Nat Rev Cancer* **9**, 28-39, doi:10.1038/nrc2559 (2009).
- 19 Delpire, E. The mammalian family of sterile 20p-like protein kinases. *Pflugers Arch* **458**, 953-967, doi:10.1007/s00424-009-0674-y (2009).

13 References

- 20 Fedorov, O., Müller, S. & Knapp, S. The (un) targeted cancer kinome. *Nature chemical biology* **6**, 166-169 (2010).
- 21 Roskoski Jr, R. Properties of FDA-approved small molecule protein kinase inhibitors: a 2020 update. *Pharmacological Research*, 104609 (2019).
- 22 Müller, S., Chaikuad, A., Gray, N. S. & Knapp, S. The ins and outs of selective kinase inhibitor development. *Nature chemical biology* **11**, 818-821 (2015).
- 23 Kornev, A. P., Taylor, S. S. & Ten Eyck, L. F. A helix scaffold for the assembly of active protein kinases. *Proc Natl Acad Sci U S A* **105**, 14377-14382, doi:10.1073/pnas.0807988105 (2008).
- 24 Bradshaw, J. M. *et al.* Prolonged and tunable residence time using reversible covalent kinase inhibitors. *Nature chemical biology* **11**, 525-531 (2015).
- 25 Klaeger, S. *et al.* The target landscape of clinical kinase drugs. *Science* **358**, eaan4368 (2017).
- 26 Copeland, R. A., Pompliano, D. L. & Meek, T. D. Drug-target residence time and its implications for lead optimization. *Nat Rev Drug Discov* **5**, 730-739, doi:10.1038/nrd2082 (2006).
- 27 Parker, R. B. & Waud, D. R. Pharmacological estimation of drug-receptor dissociation constants. Statistical evaluation. I. Agonists. *J Pharmacol Exp Ther* **177**, 1-12 (1971).
- 28 Cheng, Y.-C. & Prusoff, W. H. Relationship between the inhibition constant (K₁) and the concentration of inhibitor which causes 50 per cent inhibition (I₅₀) of an enzymatic reaction. *Biochemical pharmacology* **22**, 3099-3108 (1973).
- 29 Davis, M. I. *et al.* Comprehensive analysis of kinase inhibitor selectivity. *Nat Biotechnol* **29**, 1046-1051, doi:10.1038/nbt.1990 (2011).
- 30 Karaman, M. W. *et al.* A quantitative analysis of kinase inhibitor selectivity. *Nat Biotechnol* **26**, 127-132, doi:10.1038/nbt1358 (2008).
- 31 Anastassiadis, T., Deacon, S. W., Devarajan, K., Ma, H. & Peterson, J. R. Comprehensive assay of kinase catalytic activity reveals features of kinase inhibitor selectivity. *Nat Biotechnol* **29**, 1039-1045, doi:10.1038/nbt.2017 (2011).
- 32 Fabian, M. A. *et al.* A small molecule-kinase interaction map for clinical kinase inhibitors. *Nat Biotechnol* **23**, 329-336, doi:10.1038/nbt1068 (2005).
- 33 Copeland, R. A. The drug-target residence time model: a 10-year retrospective. *Nat Rev Drug Discov* **15**, 87-95, doi:10.1038/nrd.2015.18 (2016).
- 34 Copeland, R. A. The dynamics of drug-target interactions: drug-target residence time and its impact on efficacy and safety. *Expert opinion on drug discovery* **5**, 305-310 (2010).
- 35 Copeland, R. A., Pompliano, D. L. & Meek, T. D. Drug-target residence time and its implications for lead optimization. *Nature reviews Drug discovery* **5**, 730-739 (2006).
- 36 Swinney, D. C. The role of binding kinetics in therapeutically useful drug action. *Current opinion in drug discovery & development* **12**, 31-39 (2009).
- 37 Swinney, D. C. Can binding kinetics translate to a clinically differentiated drug? From theory to practice. *Letters in Drug Design & Discovery* **3**, 569-574 (2006).
- 38 Swinney, D. C. Applications of binding kinetics to drug discovery. *Pharmaceutical medicine* **22**, 23-34 (2008).
- 39 Dahl, G. & Akerud, T. Pharmacokinetics and the drug-target residence time concept. *Drug discovery today* **18**, 697-707 (2013).
- 40 Ehrlich, P. Chemotherapeutics: scientific principles, methods and results. *Lancet* **2**, 353-359 (1913).

13 References

- 41 Copeland, R. A. Evaluation of enzyme inhibitors in drug discovery. A guide for medicinal chemists and pharmacologists. *Methods Biochem Anal* **46**, 1-265 (2005).
- 42 Keighley, W. The need for high throughput kinetics early in the drug discovery process. *Drug Discovery World* **12**, 39-45 (2011).
- 43 Núñez, S., Venhorst, J. & Kruse, C. G. Target–drug interactions: first principles and their application to drug discovery. *Drug discovery today* **17**, 10-22 (2012).
- 44 Georgi, V. *et al.* Binding kinetics survey of the drugged kinome. *Journal of the American Chemical Society* **140**, 15774-15782 (2018).
- 45 Copeland, R. A. Conformational adaptation in drug-target interactions and residence time. *Future Med Chem* **3**, 1491-1501, doi:10.4155/fmc.11.112 (2011).
- 46 Disse, B., Speck, G. A., Rominger, K. L., Witek Jr, T. J. & Hammer, R. Tiotropium (SPIRIVA[™]): Mechanistical considerations and clinical profile in obstructive lung disease. *Life sciences* **64**, 457-464 (1999).
- 47 Tummino, P. J. & Copeland, R. A. Residence time of receptor– ligand complexes and its effect on biological function. *Biochemistry* **47**, 5481-5492 (2008).
- 48 Keighley, W. The need for high throughput kinetics early in the drug discovery process. *Drug Discov World* **12**, 39-45 (2011).
- 49 Vanderheyden, P. M., Fierens, F. L. & Vauquelin, G. Angiotensin II type 1 receptor antagonists: why do some of them produce insurmountable inhibition? *Biochemical pharmacology* **60**, 1557-1563 (2000).
- 50 FUCHS, B. *et al.* Comparative pharmacodynamics and pharmacokinetics of candesartan and losartan in man. *Journal of pharmacy and pharmacology* **52**, 1075-1083 (2000).
- 51 Kalgutkar, A. S. *et al.* Aspirin-like molecules that covalently inactivate cyclooxygenase-2. *Science* **280**, 1268-1270, doi:DOI 10.1126/science.280.5367.1268 (1998).
- 52 Nunez, S., Venhorst, J. & Kruse, C. G. Target-drug interactions: first principles and their application to drug discovery. *Drug Discov Today* **17**, 10-22, doi:10.1016/j.drudis.2011.06.013 (2012).
- 53 Dahl, G. & Akerud, T. Pharmacokinetics and the drug-target residence time concept. *Drug Discov Today* **18**, 697-707, doi:10.1016/j.drudis.2013.02.010 (2013).
- 54 Hong, Y., Gengo, F. M., Rainka, M. M., Bates, V. E. & Mager, D. E. Population pharmacodynamic modelling of aspirin-and ibuprofen-induced inhibition of platelet aggregation in healthy subjects. *Clinical pharmacokinetics* **47**, 129-137 (2008).
- 55 Schoop, A. & Dey, F. On-rate based optimization of structure–kinetic relationship–surfing the kinetic map. *Drug Discovery Today: Technologies* **17**, 9-15 (2015).
- 56 Sullivan, S. M. & Holyoak, T. Enzymes with lid-gated active sites must operate by an induced fit mechanism instead of conformational selection. *Proceedings of the National Academy of Sciences* **105**, 13829-13834 (2008).
- 57 McDonnell, D. P. The molecular pharmacology of SERMs. *Trends in Endocrinology & Metabolism* **10**, 301-311 (1999).
- 58 Copeland, R. A. Conformational adaptation in drug–target interactions and residence time. *Future medicinal chemistry* **3**, 1491-1501 (2011).
- 59 Shan, Y. *et al.* How does a drug molecule find its target binding site? *Journal of the American Chemical Society* **133**, 9181-9183 (2011).

13 References

- 60 Englert, L. *et al.* Displacement of disordered water molecules from hydrophobic pocket creates enthalpic signature: Binding of phosphoramidate to the S1'-pocket of thermolysin. *Biochimica et Biophysica Acta (BBA)-General Subjects* **1800**, 1192-1202 (2010).
- 61 Schmidtke, P., Luque, F. J., Murray, J. B. & Barril, X. Shielded hydrogen bonds as structural determinants of binding kinetics: application in drug design. *Journal of the American Chemical Society* **133**, 18903-18910 (2011).
- 62 Heroven, C. *et al.* Halogen–aromatic π interactions modulate inhibitor residence times. *Angewandte Chemie International Edition* **57**, 7220-7224 (2018).
- 63 Regan, J. *et al.* The kinetics of binding to p38 MAP kinase by analogues of BIRB 796. *Bioorganic & medicinal chemistry letters* **13**, 3101-3104 (2003).
- 64 Klein, T. *et al.* Structural and dynamic insights into the energetics of activation loop rearrangement in FGFR1 kinase. *Nature communications* **6**, 1-12 (2015).
- 65 Schuetz, D. A. *et al.* Ligand desolvation steers on-rate and impacts drug residence time of heat shock protein 90 (Hsp90) inhibitors. *Journal of medicinal chemistry* **61**, 4397-4411 (2018).
- 66 Vauquelin, G. & Charlton, S. J. Long-lasting target binding and rebinding as mechanisms to prolong in vivo drug action. *Br J Pharmacol* **161**, 488-508, doi:10.1111/j.1476-5381.2010.00936.x (2010).
- 67 Schuetz, D. A. *et al.* Kinetics for drug discovery: an industry-driven effort to target drug residence time. *Drug discovery today* **22**, 896-911 (2017).
- 68 Basavapathruni, A. *et al.* Conformational adaptation drives potent, selective and durable inhibition of the human protein methyltransferase DOT1L. *Chemical biology & drug design* **80**, 971-980 (2012).
- 69 Miller, D. C., Klute, W. & Brown, A. D. Discovery of potent, metabolically stable purine CRF-1 antagonists with differentiated binding kinetic profiles. *Bioorganic & medicinal chemistry letters* **21**, 6108-6111 (2011).
- 70 Jin, M. *et al.* Discovery of novel insulin-like growth factor-1 receptor inhibitors with unique time-dependent binding kinetics. *ACS medicinal chemistry letters* **4**, 627-631 (2013).
- 71 Gaspari, R. *et al.* Kinetic and structural insights into the mechanism of binding of sulfonamides to human carbonic anhydrase by computational and experimental studies. *Journal of medicinal chemistry* **59**, 4245-4256 (2016).
- 72 Anastassiadis, T., Deacon, S. W., Devarajan, K., Ma, H. & Peterson, J. R. Comprehensive assay of kinase catalytic activity reveals features of kinase inhibitor selectivity. *Nature biotechnology* **29**, 1039 (2011).
- 73 Davis, M. I. *et al.* Comprehensive analysis of kinase inhibitor selectivity. *Nature biotechnology* **29**, 1046 (2011).
- 74 Elkins, J. M. *et al.* Comprehensive characterization of the published kinase inhibitor set. *Nature biotechnology* **34**, 95 (2016).
- 75 Karaman, M. W. *et al.* A quantitative analysis of kinase inhibitor selectivity. *Nature biotechnology* **26**, 127-132 (2008).
- 76 Fabian, M. A. *et al.* A small molecule–kinase interaction map for clinical kinase inhibitors. *Nature biotechnology* **23**, 329-336 (2005).
- 77 Kuramochi, S. *et al.* Molecular cloning of the human gene STK10 encoding lymphocyte-oriented kinase, and comparative chromosomal mapping of the human, mouse, and rat homologues. *Immunogenetics* **49**, 369-375 (1999).

13 References

- 78 Walter, S. A., Cutler, R. E., Jr., Martinez, R., Gishizky, M. & Hill, R. J. Stk10, a new member of the polo-like kinase kinase family highly expressed in hematopoietic tissue. *J Biol Chem* **278**, 18221-18228, doi:10.1074/jbc.M212556200 (2003).
- 79 Kuramochi, S. *et al.* LOK is a novel mouse STE20-like protein kinase that is expressed predominantly in lymphocytes. *J Biol Chem* **272**, 22679-22684, doi:DOI 10.1074/jbc.272.36.22679 (1997).
- 80 Oliver, A. W., Knapp, S. & Pearl, L. H. Activation segment exchange: a common mechanism of kinase autophosphorylation? *Trends in biochemical sciences* **32**, 351-356 (2007).
- 81 Tao, L. *et al.* Opposing roles of serine/threonine kinases MEKK1 and LOK in regulating the CD28 responsive element in T-cells. *Biochem J* **363**, 175-182 (2002).
- 82 Belkina, N. V., Liu, Y., Hao, J. J., Karasuyama, H. & Shaw, S. LOK is a major ERM kinase in resting lymphocytes and regulates cytoskeletal rearrangement through ERM phosphorylation. *Proc Natl Acad Sci U S A* **106**, 4707-4712, doi:10.1073/pnas.0805963106 (2009).
- 83 Viswanatha, R., Ohouo, P. Y., Smolka, M. B. & Bretscher, A. Local phosphocycling mediated by LOK/SLK restricts ezrin function to the apical aspect of epithelial cells. *J Cell Biol* **199**, 969-984, doi:10.1083/jcb.201207047 (2012).
- 84 Qian, Y. W., Erikson, E. & Maller, J. L. Purification and cloning of a protein kinase that phosphorylates and activates the polo-like kinase Plx1. *Science* **282**, 1701-1704, doi:DOI 10.1126/science.282.5394.1701 (1998).
- 85 Jang, Y. J., Ma, S., Terada, Y. & Erikson, R. L. Phosphorylation of threonine 210 and the role of serine 137 in the regulation of mammalian polo-like kinase. *J Biol Chem* **277**, 44115-44120, doi:10.1074/jbc.M202172200 (2002).
- 86 Lacouture, M. E. Mechanisms of cutaneous toxicities to EGFR inhibitors. *Nature Reviews Cancer* **6**, 803-812 (2006).
- 87 Robert, C. *et al.* Cutaneous side-effects of kinase inhibitors and blocking antibodies. *The lancet oncology* **6**, 491-500 (2005).
- 88 Shepherd, F. A. *et al.* Erlotinib in previously treated non-small-cell lung cancer. *New England Journal of Medicine* **353**, 123-132 (2005).
- 89 Liu, H.-b. *et al.* Skin rash could predict the response to EGFR tyrosine kinase inhibitor and the prognosis for patients with non-small cell lung cancer: a systematic review and meta-analysis. *PLoS one* **8** (2013).
- 90 Parmar, S. *et al.* Pharmacogenetic predictors for EGFR-inhibitor-associated skin toxicity. *The pharmacogenomics journal* **13**, 181-188 (2013).
- 91 Petrelli, F., Borgonovo, K., Cabiddu, M., Lonati, V. & Barni, S. Relationship between skin rash and outcome in non-small-cell lung cancer patients treated with anti-EGFR tyrosine kinase inhibitors: a literature-based meta-analysis of 24 trials. *Lung cancer* **78**, 8-15 (2012).
- 92 Sugiura, Y. *et al.* Skin rash by gefitinib is a sign of favorable outcomes for patients of advanced lung adenocarcinoma in Japanese patients. *Springerplus* **2**, 22 (2013).
- 93 Wacker, B. *et al.* Correlation between development of rash and efficacy in patients treated with the epidermal growth factor receptor tyrosine kinase inhibitor erlotinib in two large phase III studies. *Clinical Cancer Research* **13**, 3913-3921 (2007).

13 References

- 94 Brahmer, J. *et al.* Dosing to rash: a phase II trial of the first-line erlotinib for patients with advanced non-small-cell lung cancer an Eastern Cooperative Oncology Group Study (E3503). *European Journal of Cancer* **50**, 302-308 (2014).
- 95 Guttman-Yassky, E. *et al.* Characterisation of the cutaneous pathology in non-small cell lung cancer (NSCLC) patients treated with the EGFR tyrosine kinase inhibitor erlotinib. *Eur J Cancer* **46**, 2010-2019, doi:10.1016/j.ejca.2010.04.028 (2010).
- 96 Lilenbaum, R. *et al.* Randomized phase II trial of erlotinib or standard chemotherapy in patients with advanced non-small-cell lung cancer and a performance status of 2. *Journal of Clinical Oncology* **26**, 863-869 (2008).
- 97 Takeda, M., Okamoto, I. & Nakagawa, K. Pooled safety analysis of EGFR-TKI treatment for EGFR mutation-positive non-small cell lung cancer. *Lung Cancer* **88**, 74-79 (2015).
- 98 Udupa, K. S., Rajendranath, R., Sagar, T. & Thomas, J. Differential toxicities of tyrosine kinase inhibitors in the management of metastatic lung cancer. *Indian journal of medical and paediatric oncology: official journal of Indian Society of Medical & Paediatric Oncology* **38**, 15 (2017).
- 99 Yamamoto, N., Honma, M. & Suzuki, H. Off-target serine/threonine kinase 10 inhibition by erlotinib enhances lymphocytic activity leading to severe skin disorders. *Mol Pharmacol* **80**, 466-475, doi:10.1124/mol.110.070862 (2011).
- 100 Schlaepfer, D. D., Hauck, C. R. & Sieg, D. J. Signaling through focal adhesion kinase. *Progress in biophysics and molecular biology* **71**, 435-478, doi:10.1016/s0079-6107(98)00052-2 (1999).
- 101 Sasaki, H. *et al.* Cloning and Characterization of Cell Adhesion Kinase β , a Novel Protein-tyrosine Kinase of the Focal Adhesion Kinase Subfamily. *J Biol Chem* **270**, 21206-21219, doi:10.1074/jbc.270.36.21206 (1995).
- 102 Avraham, H., Park, S.-Y., Schinkmann, K. & Avraham, S. RAFTK/Pyk2-mediated cellular signalling. *Cellular Signalling* **12**, 123-133, doi:10.1016/s0898-6568(99)00076-5 (2000).
- 103 Schaller, M. D. *et al.* pp125FAK a structurally distinctive protein-tyrosine kinase associated with focal adhesions. *Proceedings of the National Academy of Sciences* **89**, 5192-5196 (1992).
- 104 Lipinski, C. A. & Loftus, J. C. Targeting Pyk2 for therapeutic intervention. *Expert Opin Ther Targets* **14**, 95-108, doi:10.1517/14728220903473194 (2010).
- 105 Fan, H. & Guan, J.-L. Compensatory function of Pyk2 protein in the promotion of focal adhesion kinase (FAK)-null mammary cancer stem cell tumorigenicity and metastatic activity. *The Journal of biological chemistry* **286**, 18573-18582, doi:10.1074/jbc.M110.200717 (2011).
- 106 Wendt, M. K. *et al.* TGF- β stimulates Pyk2 expression as part of an epithelial-mesenchymal transition program required for metastatic outgrowth of breast cancer. *Oncogene* **32**, 2005-2015, doi:10.1038/onc.2012.230 (2013).
- 107 Tai, Y.-L., Chen, L.-C. & Shen, T.-L. Emerging roles of focal adhesion kinase in cancer. *BioMed research international* **2015**, 690690, doi:10.1155/2015/690690 (2015).
- 108 Lv, P. C., Jiang, A. Q., Zhang, W. M. & Zhu, H. L. FAK inhibitors in Cancer, a patent review. *Expert Opin Ther Pat* **28**, 139-145, doi:10.1080/13543776.2018.1414183 (2018).
- 109 Buckbinder, L. *et al.* Proline-rich tyrosine kinase 2 regulates osteoprogenitor cells and bone formation, and offers an anabolic treatment approach for

13 References

- osteoporosis. *Proceedings of the National Academy of Sciences* **104**, 10619-10624 (2007).
- 110 Roberts, W. G. *et al.* Antitumor activity and pharmacology of a selective focal adhesion kinase inhibitor, PF-562,271. *Cancer Res* **68**, 1935-1944, doi:10.1158/0008-5472.CAN-07-5155 (2008).
- 111 Infante, J. R. *et al.* Safety, pharmacokinetic, and pharmacodynamic phase I dose-escalation trial of PF-00562271, an inhibitor of focal adhesion kinase, in advanced solid tumors. *Journal of Clinical Oncology* **30**, 1527-1533 (2012).
- 112 Slack-Davis, J. K. *et al.* Cellular characterization of a novel focal adhesion kinase inhibitor. *J Biol Chem* **282**, 14845-14852, doi:10.1074/jbc.M606695200 (2007).
- 113 Tse, K. W. *et al.* Small molecule inhibitors of the Pyk2 and FAK kinases modulate chemoattractant-induced migration, adhesion and Akt activation in follicular and marginal zone B cells. *Cell Immunol* **275**, 47-54, doi:10.1016/j.cellimm.2012.03.002 (2012).
- 114 Stratagene. *QuickChange Site/Directed Mutagenesis Kit Instruction Manual*, (2005).
- 115 Yung-Chi, C. & Prusoff, W. H. Relationship between the inhibition constant (K_i) and the concentration of inhibitor which causes 50 per cent inhibition (I₅₀) of an enzymatic reaction. *Biochemical pharmacology* **22**, 3099-3108 (1973).
- 116 Schiele, F., Ayaz, P. & Fernández-Montalván, A. A universal homogeneous assay for high-throughput determination of binding kinetics. *Analytical biochemistry* **468**, 42-49 (2015).
- 117 Motulsky, H. J. & Mahan, L. C. The kinetics of competitive radioligand binding predicted by the law of mass action. *Mol Pharmacol* **25**, 1-9 (1984).
- 118 Fedorov, O., Niesen, F. H. & Knapp, S. in *Kinase Inhibitors* 109-118 (Springer, 2012).
- 119 Liedberg, B., Nylander, C. & Lunström, I. Surface plasmon resonance for gas detection and biosensing. *Sensors and actuators* **4**, 299-304 (1983).
- 120 Shults, M. D. & Imperiali, B. Versatile fluorescence probes of protein kinase activity. *Journal of the American Chemical Society* **125**, 14248-14249 (2003).
- 121 Robers, M. B. *et al.* Target engagement and drug residence time can be observed in living cells with BRET. *Nature communications* **6**, 10091, doi:10.1038/ncomms10091 (2015).
- 122 Machleidt, T. *et al.* NanoBRET • A Novel BRET Platform for the Analysis of Protein–Protein Interactions. *ACS chemical biology* **10**, 1797-1804 (2015).
- 123 Vasta, J. D. *et al.* Quantitative, wide-spectrum kinase profiling in live cells for assessing the effect of cellular ATP on target engagement. *Cell chemical biology* **25**, 206-214. e211 (2018).
- 124 Leslie, A. G. & Powell, H. R. in *Evolving methods for macromolecular crystallography* 41-51 (Springer, 2007).
- 125 Evans, P. R. An introduction to data reduction: space-group determination, scaling and intensity statistics. *Acta Crystallographica Section D: Biological Crystallography* **67**, 282-292 (2011).
- 126 McCoy, A. J. *et al.* Phaser crystallographic software. *Journal of applied crystallography* **40**, 658-674 (2007).
- 127 Emsley, P., Lohkamp, B., Scott, W. G. & Cowtan, K. Features and development of Coot. *Acta Crystallographica Section D: Biological Crystallography* **66**, 486-501 (2010).

13 References

- 128 Murshudov, G. N. *et al.* REFMAC5 for the refinement of macromolecular crystal structures. *Acta Crystallographica Section D: Biological Crystallography* **67**, 355-367 (2011).
- 129 Robers, M. B. *et al.* (AACR, 2015).
- 130 Lietha, D. *et al.* Structural basis for the autoinhibition of focal adhesion kinase. *Cell* **129**, 1177–1187, doi:10.1016/j.cell.2007.05.041 (2007).
- 131 Lietha, D. & Eck, M. J. Crystal structures of the FAK kinase in complex with TAE226 and related bis-anilino pyrimidine inhibitors reveal a helical DFG conformation. *PLoS one* **3** (2008).
- 132 Han, S. *et al.* Structural characterization of proline-rich tyrosine kinase 2 (PYK2) reveals a unique (DFG-out) conformation and enables inhibitor design. *J Biol Chem* **284**, 13193-13201, doi:10.1074/jbc.M809038200 (2009).
- 133 Walker, D. P. *et al.* Trifluoromethylpyrimidine-based inhibitors of proline-rich tyrosine kinase 2 (PYK2): structure-activity relationships and strategies for the elimination of reactive metabolite formation. *Bioorg Med Chem Lett* **18**, 6071-6077, doi:10.1016/j.bmcl.2008.10.030 (2008).
- 134 Markevich, N. I., Hoek, J. B. & Kholodenko, B. N. Signaling switches and bistability arising from multisite phosphorylation in protein kinase cascades. *The Journal of cell biology* **164**, 353-359 (2004).
- 135 Consortium, S. G. PF-04554878 - a highly selective FAK probe, <<https://www.sgc-ffm.uni-frankfurt.de/#!specificprobeoverview/PF-04554878>> (2020).
- 136 Bantscheff, M. *et al.* Quantitative chemical proteomics reveals mechanisms of action of clinical ABL kinase inhibitors. *Nature biotechnology* **25**, 1035-1044 (2007).
- 137 Klaeger, S. *et al.* The target landscape of clinical kinase drugs. *Science* **358**, doi:10.1126/science.aan4368 (2017).
- 138 Frohna, P. *et al.* Evaluation of the absolute oral bioavailability and bioequivalence of erlotinib, an inhibitor of the epidermal growth factor receptor tyrosine kinase, in a randomized, crossover study in healthy subjects. *The Journal of Clinical Pharmacology* **46**, 282-290 (2006).
- 139 Ault, P. S., Rose, J. & Kaled, E. S. Bosutinib therapy in patients with chronic myeloid leukemia: practical considerations for management of side effects. *Journal of the advanced practitioner in oncology* **7**, 160 (2016).
- 140 Uchida, T., Ishimori, K. & Morishima, I. The effects of heme pocket hydrophobicity on the ligand binding dynamics in myoglobin as studied with leucine 29 mutants. *J Biol Chem* **272**, 30108-30114 (1997).
- 141 Mohanty, A. *et al.* FAK-targeted and combination therapies for the treatment of cancer: an overview of phase I and II clinical trials. *Expert Opinion on Investigational Drugs* **29**, 399-409 (2020).
- 142 Farand, J. *et al.* Selectivity switch between FAK and Pyk2: Macrocyclization of FAK inhibitors improves Pyk2 potency. *Bioorg Med Chem Lett* **26**, 5926-5930, doi:10.1016/j.bmcl.2016.10.092 (2016).
- 143 Yen-Pon, E. *et al.* Structure-based design, synthesis, and characterization of the first irreversible inhibitor of focal adhesion kinase. *ACS chemical biology* **13**, 2067-2073 (2018).
- 144 Pan, A. C., Borhani, D. W., Dror, R. O. & Shaw, D. E. Molecular determinants of drug-receptor binding kinetics. *Drug Discov Today* **18**, 667-673, doi:10.1016/j.drudis.2013.02.007 (2013).